Finite Element Analysis and Design Optimization of Deep Cold Rolling of Titanium Alloy at Room and Elevated Temperatures

Armin Hadadian

A Thesis

in the Department of

Mechanical, Industrial and Aerospace Engineering

Presented in Partial Fulfilment of the Requirements
for the Degree of
Doctor of Philosophy (Mechanical Engineering) at
Concordia University
Montreal, Quebec, Canada

October 2019

CONCORDIA UNIVERSITY

SCHOOL OF GRADUATE STUDIES

This is to certify that the thesis prepared

By: Armin Hadadian

Entitled: Finite Element Analysis and Design Optimization of Deep Cold Rolling of Titanium Alloy at Room and Elevated Temperatures

and submitted in partial fulfillment of the requirements for the degree of

Doctor of Philosophy (Mechanical Engineering)

complies with the regulations of the University and meets the accepted standards with respect to originality and quality.

Signed by the final examining committee:

_____ Chair
Dr. Nikolaos Tsantalis

_____ External Examiner
Dr. Kamran Behdinan

_____ External to Program
Dr. Lucia Tirca

_____ Examiner
Dr. Ion Stiharu

_____ Examiner
Dr. Sivakumar Narayanswamy

_____ Thesis Supervisor
Dr. Ramin Sedaghati

Approved by _____
Dr. Ivan Contreras, Graduate Program Director

Thursday, December 5, 2019

_____
Dr. Amir Asif, Dean
Faculty of Engineering and Computer Science

Abstract

Finite Element Analysis and Design Optimization of Deep Cold Rolling of Titanium Alloy at Room and Elevated Temperatures

Armin Hadadian

Concordia University, 2019

High strength-to-density ratio, high corrosion resistance and superior biocompatibility are the main advantages of Ti-6Al-4V (Ti64), making it a long been favored titanium alloy for aerospace and biomedical applications. Designing titanium components to last longer and refurbishing of aged ones using surface treatments have become a desirable endeavor considering high environmental damage, difficulty in casting, scarcity and high cost associated with this metal.

Among mechanical surface treatments, Deep Cold Rolling (DCR) has been shown to be a very promising process to improve fatigue life by introducing a deep compressive residual stress and work-hardening in the surface layer of components. This process has shown to be superior compared with other surface treatment methods as it yields a better surface quality and induces a deeper residual stress profile which can effectively be controlled through the process parameters (i.e. ball diameter, rolling pressure and feed). However, residual stresses induced through this process at room temperature are generally relaxed upon exposure of the components to elevated operating temperatures.

In this work, high-fidelity Finite Element (FE) models have been developed to simulate the DCR process in order to predict the induced residual stresses at room temperature and their subsequent relaxation following exposure to temperature increase. Accuracy of the developed models has been validated using experimental measurements available in the literature. A design optimization strategy has also been proposed to identify the optimal process parameters to maximize the induced beneficial compressive residual stress on and under the surface layer and thus prolong the fatigue life. Conducting optimization directly on the developed high-fidelity FE model is not practical due to high computational cost associated with nonlinear dynamic models. Moreover, responses from the FE models are typically noisy and thus cannot be utilized in gradient based optimization algorithms. In this research study, well-established machine learning principles are employed to

develop and validate surrogate analytical models based on the response variables obtained from FE simulations. The developed analytical functions are smooth and can efficiently approximate the residual stress profiles with respect to the process parameters. Moreover the developed surrogate models can be effectively and efficiently utilized as explicit functions for the optimization process.

Using the developed surrogate models, conventional (one-sided) DCR process is optimized for a thin Ti64 plate considering the material fatigue properties, operating temperature and external load. It is shown that the DCR process can lead to a tensile balancing residual stress on the untreated side of the component which can have a detrimental effect on the fatigue life. Additionally, application of conventional DCR on thin geometries such as compressor blades can cause manufacturing defects due to unilateral application of the rolling force and can also lead to thermal distortion of the part due to asymmetric profile of the induced residual stresses.

Double-sided deep rolling has been shown as a viable alternative to address those issues since both sides of the component are treated simultaneously. The process induces a symmetric residual stress which can be further optimized to achieve a compressive residual stress on both sides of the component. For this case, a design optimization problem is formulated to improve fatigue life in high stress locations on a generic compressor blade.

All the optimization problems are formulated for multi-objective functions to achieve most optimal residual stress profiles both at room temperature as well as elevated temperature of 450℃. A hybrid optimization algorithm based on combination of sequential quadratic programming (SQP) technique with stochastic based genetic algorithm (GA) has been developed to accurately catch the global optimum solutions. It has been shown that the optimal solution depends on the stress distribution in the component due to the external load as well as the operating temperature.

Acknowledgment

Foremost, I would like to thank my supervisor Professor Ramin Sedaghati for his continuous support and encouragement throughout my PhD study. I would not be able to thank him enough in any words for always being flexible with his daily schedule in order to make it possible for me to have regular meetings with him despite my work and life obligations. His knowledge and guidance have been vital to the progress of this work.

I would like to express my gratitude to my examiners Professor Mehdi Hojjati, Professor Ion Stiharu, Dr. Lucia Tirca and Dr. Sivakumar Narayanswamy for their invaluable input and insightful questions which helped me to better shape the direction of the thesis. I also would like to thank Professor Kamran Behdinan for accepting to be the external examiner.

I need to thank Ms. Leslie Hosein, our Graduate Program Coordinator for her tremendous support and her willingness to help where possible.

Completing a PhD degree as a full-time employee requires working on evenings and many weekends which inevitably put extra stress on my young family over the past few years. As such, I owe a great debt of gratitude to my wife, Tahoura. Without her support and continuous motivation this work would have not been possible. I also like to thank my two daughters for their patience as their playtime had to be postponed many times during this time. I intend to make it up to all of them.

Table of Contents

List of Figures

List of Tables

List of Abbreviations

CCD	Central Composite Design
CNC	Computer Numerical Control
DCR	Deep Cold Rolling
DoE	Design of Experiments
DOD	Domestic Object Damage
DR	Deep Rolling
FE	Finite Element
FOD	Foreign Object Damage
GA	Genetic Algorithm
HCF	High Cycle Fatigue
LCF	Low Cycle Fatigue
LPB	Low Plasticity Burnishing
LSP	Laser Shock Peening
RS	Residual Stress
RSM	Response Surface Method
SQP	Sequential Quadratic Programming
SSE	Residual Sum of Squares
SST	Total Sum of Squares
Ti64	Ti-6Al-4V
XRD	X-Ray Diffraction

1 Research objectives and Scopes

1.1 Motivation

The current intense competition in every market pushes all companies to optimize the production processes to reduce the final cost while producing more reliable products. Shortening the process chain is a very important factor in reducing new project lead time. Numerical analysis methods have found their exceptional place particularly in high-tech industries to reduce the manufacturing cost by virtually simulating the manufacturing processes scenarios and predicting the effect of every single manufacturing process factor on the final product.

The life, performance and life cycle cost of a gas turbine is to a large extent dependent on some critical components which are heavily loaded at high temperatures. These components are usually made of super alloys such as Inconel 718 and Ti-6Al-4V (Ti64). These materials are difficult-to cut, and the machining processes are detrimental to their surface quality and mechanical integrity. Controlling the fatigue failure in such critical components is challenging with an impact on the safety, reliability and the life cycle cost of the engine.

Ti64 is a titanium alloy with a high strength-to-weight ratio and excellent corrosion resistance making it an excellent material for aero-derivative gas turbine applications. The main usage of this alloy is in compressor blades which their lives are mainly limited by fatigue failure. Therefore, improving their fatigue life while maintaining the airfoil shape without undergoing an expensive full-scale redesign is a keen desire of aerospace industry.

It is known that the fatigue strength of such highly stressed components can be significantly improved by introducing a compressive residual stress and strain hardening in near surface layers. Deep Cold Rolling (DCR) is an inexpensive but efficient mechanical surface treatment method to create the beneficial compressive surface residual stresses while maintaining a good surface quality.

Some experimental research studies have been conducted to establish the correlation between the process parameters and the introduced residual stress profiles using statistical methods. However, considering all relevant design variable in experimental studies is not practical due to the high cost associated to a reliable experimental processing and measurement. Therefore, there is a tendency to

replace experimental measurement with high-fidelity numerical simulation which is accurate to predict the residual stress profile induced by the process.

On the other hand, the residual stresses are introduced in the room temperature while most of highly stressed component are intended to operate at elevated temperature. The exposure to elevated temperature results in relaxation and redistribution of the induced residual stress which needs to be considered in the design stage to avoid overestimating the beneficial impact of the residual stress on the fatigue life improvement of the treated component. In addition, empirical determination of the residual stresses at elevated temperature is challenging as it is difficult, costly and inherits measurement errors. Therefore, reliable FE model need to be developed to simulate the thermal relaxation and predict the residual stress at elevated temperature.

Considering above the general aim of the present research study is twofold. Firstly, it attempts to develop high-fidelity finite element models to simulate conventional as well as double-sided DCR process of Ti-6Al-4V components and the following thermal exposure to elevated temperature 450°C. The accuracy of the developed models will be validated by comparing predicted residual stress profiles obtained by the developed FE models to those available experimental measurements. Secondly, the experimentally validated FE models are utilized to generate a training set of data using well-established machine learning methods to develop surrogate models for formulated design optimization problems. The surrogate models can accurately and efficiently describe the correlation between the process parameters and the achievable residual stresses both at room temperature and elevated temperature of 450°C without using computationally expensive FE models. The surrogate models can then be effectively utilized to perform sensitivity analysis and for design optimization problems. The multi-objective optimization problems can be thus practically formulated in order to achieve the most optimal residual stress profiles both at room temperature and elevated temperature, based on a given duty.

As mentioned above, while the influence of DCR on the fatigue life has been widely studied experimentally at the ambient temperature, limited research has been conducted on the development of predictive analysis and design optimization models to accurately estimate and optimize the induced residual stresses in the subsurface layers. As much less experimental information is available for the effectiveness of such a surface treatment at elevated temperature, these predictive models would be of paramount importance to shed light on the effectiveness of DCR at the elevated temperatures.

The analytical predictive models are presented for both conventional and double-sided DCR process of thin-walled Ti-6Al-4V components which can replace further experimental assessment and FE simulation. These surrogate models can be subsequently considered in stress analysis and fatigue life assessment of Ti-6Al-4V components for design optimization and process parameter selection to achieve a design target.

1.2 Specific Research Objectives

The main specific objectives of the present research study can be outlined as follow:

1. Development of a reliable high-fidelity finite element model to simulate the deep cold rolling process on Ti-6Al-4V specimens and the following short-term exposure of the treated components to elevated temperature of 450°C, in order to predict induced residual stresses and their subsequent relaxations. The validated proposed FE models could potentially replace further expensive experimental investigation.
2. Utilizing the developed FE models to simulate the conventional and double-sided DCR processes on a thin-walled geometry with the thickness of 1mm and the following thermal relaxation, in order to predict residual stress profiles.
3. Train and validate surrogate analytical models based on results obtained from high-fidelity FE models, using well-established machine learning principles. The developed analytical functions are smooth and can explicitly describe the residual stress profiles with respect to the process parameters including ball diameter, rolling pressure and feed.
4. A systematic sensitivity study on the process parameters to determine the effect and interaction level of each process parameters on the residual stress profiles both right after the process at room temperature and then after thermal relaxation due to short time exposure to elevated temperature 450°C.
5. Establish a formal design optimization of the DCR process and present design guidelines for proper selection of the process parameters to achieve desirable residual stress profiles both at room and elevated temperature to enhance fatigue strength of a Ti64 blade.

1.3 Thesis Outline

Chapter 1 outlines the motivations for finite element (FE) modeling of DCR process on Ti64 components in order to predict residual stress profiles and ultimately developing surrogate models to approximate FE models. Research objectives are briefly discussed which draw a framework in the current study.

Chapter 2 presents an introduction to DCR process and its beneficial impact on mechanical integrity of treated components both at room and elevated temperatures. A detailed literature review on the finite element modeling of DCR process will be elaborated to identify the research gaps in this field which will be accordingly addressed in the following chapters.

Chapter 3 explains the FE model development of deep cold rolling process on Ti-6Al-4V specimens and the following short-term exposure of the treated components to elevated temperature. The process is simulated using ABAQUS/Explicit which can effectively handle non-linearities associated to the friction contact and plastic deformation under the rolling element. The thermal relaxation is performed in ABAQUS/Standard using a visco-plastic model which couples the creep and plasticity deformation mechanisms to predict the state of residual stresses at the elevated temperature. A new set of hyperbolic creep law coefficients are introduced to describe the primary creep of Ti-6Al-4V at 450˚C. The accuracy of the developed finite element model to predict residual stresses is validated by comparisons of the simulation results with the experimental data available in the literature.

Chapter 4 details design optimization of DCR process on a thin Ti-6Al-4V plate aiming to achieve optimal residual stress profiles based on a given duty cycle and fatigue behaviour of the material. The application of the developed FE model in Chapter 3 is extended to simulate the DCR process on a thin plate and the following thermal relaxation. Conducting optimization directly on the developed high-fidelity finite element (FE) model is not practical due to high computational cost associated with nonlinear dynamic finite element models. Thus, well-established machine learning principles are considered to develop and validate surrogate models which can efficiently replace the computationally expensive FE models. A set of multi-objective design optimization problems are formulated and solved using a hybrid optimization method by combining genetic algorithm with sequential quadratic programming techniques. It will be demonstrated that the optimal

solution depends on the final resultant stress state in the component and operating temperature under the defined duty cycles.

Chapter 5 covers FE simulation of double-sided DCR process on a thin walled Ti-6Al-4V components and the following thermal relaxation of the induced residual stresses at elevated temperature of 450°C. The importance of considering double-sided DCR process to prevent manufacturing damage and possible thermal distortion in thin-walled component will be elaborated. The developed FE model will be validated by comparing simulation results with experimental measurements available in the literature. The results obtained using the developed high-fidelity FE models are then used to establish analytical surrogate models which can be efficiently used to evaluate the residual stress profiles at room and the elevated temperature. Critical high stress locations on a generic compressor blade will be highlighted and considered to formulate a design optimization problem in order to improve the fatigue life of the component.

Chapter 6 summaries the main conclusions and highlights the major contributions of the present PhD dissertation to the advancement of knowledge in this filed. In addition, the possible future research topics in the field will be discussed.

2 Literature Review and Research Background

In the following, first an introduction to Deep Cold Rolling (DCR) process is provided and the beneficial impact of the process on mechanical integrity of treated components at room and elevated temperatures will be discussed. This is followed by a critical literature review on this promising mechanical surface treatment to understand the current state of the art in DCR process with emphasis on Ti-6Al-4V alloy.

2.1 Deep Cold Rolling

Ti-6Al-4V is a titanium alloy with a high strength-to-weight ratio and excellent corrosion resistance. It has been widely used in highly stressed components operating at elevated temperatures, such as turbine blades, discs and aircraft containment structures. Controlling the fatigue failure is of paramount importance and a main challenge in such critical components. It is known that the fatigue life of highly stressed component such as turbine blades, crankshafts and connecting rods can be significantly improved by the introduction of a compressive residual stress and strain hardening in near surface layers [1].

Various thermo-chemical surface modifications such as carburizing, plasma-carburizing nitriding, and oxidation have been widely studied and employed to improve wear resistance of titanium alloys by producing a high hardness surface layer. However, these diffusion treatments are not very effective in improving the fatigue strength of the alloy particularly at high temperatures as the induced high-hardness surface layer is brittle and the resultant compressive residual stresses can easily relax at elevated temperature [2]. Thus mechanical surface treatments are preferred if the aim of the process is to enhance the fatigue strength of a component [2, 3].

Shot-peening (SP), liquid jet peening (LJP), laser shock peening (LSP or simply LP), ultrasonic surface rolling (USRP), low plasticity burnishing (LPB) and deep cold rolling (DCR) are among popular mechanical surface treatments that have been well employed to improve wear resistance, fatigue strength and corrosion resistance of titanium components by introducing a compressive residual stress in the surface and sub-surface layers [2-6].

It is worth mentioning that that Deep Rolling (DR), Deep Cold Rolling (DCR), Low Plasticity Burnishing (LPB), Ball Burnishing (BB) and Roller Burnishing (RB) are fundamentally similar surface treatment processes where a hydrostatically suspended ball plastically deforms a

component surface through mechanical interaction. The main difference between these methods is in the tooling design and the way the load is applied or controlled during the process [7]. However, the plastic deformation mechanism in the workpiece under these processes is identical and the relevant research works on this topic are elaborated in the current literature review. Figure 2-1 (a) shows the schematic of the process. The process parameters are rolling speed, rolling feed rate, applied fluid pressure or normal displacement and the ball diameter.

The deformation introduced by DCR results in plastic strain, yield surface, and residual stress profiles that vary through the depth from the surface. The process makes three important changes in the near surface layers of a treated material: (1) hardening of the material, i.e., raising the yield strength; (2) large biaxial compressive residual stresses in surface layer constrained by balancing tensile stresses in deeper depth, and (3) severe plastic deformation near the surface layer which may become unstable under cyclic and thermal loads.

The process creates a deep residual stress field beneath the treated surface which can be typically represented by residual stress depth profile $\sigma(y)$ as shown in Figure 2-1 (b). The residual stress profile can be characterized by four significant output variables including the residual stress at the surface σ_o (at Y=0), the minimum residual stress σ_{min} located at $Y = Y_{min}$, the maximum residual stress σ_{max} located at $Y = Y_{max}$ and the location through the thickness from which residual stress changes from compressive to tensile ($Y = Y_o$) [1]. In addition, in the current study, the areas under the curve (areas between the residual stress curve and $\sigma = 0$) are also introduced which are deemed to describe the overall shape of the stress profile. The total area of the residual stress can then be calculated using both negative $A_{(-)}$ and positive areas $A_{(+)}$ of the stress components throughout the thickness. These significant parameters can be effectively utilized to describe the variation of the residual stress through the thickness. These parameters can also be considered as desired output responses to establish surrogate meta models which can be efficiently used for design optimization problems.

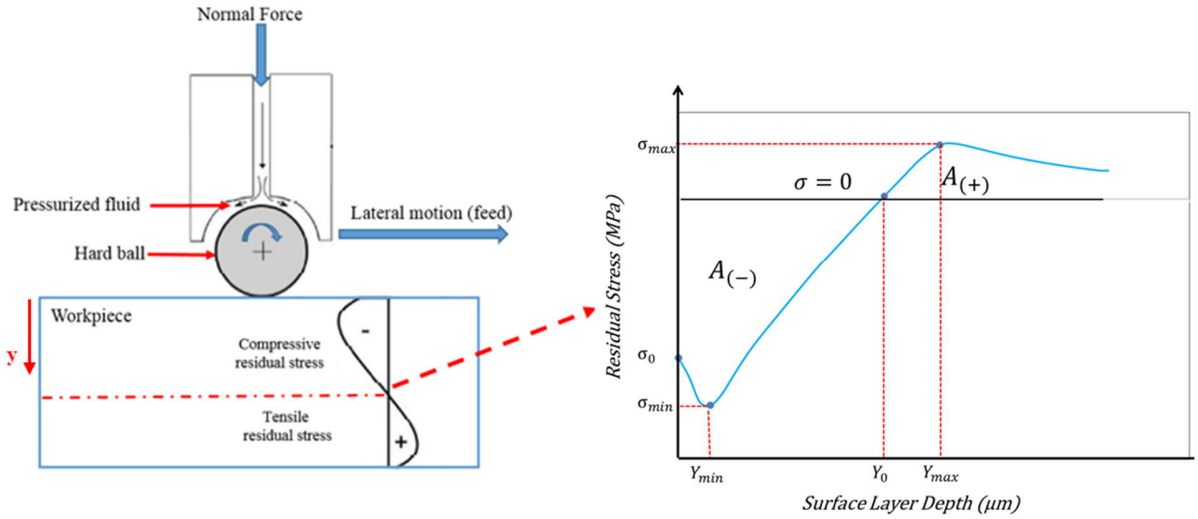

(a) (b)

Figure 2-1:(a) Schematic of deep rolling process [7], and (b) Characterization of a residual stress depth profile

DCR in particular is considered to be a promising low cost process which is found to be superior to other surface treatment methods, as the profile of the induced residual stresses is generally controllable through the process parameters thus enabling generation of beneficial residual stresses with higher magnitude and depth while retaining a high quality smooth surface [4, 6].

Figure 2-2 shows the typical depth and profile of the residual stresses induced in SP, LP, and DR in Ti-6Al-4V samples.

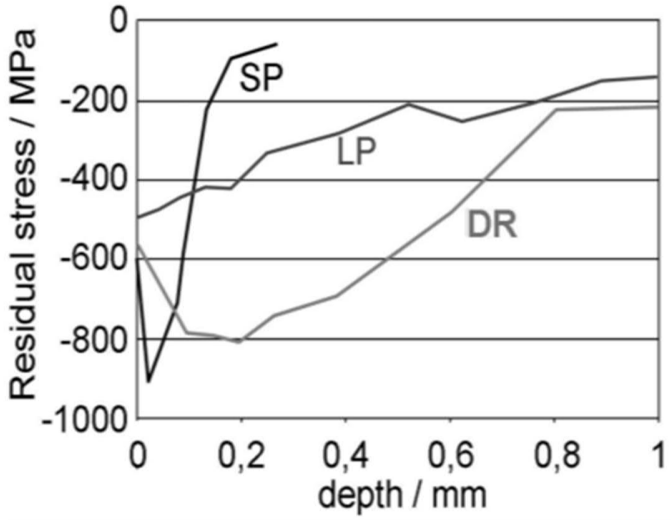

Figure 2-2: Comparison of residual stress state in Ti-6Al-4V material using different strain hardening techniques [4]

As it can be realized DR or DCR process can introduce deeper compressive residual stress under the surface. The residual stress up to a depth of 500 µm can be easily reached in DCR process while in shot-peening process of titanium alloys the achievable depth of the residual stresses is mainly limited to 250 µm as shown in

Figure 2-2. The DCR process can improve the surface roughness of an untreated titanium workpiece from 0.22 µm to 0.07 µm [2]. This is a very important fact as a lower surface quality (higher surface roughness) is known to increase the chance of fatigue crack initiation [8]. More importantly, in terms of application, the magnitude and depth of the induced residual stress profile can be easily controlled by the process parameters [1, 7, 9, 10] which can be effectively used to reach an optimized profile based on a given operating load and cycle.

The effect of a compressive residual stress on the crack opening can be schematically presented in Figure 2-3. The superposition of the induced compressive residual stresses (created by the process) onto the applied tensile stresses (due to external load) defines the final state of the resultant stress in the crack tip. As it can be realized, the amount and the nature of the residual stress play an important role in the crack propagation and consequently the fatigue failure of the component. If the resultant stress remains compressive at the crack tip, the crack is closed and thus its propagation is suppressed while a tensile residual stress can severe the effect of the external load on the opening of the crack.

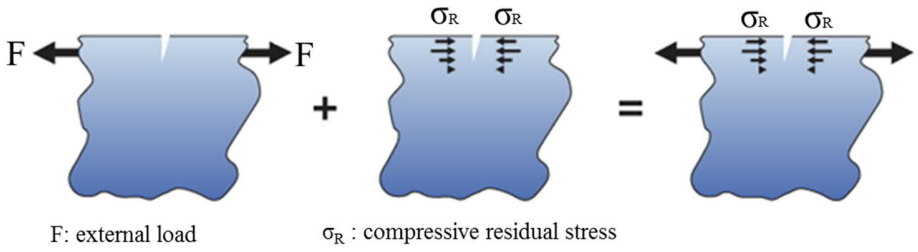

Figure 2-3: Effect of residual stress on crack opening

Klocke et al. [11] investigated the effect of the component thickness on the residual stress distribution induced by deep rolling on IN718 specimens with different thicknesses. The experimental results showed that the thickness of the treated component can significantly influence the near surface residual stresses.

A thick component; with a thickness larger in order of magnitude than the depth of residual stress, is only locally affected in the surface layer while a thin-walled geometry with a thickness

comparable to the depth of the residual stress is affected over the complete thickness. In addition, as presented in Figure 2-1, the process tends to create a compressive residual stress on the surface layer which is balanced by tensile residual stress in the inner sub-surface region of the component. The compensatory tensile stress can spread over a large domain in thick components, while in thin-walled components, the magnitude of tensile residual stress needs to increase due to lower thickness. This results in a significantly different residual distribution through the thickness in thin-walled components compared with that in thick components [12].

As a result, the component thickness needs to be considered in the selection of process parameters particularly for thin-walled geometries where the thickness of the component is comparable to the residual stress depth. Otherwise, the process may result in a detrimental tensile residual stress on the surface which can negatively impact the fatigue life of the treated component.

Avoiding manufacturing defects due to permanent deflection of thin-walled surfaces under the unilateral rolling loads is one of the main challenges in DCR process of fan and compressor blades [12]. Additionally, the induced strain states in conventional roller burnishing of thin-walled components is asymmetrical as the load is applied on only one side of the component. This is usually observed in form of bulging of the blade toward the direction of applied force after the completion of the process as it is shown in Figure 2-4 (a). This permanent deflection of the blade is accompanied with increase of the plastic strain in the surface layer [12]. Considering this, performing the conventional DCR on thin-walled geometries is not generally recommended and deep rolling process of turbine blade is a demanding production challenge [13].

Another risk associated to conventional DCR process of thin-walled component is thermal distortion caused by thermal relaxation of asymmetrical residual stresses. The distortion will be more severe in component with a thickness in the order of the depth of the induced compressive layer and especially under a non-uniform thermal relaxation [14].

ECOROLL Corporation Tool Technology [15] has designed a special tool to perform double-sided DCR process on thin-walled components such as turbine blades which is shown in Figure 2-4 (b). This tool compromises a double-sided hydrostatic deep rolling tool which pressures the balls on both sides of the component simultaneously to avoid the permanent deflection of the part under the process. The double-sided process introduces a symmetrical residual stress and plastic deformation through the component thickness which can also mitigate the thermal distortion issue.

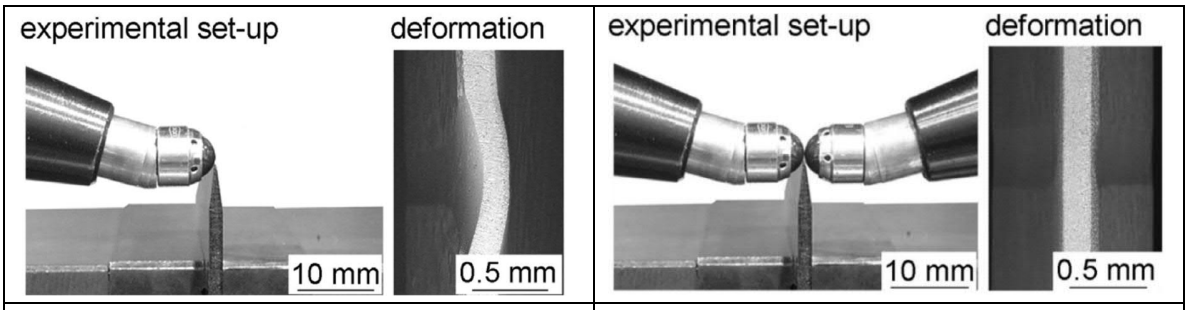

Figure 2-4: (a) conventional deep rolling and (b) double-sided deep rolling [12].

2.2 Effcet of Elevated Temperature on Residual Stresses

The surface treatments are usually performed at ambient temperature while many highly stressed components operate at elevated temperature. The experimental measurements confirm that the exposure of the deep cold rolled components to elevated temperature relaxes and redistributes the residual stress induced at the room temperature by the DCR process [3, 7, 16]. The beneficial influence of the surface treatments may, thus, decrease due the thermal relaxation of residual stresses. Stress relaxation is defined as the decrease or redistribution of residual stress because of external loading conditions. Thermal load, static over load beyond yield strength, cyclic load and crack extension are among the sources of residual stress relaxation [14, 17]. Fatigue life prediction would be inaccurate without consideration of the residual stress relaxation in the component [18].

An example of stress relaxation of deep rolled Ti64 after half the cycles to failure at ambient temperature under cyclic load of 670 MPa is shown in Figure 2-5 (a). It appears that a more uniform compressive residual stress remains in place after cycling and the maximum compressive stress level is remarkably reduced [3]. Figure 2-5 (b) displays the level of residual stress relaxation due to annealing at elevated temperature of 450°C.

The thermal relaxation of the residual stress in deep-rolled Ti64 alloy has been widely studied experimentally [3, 19-21]. The results showed that the relaxation is greater in the region closer to the surface nearly less than 50µm from the surface [3, 21] and the relaxation of the stresses on the surface layer is faster than beneath the surface which is fundamentally due to formation of high dislocation densities and nanocrystalline in the surface layer [3, 17].

The microstructure of the subsurface layer in deep rolled Ti64 has a high dislocation density which is thermally unstable [21]. While untreated Ti64 has an average α-grain size of about 10µm, after

deep rolling the nanocrystalline layer with crystallite sizes of about 50nm is created directly on the surface. The nanocrystalline layer exhibits high dislocation densities and has a complex lamellar substructure [21].

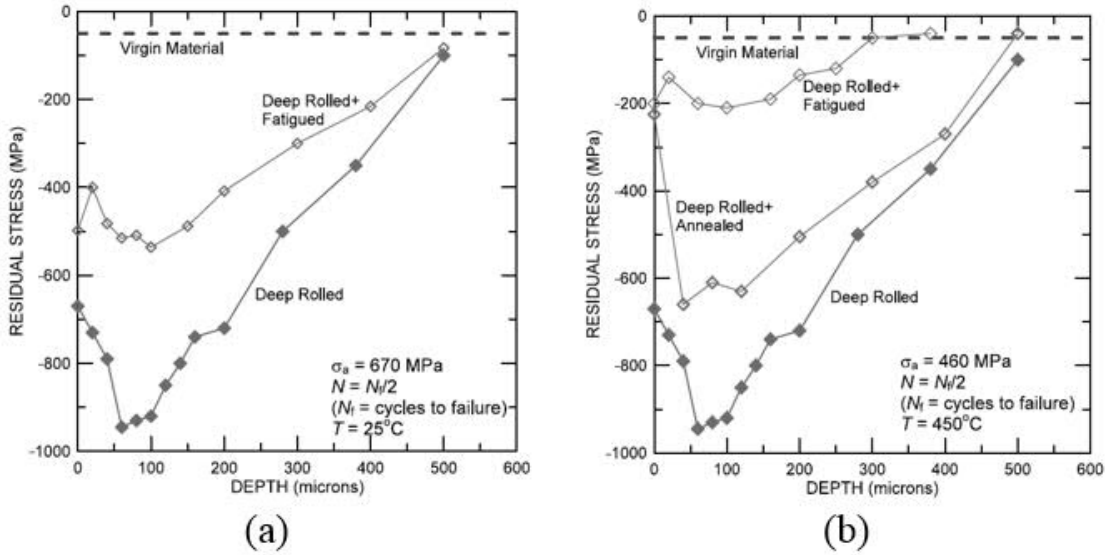

Figure 2-5: Stress relaxation of deep rolled Ti64 (a) cyclic load at 25°C (b) effect of elevated temperature and cyclic load at 450 °C [3].

Experimental investigations strongly suggest that the thermal stability of the residual stresses in the surface layer depends on the material state, and particularly on the induced dislocation density. Surface layers with medium dislocation density show enhanced thermal stability of residual stresses while surface layers with extremely high dislocation densities (as induced by shot peening and high ball burnishing pressure) have a poor thermal stability [14, 22].

The thermal relaxation of residual stress is fundamentally due to the annihilation and reorganization of meta-stable crystalline defects induced by treatment process, creep-controlled dislocation rearrangement and material softening at elevated temperatures [23]. Exposure to temperatures above 0.5 T_m (melting temperature) for several hours leads to recrystallization of the material. Recrystallization causes grain reformation which relaxes all macro residual stresses and majority of micro residual stresses. Stress relaxation at temperatures lower than 0.5 *Tm* is governed by diffusion-controlled dislocation movements, and changes from dislocation core diffusion to volume diffusion as temperature raises [17].

The initial thermal relaxation is prompt and caused by the change in the yield strength and Young's modulus at elevated temperature. Decreasing the Young's modulus leads to an elastic temporary

relaxation. Also with the temperature increase, the yield stress decreases and may be lower than the high compressive residual stresses induced at room temperature. This may result in a local plastic deformation which can cause permanent residual stress relaxation.

Zener-Wert-Avrami model is an analytical function which describes the thermal relaxation of macro residual stresses and changes of work hardening states quantitatively and it is applicable to a wide range of temperatures. The function formulates the thermal relaxation based on activation enthalpy which is roughly the enthalpy for self-diffusion. Zener-Wert-Avrami model to describe the residual stress relaxation during thermal loading can be written as [17, 18, 23]:

$$\frac{\sigma^{rs}(T,t)}{\sigma_0^{rs}} = exp\left\{-[Cexp\left(\frac{-\Delta H_A}{\kappa T}\right)t]^m\right\} \tag{2-1}$$

where $\sigma^{rs}(T,t)$ is the residual stress value after annealing at temperature T and time t. σ_0^{rs} is the initial residual stress. ΔH_A is the activation enthalpy and C is velocity constant. κ is Boltman constant and m represents material property parameter found by the experimental test.

Thermal stress relaxation is the decay of the stress due to temperature and time while the strain is constant [24]. On the other hand, creep is the time dependent plastic deformation of the material under a constant load at elevated temperature. It has been shown that the time dependent thermal relaxation can also be described by creep behaviour as shown experimentally for Ti64 [20, 24]. Correlation between time dependent plastic strains and mean residual stress are established in such approach [17].

Norton and Hyperbolic-sine function are among widely used creep laws and have been employed to describe the creep behaviour of Ti64 [20, 25]. Hyperbolic-sine creep model which has been found to be suitable for the primary creep can be described as:

$$\dot{\varepsilon}_c = A(sinhB\sigma)^n \exp(-\frac{\Delta H}{RT}) \tag{2-2}$$

where T is temperature [K]; ΔH is creep activation energy [kJ/(mol·K)]; R is gas constant, [kJ/mol]; A is material structure factor, [s^{-1}]; B is stress level factor, [MPa^{-1}]; n is stress exponent.

2.3 The Effect of DCR on Mechanical Integrity of Ti-6Al-4V

Prevéy et al. [22] showed that a deeper compressive residual stress can significantly improve foreign object damage (FOD) tolerance in Ti64. Investigation on 450 stainless steel revealed that

the compressive residual stresses can significantly improve the corrosion fatigue strength, and the level of improvement highly depends on the depth and the magnitude of the induced compressive residual stress [26].

All mechanical surface treatments influence the fatigue life through surface strengthening by inducing a high dislocation density (cold work) layer which delays crack nucleation at the surface and developing a compressive residual stress which retards micro-crack growth from the surface and slows the crack propagation rate [19, 27, 28]. Surface treatments can also have secondary effects on the fatigue strength through the surface roughness and deformation-induced phase transformations which could be beneficial if the process and associated parameters are chosen properly [19].

Since the depth and magnitude of the residual stress achieved by DCR is controllable by the process parameters and typically higher than other mechanical surface treatments, this process can be effectively utilized to improve the fatigue corrosion strength and FOD resistance of Ti64 alloys used in the gas turbine blades.

Deep rolling process is typically applied to enhance the fatigue strength of materials. The effectiveness of the deep rolling treatment highly depends on the fatigue mechanism i.e. whether it is dominated by crack initiation or crack propagation. Generally speaking, the fatigue of smooth unnotched components is mainly crack initiation controlled whereas fatigue of notched components is mainly dominated by crack propagation [6]. LPB has been applied to titanium, iron, and nickel based aero-turbine engine alloys to improve the damage tolerance, high cycle and low cycle fatigue performance of blades. The reported studies have shown that the LPB process can improve the damage tolerance of Ti64 fan blade in order of magnitude [29, 30].

The residual stresses induced by the DCR in Ti64 and its effect on improving low-cycle fatigue (LCF) and high-cycle fatigue (HCF) behavior of this alloy has been extensively investigated [2, 3, 31] . All the experimental results unanimously confirm that the process can enhance the fatigue strength of the treated specimens both at room and elevated temperatures.

Figure 2-6 demonstrates the comparison of the fatigue lives of untreated, deep-rolled, carburized, and deep-rolled carburized of Ti64 samples which has been reported by Tsuji et al. [2] . It is seen that the fatigue life of the titanium alloy is significantly improved by deep rolling process. For the fatigue lives of less than 10^5 cycles, the crack initiated from the surface and propagated toward the

interior region for all samples. However, in the long-life regimes i.e. $N_f > 10^6$ cycles, crack initiations were observed on the surface layer for both untreated and carburized samples, while in the deep-rolled samples the crack initiated from subsurface layers. This can be realized by examination of the S-N curves for deep rolled samples in which the two regions controlled by surface crack and interior crack are noticeable as shown in Figure 2-6.

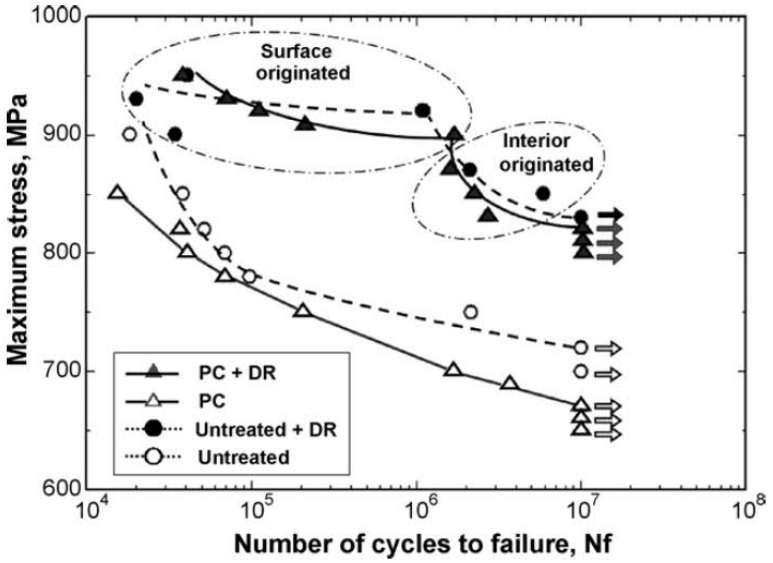

Figure 2-6: S–N curve for untreated, as-carburized (PC), deep-rolled (DR), and deep-rolled carburized (PC + DR) Ti64 samples [2].

The High Cycle Fatigue (HCF) tests conducted on Ti64 specimens at room temperature show that the deep rolling process increased the fatigue strength almost by 13% [32] and 16% [2] for R=0.1, by 20% for R=-1 [33, 34], by 25% for R=-1 [35] , and by 12.5% for R=-1 [27] in which R is the stress ratio defined as $\sigma_{min}/\sigma_{max}$.

It has been shown that the depth of the crack nucleation site can be correlated with the rolling pressure [28] as presented in Figure 2-7 (a). A sample of fractographic observations of HCF failure in deep-rolled Ti–6Al–7Nb is presented in Figure 2-7 (b). Fractographic observations showed that the HCF crack nucleation in deep rolled Ti64 specimens occurs in regions of peak tensile residual stresses under the surface, where tensile residual stresses balance the outer compressive stress field [27, 28, 32-34, 36].

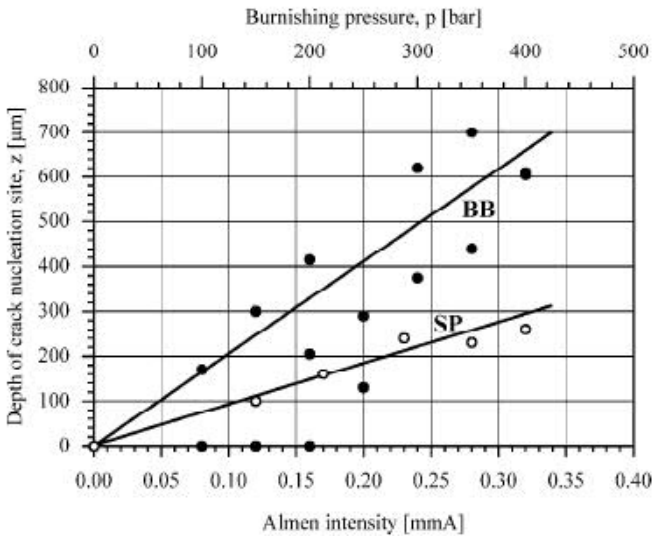

(a)

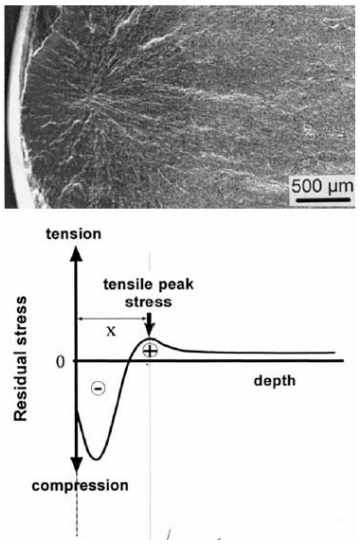

(b)

Figure 2-7: (a) Depth of crack nuclition site in deep-rooled and shot-peened Ti64 [28], and (b) Subsurface fatigue crack nucleation in deep-rolled Ti–6Al–7Nb [36]

Fatigue behavior of Ti64 also shows Anomalous Mean stress Sensitivities (AMSS) that a low mean tensile stress can lead to severe losses in HCF strength [37]. Therefore, none of the conventional life approaches such as Goodman, Soderberg, and Gerber parabola relationship is able to predict the fatigue life of untreated Ti64 [37-39] and as a result to explain the effect of the deep rolling on HCF of Ti64.

Comparing the fatigue properties of untreated and deep-rolled Ti64 as presented in Figure 2-8 (a) shows that the fatigue life improvement is not limited to HCF regime, and the process can also have beneficial effect on the LCF at room temperature and at elevated temperatures [2, 3] . Even though it is generally considered that mechanical surface treatment enhances the fatigue life primarily by mitigating the initiation of cracks, deep rolling has an additional positive influence on fatigue properties by lowering the initial fatigue-crack growth rates, typically by a factor of 2-3 for Ti64, compared with the untreated material [3]. Figure 2-8 (b) also shows the plastic strain amplitude versus the number of cycles during fatigue testing of untreated, deep-rolled and laser shock peened Ti64 at 450 °C. An initial cyclic softening followed by cyclic hardening in the plastic strain amplitude was observed in all three cases [3, 8]. Compared with the untreated material, DCR lowers the plastic strain amplitude throughout the majority of the lifetime for a given applied stress. Such a plastic strain reduction significantly extends the fatigue life of the treated component.

Hence, the plastic strain amplitude can be a reliable measure to describe the extent of accumulated 'damage' during the fatigue of ductile materials [3].

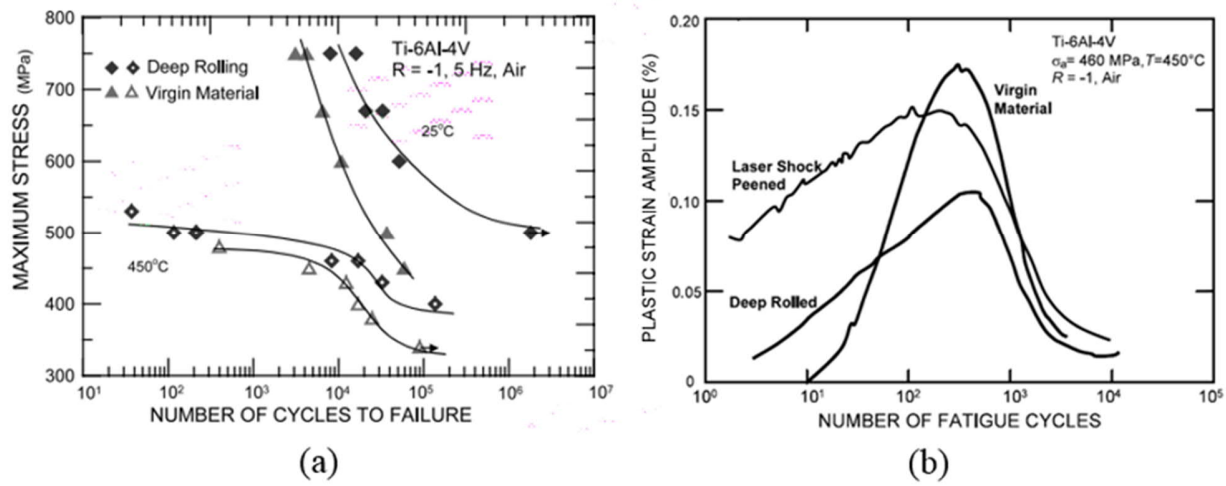

Figure 2-8:(a) Stress/life (S/N) data obtained at 25 and 450 °C for the virgin and deep-rolled Ti–6Al–4V material and (b) Plastic strain amplitudes for the virgin, deep-rolled and laser shock peened Ti–6Al–4V [3].

Nalla et. al. [3] studied the effect of DR process on the LCF and HCF behavior of Ti64 alloy at room and elevated temperatures. The thermal and mechanical stability of the induced residual stresses and near-surface microstructures were investigated. The results showed that despite the relaxation of the near-surface residual stresses, deep rolling effectively retards the initiation and initial propagation of fatigue cracks in Ti64 at elevated temperature up to 450°C (~0.4T/Tm). The effect of strain hardening on the fatigue life is more remarkable at high temperatures, where the noticeable relaxation of RS is observed while the strain hardening is barely influenced [3].

In addition to the crack closure due to compressive residual stresses, changes of local plastic deformation and local yield stress because of cyclic hardening contribute to the fatigue life improvement by lowering the fatigue crack growth rate [25]. The micro structure investigation of deep-rolled Ti64 also shows a layer of work hardened nanoscale grains which plays a critical role in the enhancement of fatigue life in the absence of residual stresses at elevated temperatures [3]. This layer restricts or impedes dislocation slip and the formation of slip bands at the surface. The thickness of the nanocrystalline layer in deep-rolled Ti64 is determined by the deep rolling parameters (rolling pressure and coverage) [21].

In a comprehensive study, Altenberger et al. [8] investigated the fatigue behavior of deep-rolled and laser-shock peened and untreated Ti–6Al–4V in the regime of 10^2-10^6 cycles under fully reversed stress-controlled isothermal push–pull ($R = -1$) loading in temperature range between 25°C and 550 °C. As it is shown in Figure 2-9, deep rolling process can improve the fatigue lives significantly at temperatures as high as 550°C while fatigue enhancement was observed to be much more pronounced at low temperature levels. Their results also show that the LCF-regime of both the untreated and deep-rolled Ti–6Al–4V alloys can be well explained by Manson-Coffin relation which describes plastic strain amplitude as a function of the number of cycles to failure.

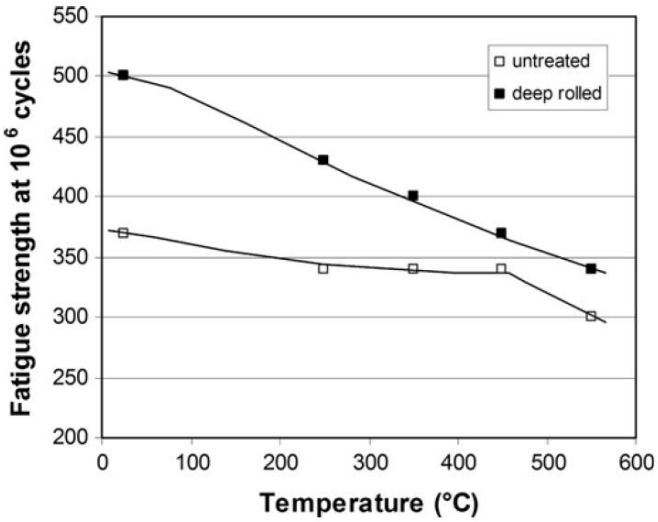

Figure 2-9: Fatigue strength of untreated and deep-rolled Ti–6Al–4V as a function of test temperature at 10^6 cycles to failure [8]

From above, it can be concluded that while DCR can enhance LCF life by introducing a deep compressive residual stress in the surface layer; if the process parameters are not selected appropriately, it may have a detrimental secondary effect on HCF life due to sub-surface cracking caused by balancing tensile residual stresses.

2.4 Finite Element Prediction of Residual Stresses Induced by DCR Process

The residual stress generated in the workpiece during the DCR process is the result of a complex cyclic plastic deformation and microstructural textural evolution occurring in the surface layer. The process is a complex nonlinear dynamic phenomenon due to the movement of the ball, the presence of plasticity beneath the rolling ball and nonlinear contact between the ball and the component. Although the closed form (analytical) solutions with a certain level of accuracy exist

for elastic rolling contact, application of semi-analytical methods and finite element (FE) methods are inevitable for the elastic-plastic rolling contact problems. The apparent shortcoming of semi-analytical methods are the inherited inaccuracies in solving large plastic deformation especially under highly nonlinear contact conditions and their limitations to two-dimensional rolling contact problems [13].

The correlations between the induced residual stresses and process parameters have been mostly determined empirically by cumbersome, time and cost expensive experiments. However, the applicability of empirical models is limited to the considered process parameters in a given experiment. Finite Element (FE) analysis has been proposed as an effective and cost reducing alternative to experimental and analytical methods. Although FE method has shown some promises to predict the correlation between the rolling process parameters and the induced residual stress, careful experimental study is still required for validation of the FE models.

In this section a systematic literature review is presented to cover the research background on finite element (FE) modeling of the DCR process and to identify the research gap. The governing equations to be solved by FE methods, FE techniques and material constitutive models are briefly explained. The most relevant research work with emphasise on predicting residual stresses are then presented with pertinent details. Where possible, the accuracy of the models is compared with the related experimental measurements. Establishing the knowledge and techniques to build a reliable FE model to predict residual stresses is the main objective of the current literature survey.

2.4.1 Solution of Governing Equations using Explicit and Implicit Methods

The final governing equations in the finite element format at a specific instant of time may be describes as:

$$M\ddot{u} + Ku - F = 0 \tag{2-3}$$

where M and K represent mass and stiffness matrixes, respectively. F is external forces vectors, u and $\ddot{u}$ are the nodal displacement and acceleration vectors, respectively. Direct integration methods are used in ABAQUS to solve time history analysis and are generally categorized into explicit and implicit methods.

2.4.1.1 Explicit Method

The central difference time integration algorithm is mainly used in ABQUS/Explicit [40] to integrate through time by using many small time increments. In direct integration method, the governing equations of motion as stated in Eq. (2-3) is generally written at specific instant of time as:

$$M\ddot{u}_n + Ku_n - F_n = 0 \tag{2-4}$$

where the subscript n represents time $n\Delta t$ in which Δt is the time step (size of time increment), $\ddot{u}_n$, u_n and F_n are respectively nodal acceleration, displacement and external force vectors, at time $n\Delta t$. Ignoring the effect of damping, the internal force vector can also be described using the system stiffness matrix, as $I_n = K\, u_n$ in which the stiffness matrix is also function of current nodal displacement vector, u_n , which should be updated at each iteration. The explicit central difference integration method is then employed to update the velocity and acceleration vector at time $n\Delta t$ as:

$$\dot{u}_n = \frac{1}{2\,\Delta t}(u_{n+1} - u_{n-1}) \tag{2-5}$$

$$\ddot{u}_n = \frac{1}{\Delta t^2}(u_{n+1} - 2u_n + u_{n-1}) \tag{2-6}$$

It is noted that above equation can be easily obtained by expanding displacement vectors at time $n+1$ and $n-1$ (u_{n+1} and u_{n-1}) using Taylor series about time $n\Delta t$ and truncate it up to the second order. Thus the central difference method is second-order accurate. Substituting Eq. (2-6) into Eq. (2-4) yields:

$$\left[\frac{1}{\Delta t^2}M\right]u_{n+1} = F_t - \left[K - \frac{2}{\Delta t^2}M\right]u_{n+1} - \left[\frac{1}{\Delta t^2}M\right]u_{n-1} \tag{2-7}$$

From which we can solve for u_{n+1}. It should be noted that the solution of u_{n+1} is thus based on using the equilibrium conditions at time n and $n-1$. For this reason, the integration procedure is called an explicit integration method as it permits u_{n+1} to be determined using the complete historical information of displacement vector at time $n\Delta t$ and before [41]. It is noted using Taylor series that, $\dot{u}_{-1} = u_0 - \Delta t\, \dot{u}_0$ in which u_0 and $\dot{u}_0$ are known initial velocity and displacement vectors. Eq. (2-7) is conditionally stable and the time increment must be smaller than the time required for a dilatational wave to cross any element in the mesh which is estimated as [40]:

$$\Delta t \leq \frac{L_{\min}}{\sqrt{E/\rho}} \tag{2-8}$$

In which L_{min} is the smallest element dimension in the FE model and ρ and E are the density and Young modulus of the material, respectively. Therefore the size of the smallest element in the FE model dominates the stable time increments. Although the time increments are typically very small compared to the cycle time of forming processes, the computation time for each time increment in the explicit procedure is very short because the solution requires no iterations.

The explicit method could be computationally very expensive for quasi-static problems such as metal forming processes because it requires a long-time solution and needs very small elements in the contact zone due to a high level of nonlinearity. The run time of dynamic explicit program can be further reduced by artificially increasing the forming rate (time scaling) or artificially increasing the density of the elements (mass scaling technique). However, the solution accuracy can be compromised because of the introduction of unrealistic dynamic effects if proper care is not considered using these techniques. In the following, time and mass scaling are briefly described.

Time scaling

The number of increments required to simulate an event with time period of, T, is given by $n=T/\Delta t$ in which the minimum time increment, Δt , is given by Eq. (2-8) at each time step. It is noted that the time increment is not constant as the element distortion and also nonlinear material response cause L_{min} and young modulus to change, respectively [40].

Time scaling is a technique in which the time period of the event, T, is artificially reduced compared with the actual time of the process, thus decreasing the number of required increments. However, time scaling if not applied carefully can substantially change the rate of the applied load which may generate erroneous results [40]. Speeding up the simulation too much, will increase inertia forces that can change the predicted response. For example, very large time scaling can cause unreal wave propagation in system which is far away from the actual dynamic response. Therefore, large time scaling should be avoided to control this numerical error.

Moreover other aspects of the problem may also be rate dependent and as a result sensitive to the rate of the loading. For instance, the material behaviour is typically strain rate dependent and

changing the rate of the applied load by time scaling may result in a different stress state in the material.

Mass scaling

Increasing the critical time increment in explicit simulations can effectively reduce the computation time significantly. According to Eq. (2-8) , by artificially increasing the material density, ρ, by a factor f^2, the minimum time increment can be increased by a factor of f which proportionally reduces the simulation time. This concept is called mass scaling. The "mass scaling" can be physically expressed as the reducing the ratio of the event time to the time for wave propagation across an element while leaving the event time fixed. One of the advantages of the mass scaling concept is the possibility to include rate-dependent behaviour in the analysis. The effects of the mass scaling and time scaling on inertia forces are identical which must be monitored during the analysis [40]. In practice the mass scaling is applied only on a small part of the model where the inertia forces can be neglected due to small mass [9].

2.4.1.2 Implicit method

Most implicit numerical procedures are usually unconditionally stable direct integration techniques which do not require any restriction on the time step size such as that in Eq. (2-8) for the explicit central difference method. Newmark family of methods are the most popular and widely used implicit methods [41] as they can provide artificial damping that can effectively dissipate high-frequency numerical noise while not affecting the low frequency responses. These methods have replaced Houbolt method which once was commonly used in general purpose transient codes but now has been obsolete due to introduction of high level of artificial damping for low-frequency response. It is noted that that the ABAQUS/Standard utilizes the implicit solver for time integration of the dynamic problem using the backward Euler operator and a generalized form of Newmark method. The method implements a controllable numerical damping to provide automatic dissipation of high-frequency numerical noise while not affecting dominant low-frequency response and allows the numerical stability and automation of time stepping scheme [40]. The Newmark methods calculate the nodal displacement and velocity as follows [41]:

$$u_{n+1} = u_n + \Delta t\, \dot{u}_n + \Delta t^2 \left(\left(\frac{1}{2} - \beta \right) \ddot{u}_n + \beta\, \ddot{u}_{n+1} \right) \tag{2-9}$$

$$\dot{u}_{n+1} = \dot{u}_n + \Delta t\big((1-\gamma) + \gamma\, \ddot{u}_{n+1}\big) \tag{2-10}$$

with

$$\beta = \tfrac{1}{4}(1-\alpha)^2,\ \ \gamma = \tfrac{1}{2} - \alpha \ \text{ and } -\tfrac{1}{2} \le \alpha \le 0. \tag{2-11}$$

where α and β are control stability parameters and are chosen so that the method to be unconditionally stable. For $\gamma > 0.5,\ (\alpha < 0)$ and $\beta = \frac{1}{4}(1-\alpha)^2$, the Newmark method maximizes the dissipation of the high-frequency noises while retaining the response accuracy to first order [41] . A large system of equations is solved repeatedly at each time step to obtain the displacement field. As it can be realized from Eq. (2-9), the displacement field at the step *n*+1 depends also on the acceleration on the step *n*+1 demonstrating the implicit nature of the method.

As mentioned before, the DCR process is a highly nonlinear dynamic phenomenon in which the nonlinearity is mainly due to the geometric and material nonlinearity as well as contact between the rolling ball and the workpiece. The nonlinearity translates itself into variable stiffness matrix which depends on current nodal displacement vector. Thus at each time step in nonlinear dynamic problems, an iterative procedure requires to obtain the nodal displacement vector which generally accomplished using the Newton Raphson method. This besides the iterative nature of time steps for dynamic analysis makes simulation of DCR process highly computationally expensive for the implicit solvers.

Although there is no restriction on time step size in the implicit method, it should be generally kept small to fulfill equilibrium after each incremental step and for accuracy. In a complex problem with rapidly changing contact conditions like DCR, implicit codes are computationally very expensive because of huge number of iterations required to satisfy the equilibrium at each time increment. In contrast to the implicit solver that each increment typically requires several iterations to obtain a solution within a defined tolerance error, employing small time increments in explicit solver allows the solution to proceed without iteration and forming tangent stiffness matrices in each time increment which significantly simplifies the treatment of contact problems.

2.4.2 Material Models

The accuracy of the FE model to predict the residual stresses significantly depends on the reliability of the constitutive model used to describe cyclic inelastic behaviour of the material [42].

The calculated rolling contact stress and the components of the residual stress and strain are significantly influenced by the assumed plasticity model for the workpiece in the FE model. For example, the linear kinematic hardening plasticity model produces much smaller deformation and residual stress compared to the elastic–perfectly plastic material model under the same rolling condition [43], while the difference between the results obtained from isotropic hardening plasticity model and linear kinematic hardening plasticity model is negligible [44].

Although kinematic hardening models are more comprehensive in modeling material plasticity behavior than isotropic hardening model, they can lead to over estimating the level of residual stress after deformation if the modelling of the yield stress evolution during a cyclic loading is not precise enough [45]. Since strains are greater than 10% in metal forming simulations, the isotropic strain hardening is sufficient enough to model the deformation. Nevertheless, in case of small cold deformation and cyclic loading, the kinematic hardening effects needs to be considered in the FE model [45].

For the simulation of multi-pass surface rolling process, the material model should be able to demonstrate work-hardening effect as a result of plastic deformation, strain rate hardening effect caused by rate of the loading, as well as the cyclic deformation behaviour at ambient temperature [5]. Available material models which can be effectively used in deep rolling processes include Lemaitre-Chaboche-Plasticity (LCP) and Johnson-Cook (JC) models. These models are briefly described in the following.

Lemaitre-Chaboche-Plasticity (LCP) model

The LCP model is a combined isotropic/kinematic strain hardening law. The translation of the yield surface in stress space through back stress is described by the kinematic hardening component. The isotropic hardening component defines the change of the equivalent stress with the size of the yield surface as a function of plastic strain. The LCP model can be expressed as [46]:

$$f = \sigma_e(\boldsymbol{\sigma}, \boldsymbol{X}) - R(\varepsilon_p)$$

$$R(\varepsilon_p) = Y + R_{sat}(1 - e^{-C_r \varepsilon_p}) \tag{2-12}$$

$$d\boldsymbol{X} = C_x X_{sat} d\varepsilon_p - C_x \boldsymbol{X} d\varepsilon_p$$

where $\sigma_e(\sigma, X)$ is the equivalent stress, ε_p is the equivalent plastic strain, $\boldsymbol{X}$ represents the back stress, $R(\varepsilon_p)$ is the isotropic hardening stress. Y, R_{sat} and C_r represent the yield stress, the material parameters for the isotropic hardening model representing the critical stress and work hardening ratio, respectively. X_{sat} and C_x are the material parameters for the kinematic hardening model. The model becomes the kinematic hardening model when $R_{sat} = 0$ and it is equivalent to the isotropic hardening model when $X_{sat} = 0$.

Johnson-Cook (JC) model

The JC model is purely empirical and its ability to adequately represent the deformation and failure of Ti64 under high-rate loading, large plastic strain rate and high temperature has been verified [47]. The model can be described as:

$$\sigma = [A + B\varepsilon^n][1 + Cln\dot{\varepsilon}^*]\left[1 - \left(\frac{T - 298}{T_m - 298}\right)^m\right] \quad (2\text{-}13)$$

where σ and ε are the effective stress and strain respectively, $\dot{\varepsilon}^*$is the normalized effective plastic strain rate, n is the work hardening exponent and A, B, C, and m are constants which are determined from an empirical fit of flow stress data . T_m represents the melting temperature.

It should be noted that JC model parameters are evaluated using many experimental tests at different strain rates and temperature levels. JC model provided in Eq. (2-13) has three distinct parts (inside brackets) which explicitly relate the effective stress to strain, strain rate and temperature, respectively. The parameters A, B and n are typically evaluated using quasi-static tests or dynamic tests at very low strain rare. Once these parameters are identified, then parameters C and m which respectively describe the strain-rate and temperature dependent part of JC model are identified using series of dynamic tests at various controlled strain rates and temperatures. This can be conducted using apparatus such as Split-Hopkinson Bars or Tayler Impact Test.

The JC model has been extensively used to describe the material behavior in the simulation of cold rolling processes [48] and has been particularly studied to describe the Ti64 strain hardening behaviour under various temperature and strain rates [49, 50]. Therefore, the JC constitutive material model has been considered to model the stress-strain behaviour of Ti64 alloy in this study. Numerous sets of JC model parameters exist for Ti64 in the literature [49, 50] where each set of material constants has been identified based on the measured plastic strain and strain rates in a

specific range of temperatures. The assumed JC model for the simulation of the DCR process should cover the largest strain and strain rate typically generated during the process.

2.5 Literature Review on FE Simulation of DCR

Here a comprehensive literature review on the pertinent attempts to model DR process using 2D and 3D FE models are presented. Wherever available, the accuracy of each FE model is compared to correlated experimental measurements. Table (2-1) summarizes the detail of the models and their level of accuracy. WebPlotDigitizer [51] which is a free source online application was used to extract numerical data from plot images presented in the literatures for the sake of comparison. Despite the best attempts, the data extraction process may contain some levels of inaccuracy.

The residual stress (RS) in the rolling direction (axial) is considerably lower than the stress component perpendicular to the rolling direction (tangential). Also residual stress measurement techniques are more or less inefficient in measuring the residual stress in curved directions [52], therefore only RS profiles in the tangential direction are compared here and important remarks are presented.

Zhuang and Wicks [42] simulated multi-pass DCR process for IN718 coupons in ABAQUS/Explicit using a non-linear isotropic/ kinematic hardening constitutive model for the material and then compared the predicted residual stresses with experimental data. Comparison of residual stresses obtained using FE method and experiments shows that the developed FE model was not accurate enough to predict the residual stresses especially in the surface layer. The discrepancy of the results at the surface layer was related to probable existence of initial residual stresses caused by machining in surface layer of the specimen prior to DCR process.

Klocke et al. [53] had successfully developed a 3D FE model to simulate the deep rolling process on several geometries representing typical shapes of turbine blade and turbine disk components. Ti64 and IN718; the two widely used materials in aerospace industry, were considered in their study. Their study clearly demonstrated that the residual stress distributions in plane geometry and thin-walled geometries are significantly different. While the process affects plane geometry only in the neighborhood of the processed surface, thin walled geometries are affected over their complete thickness.

Klocke et al. [11] used 3D finite element models to investigate the influence of ball diameter, rolling pressure, feed and specimen thickness on the surface layer state after roller burnishing of IN718. It was found that the component thickness has a very significant impact on the residual stress distribution and particularly at the surface layer as it can change from compressive to tensile stresses with decreasing thickness. The impact was observed to be more significant at higher rolling pressure as resulted in higher tensile residual stresses. Therefore, optimal selection of the process parameters is more critical in thin-walled component as such tensile residual stresses on the surface can negatively impact the fatigue strength of the treated components. Their results also show that a deeper residual stress can be achieved by increasing the rolling pressure. However, they observed that there is a saturation point where increasing the rolling pressure does not change the residual stress profile significantly.

Bäcker et al. [4] proposed coupling of the FE method with Boundary Element (BE) method to simulate DCR process on a Ti64 turbine blade in order to predict the induced residual stress. It is mentioned that, the coupling between FE and BE methods can only be adopted by implicit solvers. FE was used locally for precise prediction of the residual stress field in a sub-model of the blade where the ball and specimen interact, while the global deformation of the global blade geometry was evaluated by BE. The simulations demonstrated the feasibility of the proposed coupling methods despite the discrepancy with the experimental measurement.

Klocke et al. [12] developed a 3D FE model considering a user defined isotropic hardening model to predict residual stress in Ti64 alloy. The developed model underestimates residual stress in the surface layer by more than 50%.

Liu et al. [5] developed a three-dimensional finite element model in ABAQUS/Explicit to predict the surface deformation, stress and strain in Ti64 cylinder with a radius of 40 mm and thickness of 16 mm under ultrasonic surface rolling (USRP). In USRP, ultrasonic vibration and static force are simultaneously applied on the work piece to generate residual compressive stress in the surface layers. The results predicted by explicit FE model were in a good agreement with the measured values.

Ali and Pan [54] compared residual stresses induced by cold rolling process in a plate by a rigid and elastic deformable roller using 2D plane strain FE model. The plastic behavior was modeled by nonlinear kinematic hardening rule. Results showed that the residual stress profiles are almost

the same for both kind of roller models. Therefore, a rigid ball can be used in the simulation of the process in order to reduce the computation time without compromising the accuracy.

In 2013, Balland et al. [55, 56] concluded that previous numerical studies on burnishing process had not been very successful in describing the effect of the process on surface hardening, mainly due to assumptions been made in previous research works . Three remarkable conclusions can be outlined based on their results: 1) The residual stress profile evolves gradually by increasing the number of rolling passes. 2) A minimum number of rolling passes is required to obtain a stabilized residual stress field. 3) The magnitude of the overlap between the rolling passes has a great effect on the final residual stress state.

Sayahi et al. [57] simulated the deep rolling process on Ti-6Al-7Nb components using 2D and 3D FE models and compared the simulation and experimental results. The developed 3D FE models provided results with a good agreement with experimental measurements although unable to predict the magnitude of residual stress on the surface. The authors concluded that the 2D FE models only provide a very qualitative description of the RS profile and do not yield accurate quantitative results.

The residual stresses of cold rolling process on cylindrical specimens made of IN718, 42CrMo4 and GGG60 materials have also been predicted with ABAQUS/Explicit and validated to experimental results [1]. Based on the numerical results obtained from the validated FE models and using similarity mechanics, a set of equations was derived to approximate the residual stress profile with respect to the depth from the surface layer.

Mohammadi et al. [9] employed ABAQUS/Explicit to simulate LPB process on a half-space Ti64 specimen. The residual stress of an elastic-plastic half space was calculated by a 3D explicit model and compared to results of 2D implicit model cited by Fischer-Cripps [58]. However, the number of rolling passes was considered as a design variable and the reference lacked validation to experimental measurements.

Lim et al [59] simulated DCR process on Ti64 plate using a 3D FE model in order to investigate the residual stress distribution at the boundary between the treated and untreated zone on the surface of the component. The results of the FE model in the treated zone wre compared with experimental measurements which showed significant disagreement particularly at the near to the surface area. The limitation of the residual stress measurement method at the surface layer area

was stated as a potential source of the discrepancy. They used the net material movement to explain the induced plastic deformation and the resultant residual stress.

Table 2-1: Summary of articles on FE simulations of deep rolling and their level of accuracy in comparison with experimental results

Reference	FE Model	Material	Material model	Error %			
				σ_0	σ_{min}	Y_{min}	Y_o
Guagliano (1998) [60]	3D Implicit	40CrMo4 steel	isotropic hardening	58	41	100	-
Jiang (2002) [61]	3D Implicit	AISI 1070 steel	LCP model	No validation was performed.			
Courtin (2003) [62]	2D and 3D static	Cast Iron	elastic perfectly plastic	-24	-22	∞	7
Zhuang (2004) [42]	3D Implicit	IN718	isotropic/kinematic hardening	38	31	22	12
Guo (2004) [43]	2D Implicit	AISI 52100	nonlinear isotropic hardening	RS profiles from experiment and FE don't agree to be compared.			
Saï (2005) [63]	3D Static	AISI 1042	isotropic hardening	No validation was performed.[1]			
Yen (2005) [64]	2D & 3D Implicit	AlSl 52100	linear elastic-plastic	The data were not readable to compare.			
Demurger (2006) [45]	3D Implicit	23MnCrMo5	LCP model	305	123	100	-
Partchapol (2007) [65]	2D & 3D Implicit	AISI 52100	isotropic hardening	-247	29	245	33
Manouchehrifar (2009)[66]	3D Explicit	Ti64	JC	The comparison is not valid. [2]			
Klocke (2009) [53]	3D Explicit	Ti64 and IN718 [3]	isotropic/kinematic hardening	38	10	7	17
Li (2010) [67]	3D Explicit	IN718	JC	72	18	79	8
Bäker (2010) [4]	3D Implicit	Ti64	isotropic/kinematic hardening	-16	10	32	∞
Bougharriou (2010) [68]	3D Static 2D Implicit	AISI 1042	kinematic hardening	54	54	0	75
Majzoobi (2010) [69]	3D Explicit	AISI 4340	JC	No validation was performed.			
Klocke (2011) [12]	3D Implicit	Ti64[4]	isotropic/kinematic hardening	63	32	46	12
Niţu (2011) [48]	3D Explicit	AISI 1015 steel	JC	Forces and micro-hardness measurements were used for comparison.			

Table 2-1: Summary of articles on FE simulations of deep rolling and their level of accuracy in comparison with experimental results

Reference	FE Model	Material	Material model	Error %			
				σ_0	σ_{min}	Y_{min}	Y_o
Fu (2012) [70]	3D Explicit	Nitinol	user defined	Deformation and track shape were used for comoarison.			
Mohammadi (2013) [9]	3D Explicit	Ti64	JC	No comparison was done.			
Sayahi (2013) [57]	3D Explicit	Ti-6Al-7Nb	isotropic hardening	50	5	51	7
Balland (2013) [55]	3D Implicit	11SMn30 steel	isotropic hardening	No validation was performed.			
Bougharriou (2013) [71]	2D Implicit	AISI 1042	isotropic hardening	30	30	0	50 7
Trauth (2013) [1]	3D Explicit	IN718 42CrMo4 GGG60	LCP model	Results were not available in the article.			
Liou (2014) [72]	3D Explicit	Ti64	JC	The FE model was not validated with experiments.			
Perenda (2015) [73]	3D Explicit	TORKA steel	LCP model	8	10	-	9
Perenda (2015) [74]	3D Explicit	Torka steel	LCP	No validation was performed.[5]			
Lim (2015) [59]	3D Implicit	Ti64	isotropic hardening	40	43	0	-8
Majzoobi (2016) [52]	3D Explicit	Al7075	LCP	1	17	2	13

[1] The authors mentioned that the residual stress calculated by the model level is very low compared to experimental values.
[2] FEM results of 0.9 mm ball were compared to experimental results of 6mm ball.
[3]Only the results of Ti64 has been presented in the article. The calculated error is for the plain plate.
[4] The best numerical result in terms of agreement with to experiments was considered.
[5] RS distributions were not provided in the article. But most likely the calculated errors for [73] are applicable.

The main findings that can be summarized from above investigation on the pertinent literature in the field can be described as: 1) The rolling process should be simulated by a 3D FE model since nature of the rolling contact is three dimensional and no symmetry can be found in order to reduce it to a 2D problem [61]; 2) The influence of DR on the workpiece is highly localized so the effect of surface curvature and the resultant helical rolling path is negligible in modeling of DR on

cylindrical workpiece [64, 65]. Therefore, it is possible to model the DR on a flat plate without sacrificing the accuracy.

It has been reported that the effect of friction coefficient on the simulation is negligible as long as the friction is nonzero as any level of friction will allow the ball to be in a pure rotating state of motion [59]. The pressurized fluid acts as coolant and lubricant in the process so the process is assumed to be isothermal [65], and for the interaction between the workpiece and ball a frictional coefficient between 10^{-5} and 5×10^{-3} is generally considered using isotropic Coulomb friction model [67]. Numerical investigations showed that increasing the friction coefficient decreases the maximum residual stress and for a friction coefficient higher than 0.1, the effect of friction can cause instability of the residual stress profile [66].

X-Ray Diffraction (XRD) has been widely utilized as an effective method to measure the residual stresses. In XRD, lattice spacing variation is measured using Bragg law and compared to a strain-free reference specimen to calculate residual stress and strains. XRD involves material layer removal which causes inevitable relaxation and redistribution of the initial residual stress profile and requires corrections in the measurement. Figure 2-10 shows the residuals stress distribution with and without correction to account for XRD layer removal in a 1070 steel shaft [75]. As presented in Figure 2-10, the measurement error increases with the depth from the surface if the correction for layer removal is not considered in the process. Additionally, measuring tensile residual stresses beneath the surface using XRD method is not possible due to this layer removal approach. The equilibrium of forces between the tensile region and compressive region must be maintained in each step and due to layer removal the compressive region either reduces or does not exist [25]. Also residual stress measurement techniques are more or less inefficient in measuring the residual stress in curved directions [52].

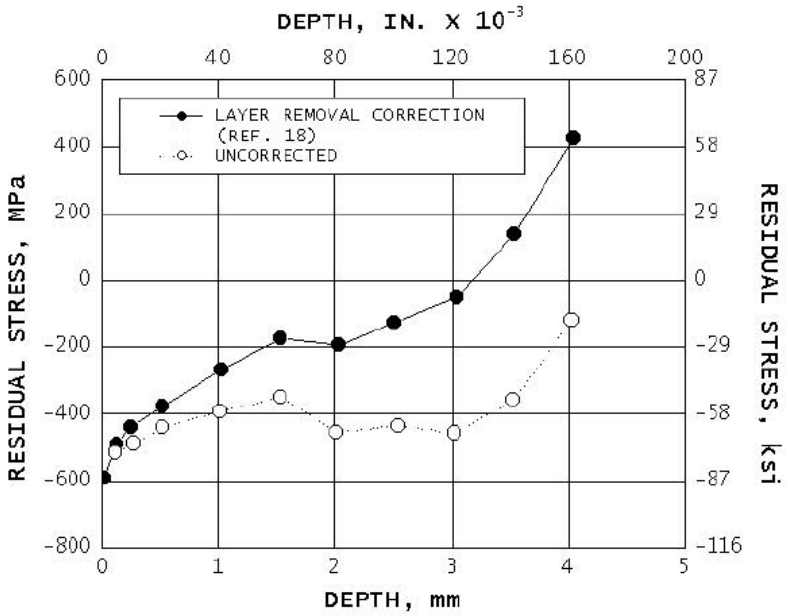

Figure 2-10: residual stress distribution with and without correction for XRD layer removal in ST1070 shaft [75]

The comprehensive literature review conducted for the current research work revealed that the available published numerical studies are mainly limited to simulation of the process to predict the induced residual stresses at the ambient temperature. There is limited number of models that can generally predict the residual stress profile with reasonable accuracy. While these models can certainly provide a fundamental understanding on the mechanism of DCR, they are not accurate enough to account for the effect of residual stresses on the fatigue life. Particularly, the accuracy of the previous numerical FE results especially in the region near to the surface layer is not sufficient enough compared with correlated available experimental data. Most importantly, they have not addressed further relaxation of the induced residual stresses under specific thermo-mechanical environments, while majority of highly stressed components treated by DCR process operate at elevated temperature where beneficial influence of the surface treatments may decrease due to the thermal relaxation of compressive residual stresses at such temperatures. In addition, a non-uniform relaxation of the induced compressive residual stress in thin-walled components can also cause shape distortion and warping in addition to the direct effect of thermal relaxation which is reduction in the amount of compressive residual stress. If the section thickness of the treated component is in the order of the depth of the compressive layer, the distortion could be more severe [14]. This can be a serious concern in surface treatment of thin turbine blades which any minor

distortion from aerodynamic shape can potentially affect the engine performance and efficiency. Therefore, it is important to investigate and accurately assess the thermal relaxation of the induced residual stresses in such cases.

Despite experimental studies; to the best of the author's knowledge, there is no prior published work detailing the modeling of the thermal relaxation of residual stresses in deep-rolled of Ti64 alloy with a systematic validation with the experimental results. One of the main objectives of the current study is to develop reliable high-fidelity FE models and simulation codes for predicting residual stresses associated with the DCR process and the following thermal relaxation at elevated temperature of 450˚C.

2.6 Regression Analysis and Optimization Studies

The experimental results show that the affected depth of the surface treatment (i,e, the depth of compressive residual stresses and strain hardening) has a significant effect on the fatigue enhancement of the treated component [3]. It was discussed that the profile of induced residual stresses can be controlled by the process parameters namely ball diameter, feed, rolling pressure and the ball rolling velocity. Therefore, it is necessary to understand the correlation between each key process parameters and the residual stress profile.

It has been mentioned that the main goal of the DCR is to mainly increase the fatigue strength of a given component. In practice the desirable results can be achieved by optimization of the process parameters. Comprehensive experimental studies performed on 2024 Al confirms that there is an optimum value of rolling force which maximizes the fatigue life. After reaching the maximum, any further increase of rolling force will have a debit on the fatigue life. [36]. Generally too low rolling forces have no noticeable effect on the fatigue behavior and in contrast too high forces may even deteriorate the fatigue behavior of the component [6]. Increasing the rolling force can increase the compressive residual stresses up to a saturation limit. Beyond the saturation level, while further increasing the force induces a deeper compressive residual stress into the component, it leads to tensile residual stresses on the surface [6].

It can be realized that a careless application of the process can damage the surface and consequently reduce the fatigue life of the component by introducing surface cracks or opening the existing ones, and creating tensile residual stress in the surface layer of the component. To avoid any undesirable outcome from the process, it is necessary to determine the correlation

between the residual stress profile and key parameters of the DCR process; and then identify process parameters to induce an optimal residual stress profile in the component surface layer.

There have been several experimental studies to investigate the impact of the DCR process parameters on the induced residual stress profile and the surface finish [10, 76-79] where the impact of each design variable and their interactions on measured output variables were systematically studied using Design of Experiment (DoE) techniques. The results have confirmed that DCR is a complex process and each parameter has a different level of interactions on the final state of the surface roughness and induced residual stress profile.

DoE generally refers to a collection of statistical techniques that maximizes the knowledge gained from minimum number of experiments (simulations) by identifying the best positions of the design points in a defined design space [80, 81]. Due to cost associated with experimental studies, it is not possible to explore a large design space and systematically explore the effect of tool and process parameters simultaneously and therefore the experiments are performed at the intelligently selected design points.

El-Axir [10] implemented Box and Hunter DoE technique to experimentally investigate the influence of roller burnishing process parameters (namely, burnishing speed, force, feed, and number of passes) on residual stress profile and surface roughness of ST 37 samples. Prabhu et al. [77] used fractional factorial DoE to study the influence of main process parameters on the surface roughness and the hardness of AISI 4140 steel for both LPB and DCR process. Burnishing force, feed rate, number of tool passes/overruns, initial roughness of the work piece, ball material, ball diameter and lubricant were considered as the input variables in the study.

Loh et al. [76] experimentally explored the effect of depth of indentation, feed, ball material, burnishing speed and lubricant on the surface roughness of AISI 1045 specimen in ball burnishing process using a full factorial DoE . Seemikeri et al. [78] studied the effect of LPB process on the surface roughness, surface integrity and fatigue life aspects of AISI 1045 work material using full factorial design of experiments. Burnishing process parameters as burnishing pressure, burnishing speed, ball diameter and number of passes were considered as design variables. Scheil et al. [79] experimentally investigated the effect of ball diameter, processing speed, line spacing between rolling traces and pressure on the surface hardness. They used a fractional factorial DoE to determine the experimental matrix design for all parameters.

Trauth et al. [1] extended the applicability of the similarity mechanics; a widely used approach in fluid mechanics, to investigate the deep rolling process more efficiently. Based on FE results validated by the experimental measurements, an efficient and accurate approach using similarity mechanics and DoE was established to study the correlation between the process parameters and the induced residual stresses. Bäcker et al. [4], considered different rolling ball diameter (3-6-13 mm), rolling pressure (50-150-250 bar) and overlap (30-60-80%) with the rolling speed of 10 mm/s to investigate the effects of the rolling process on the residual stresses. However, a formal DoE was not performed and only variation of the residual stress by changing the process parameters was studied.

The FE studies of Balland et al. [55, 56] demonstrated that that the magnitude of the overlap between the rolling passes (feed rate) has a major effect on the final residual stress state. The results also confirmed that the residual stress profile evolves gradually by increasing the number of rolling passes and therefore a minimum number of rolling passes is required to obtain a stable residual stress field. Further rolling beyond the required minimum number of rolling passes will not generally alter the induced residual stress profile in the workpiece. In addition, the previous experimental and numerical research works have unanimously confirmed that the impact of the rolling speed on the residual stress is negligible [9, 11, 52, 82]. Therefore, it can be concluded that the number of rolling passes and rolling velocity may not be treated as a design variable in the process optimization.

Applying either a gradient based optimization algorithm or a non-gradient stochastic-based algorithm such as genetic algorithms (GAs) directly on the FE results is very computationally expensive because the FE model may be called several times in every optimization iteration. In addition to that, the responses of FE models for dynamic nonlinear problems are typically noisy, thus calculation the gradient of the response functions can be erroneous which may render inaccurate optimal solution [80]. Therefore, direct use of high-fidelity gradient-based optimization algorithms on the FE results is not practical, if not impossible. To overcome this limitation, response surface method (RSM) has been effectively employed in practical large size problems to develop a smooth and analytical response function to define the correlation between the FE results and the design variables [9, 80, 81]. RSM basically fits the best polynomial function to the FEM results sampled over the selected design points in the defined design space.

Taguchi and RSM methods [83, 84], fuzzy logic method [85] and artificial neural network (ANN) [86] have been widely used in experimental studies to establish correlations between DCR process parameters and surface roughness and microhardness. The Grey based relational analysis and Taguchi method were used to establish a multi-response optimization of the burnishing process for an optimal parametric combination of surface roughness and microhardness [87]. Mohammadi et al. [9] formulated the design optimization problem for a half-space specimen of Ti64 to obtain the optimum set of LPB process parameters in order to reach an optimal profile of the residual stress. RSM was employed to create analytical objective and constraint functions using results obtained from FE models.

The comprehensive literature review shows that the main focus of previous studies was on establishing correlations and design optimization of the process at room temperature without considering the design intend of the treated component. However, the optimal profile of the induced residual stress strongly depends on the stress distribution resulted from the applied external load. While a deep residual stress is more essential in components subjected to push-pull loading, in parts under bending or torsional loads with high stress gradients, a more comprehensive stress on the surface layer is beneficial [19].

The surface treatments are usually performed at ambient temperature while many highly stressed components operate at elevated temperature. The beneficial influence of the surface treatments may decrease due the thermal relaxation of residual stresses. Since Ti64 components are designed for service temperature up to 450˚C, identifying process parameters to achieve an optimal residual stress distribution at the room temperature does not necessarily result in the most optimum solution for operations at elevated temperature. Moreover, achieving optimal selections of the process parameters in thin-walled components where the depth of the residual stress is comparable with the thickness of the component is more critical as the process can easily lead to detrimental tensile residual stress in the surface layer [11].

Another important objective of the present study is to develop a design optimization methodology to identify the optimal process parameters which can maximize the beneficial compressive residual profile in Ti64 component operating at room temperature as well as elevated operating temperature of 450˚C. To achieve this, the developed and validated high-fidelity nonlinear FE model will be utilized to simulate the DCR process to predict induced residual stress profile for a set of input

design points (process parameters) at both room temperature and its relaxation at the elevated temperature. The design points in the given design space will be optimally identified using DoE technique. Using the response surface method, analytical surrogate response functions will then be developed. These functions can efficiently replace computationally expensive FE model to predict the output residual stress parameters at both room and their relaxed states at elevated temperature with respect to the input process parameters. Finally, formal optimization problems will be formulated using developed explicit surrogate models to identify the optimal process parameters to enhance the fatigue life at the elevated temperature.

3 Prediction of Residual Stresses Induced by Deep Cold Rolling of Ti–6Al–4V Alloy and the Effect of Thermal Relaxation

In this chapter, a high-fidelity finite element model has been developed to simulate the deep cold rolling process on Ti64 specimens and the following short-term exposure of the treated components to elevated temperature. The developed model can be effectively used to predict the residual stress profiles induced by the process at room temperature and the following residual stress relaxation at the elevated temperature. The thermal relaxation stage is performed using a visco-plastic model which couples creep and plasticity deformation mechanisms to predict the state of residual stresses at the elevated temperature. For this purpose, a new set of hyperbolic creep law coefficients are identified in order to describe the primary creep at 450˚C. The accuracy of the developed finite element model to predict residual stresses is validated by comparisons of the simulation results with the experimental data available in the literature. It has been shown that the finite element predictions correlate well with experimental results with error generally less than 10%.

3.1 Simulation Frame Work

As mentioned before, the induced residual stress field cannot be determined by means of analytical methods due to highly nonlinear cyclic plastic deformation and contact between the ball and the component during of DCR process and thus the use of numerical FE based models is inevitable. In the present work, a high-fidelity 3D FE model has been developed in ABAQUS software to simulate the DCR process in order to predict the residual stress, and also to evaluate the thermal relaxation of the induce residual stresses at elevated temperatures.

ABAQUS package generally offers two powerful solvers namely ABAQUS/Standard and ABAQUS/Explicit. ABAQUS/Standard uses the iterative procedure based on the implicit time integration technique, which is unconditionally stable, but is slow convergent especially for short duration dynamic nonlinear problems. On the other hand, ABAQUS/Explicit is based on explicit time integration technique, which is conditionally stable. However with properly selected time

step, the explicit solver can be effectively used to solve complex nonlinear dynamic problems with fast convergence [40].

The proposed simulation framework has been divided into three main stages as shown in Figure 3-1. First the DCR process at room temperature is simulated using Johnson Cook material model as presented by Eq. (2-13), to evaluate the induced residual stress and strain fields which are then subsequently considered as initial conditions for the next stage of simulation in which the spring back analysis is modeled using isotropic plasticity behaviour of the material at a low strain rate. The results at the end of this stage are then validated against available experimental measurements.

The output of spring back analysis is the initial states for the thermal relaxation assessment where the effect of the elevated temperature on the induced residual stress field is modeled through the plastic softening and short-term creep relaxation mechanism. The results obtained from the analysis of this stage are also compared to those available experimental measurements for the purpose of validation of the developed FE model. This stage includes several sequentially coupled steps in which the stress and strain output of each step will be an initial state for the following step.

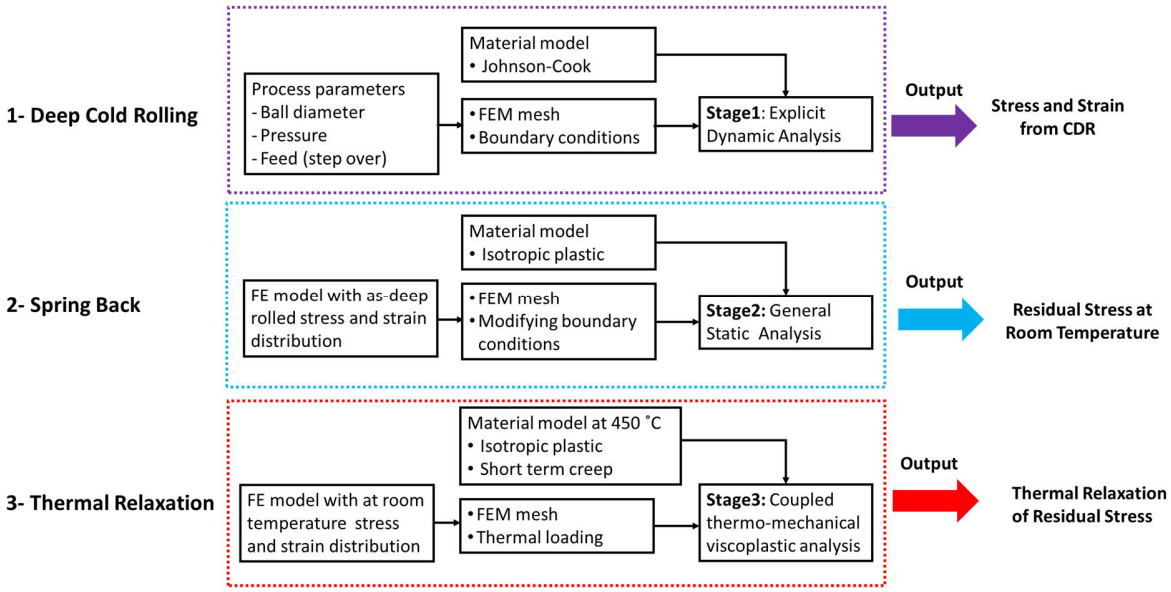

Figure 3-1: Flow chart for the simulation of the DCR process and thermal relaxation

As explained before the modeling of DCR inherits many sources of nonlinearities mainly due to the contact analysis, nonlinear behavior of the material, dynamic loading and large deformation. ABAQUS is capable of handling highly dynamic nonlinear problems efficiently and accurately using its explicit module and has shown to be effective in modeling of DCR process [9, 42].

The explicit method could be computationally very expensive for quasi-static problems such as metal forming processes because it requires a long-time solution and needs very small elements in the contact zone due to a high level of nonlinearity. The run time of dynamic explicit program can be further reduced by artificially increasing the forming rate (time scaling) or artificially increasing the density of the elements (mass scaling technique) as explained in section 2.4.1. However, the solution accuracy can be compromised because of the introduction of unrealistic dynamic effects if proper care is not taken into account using these techniques. The kinetic energy of the system needs to be carefully monitored through the simulation process to ensure that the ratio of kinetic energy to internal energy does not exceed 10%. Time scaling approach should not be used in a strain rate dependent simulation like deep rolling process [40].

It should be noted that the spring back and thermal relaxation stages due to their quasi-static nature are analyzed using Implicit solve in ABAQUS/Standard. As it was discussed in section 2.4, the implicit numerical procedures are usually unconditionally stable and ABAQUS/Standard uses the backward Euler operator and a generalized form of Newmark method for time integration of the dynamic problem.

3.2 Finite Element Simulation of DCR at Room Temperature

As mentioned before in Chapter 2, the rolling process should be simulated by a 3D FE model since nature of the rolling contact is three dimensional and no symmetry can be found in order to reduce it to 2D problem [61]. The influence of deep rolling on the workpiece is highly localized so the effect of surface curvature and the resultant helical rolling path is negligible in the modeling of DCR process on a cylindrical workpiece [64, 65] and the process can effectively be modeled on a flat plate without sacrificing the accuracy. The pressurized fluid acts as the coolant and lubricant in the process. Thus the process is assumed to be isothermal [65] and for the interaction between the workpiece and ball a frictional coefficient between 10^{-5} and 5×10^{-3} is considered using isotropic Coulomb friction model [67].

Figure 3-2 shows the 3D FE model of the ball and the work piece developed using C3D8RT elements in ABAQUS environment. C3D8RT is an 8-node thermally coupled brick element accommodating temperature degree of freedom (DOF) in addition to all possible displacement DOFs. Stresses are evaluated at the Gauss points with reduced integration to prevent shear locking. The DCR process parameters are considered to be the ball diameter, rolling force and feed. The

process parameters of experimental work of Nalla et al. [3] were considered for the modeling in order to validate the FE results.

The experimental results show that the DCR process can induce the residual stresses with high gradient up to 600µm depth from the surface of the workpiece. Hence a very refined mesh (size of 25µm) has been used in the vicinity of contact zone as shown in Figure 3-2 to achieve accurate results. However, in the regions far away from the contact zone, coarser elements were used to decrease the number of degrees of freedom and computational costs.

The geometry of the workpiece was partitioned to smooth the transition from very refined mesh to coarse mesh in order to avoid element distortion and generate a high-quality mesh. As the hardness of the moving ball is generally several times higher than that of test specimen, it has been modeled as analytical rigid body and hence its motion can be associated to a reference point. This assumption reduces the number of degrees of freedom required to describe the motion of the rolling ball, thus making the simulation more computationally efficient without compromising the accuracy.

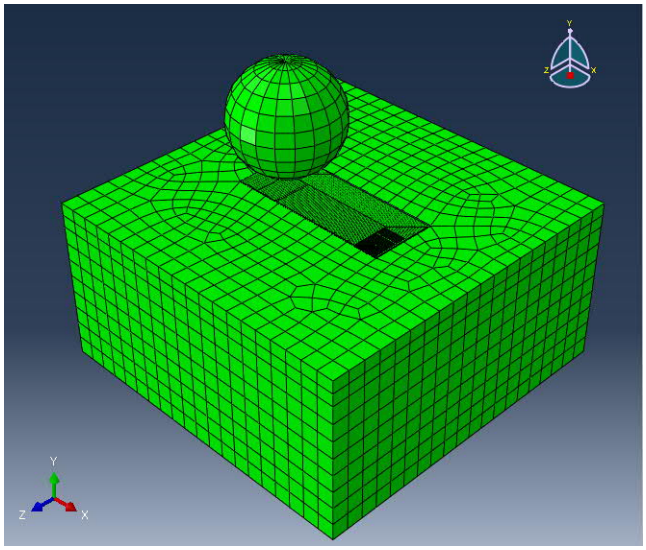

Figure 3-2: Geometric model and mesh of the workpiece in the 3D simulation

A series of simulation cycles are conducted until a stable residual stress field is achieved in the contact zone. The roller kinematics is defined by four different boundary conditions as:

(a) Indentation step where the ball is pushed into the surface of workpiece
(b) Rolling steps whereby the ball is free to rotate while the force is constantly applied

(c) Overlap steps where the ball is offset laterally (perpendicular to the rolling pass) by the amount of feed. In this step the movement of the ball in the other directions is fixed.

(d) Retraction step where the ball is removed from the surface.

When the ball rolls and finishes one trajectory in X direction, it is then offset in Z direction and rolls back in an opposite direction (-X) to complete the next trajectory. Through several trial and error, it is found that 10-number of rolling passes is sufficient to generate a stable stress state.

Numerous sets of JC model parameters for Ti64 exist in the literature [49, 50] where each set has been defined based on the measured plastic strain and strain rates in a specific range of temperatures. The assumed JC model for the simulation of the DCR process should cover the largest strain and strain rate typically generated during the process. Thus, the JC model developed by Lee and Lin [88] for Ti64 with parameters presented in Table 3-1 was used to describe the material behavior in the simulation of cold rolling processes.

Table 3-1: JC material constant parameters presented for Ti64 [88]

A (MPa)	B (MPa)	n	C	m
724.7	683.1	0.47	0.035	1

It is noted that the stable time increment depends on the material properties and the element size as shown by Eq. (2-8). The time increment is governed by the elements in the layer close to the surface through the analysis process as it requires the minimum element size which its value changes due to the loading. It is noted that to reduce the computational time, the mass scaling technique with the target time increment of 8×10^{-8} has been employed in the current work. The energy balance during the CDR process was monitored to evaluate whether the assumed mass scaling in ABAQUS/Explicit simulation is yielding an appropriate dynamic response as shown in Figure 3-3. As it can be realized, the kinetic energy (ALLKE) of the process does not exceed a small fraction (less than 5%) of its internal energy (ALLIE) throughout the majority of the process.

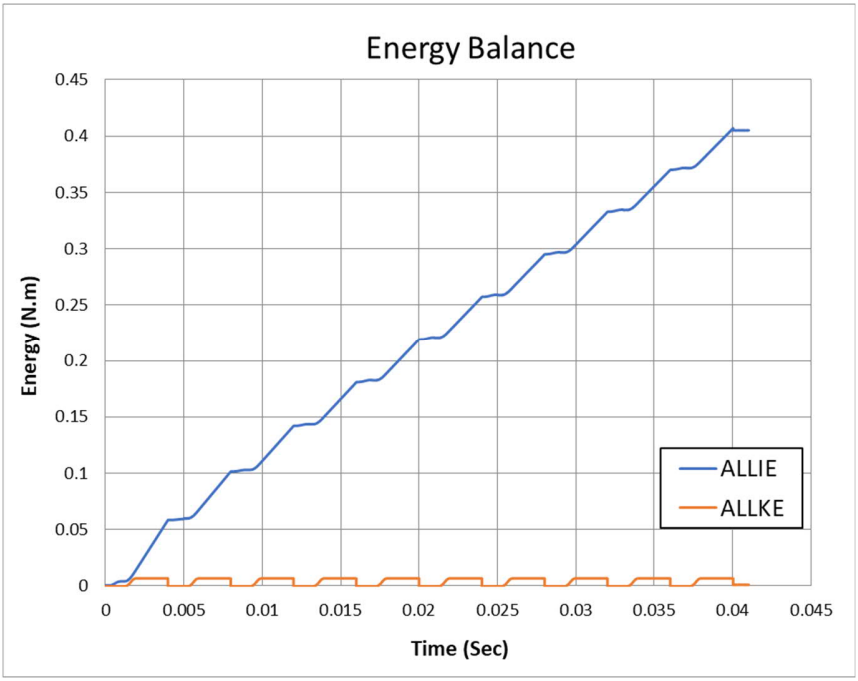

Figure 3-3: Energy balance in the DCR simulation

When the deep rolling process is completed, the stress and strain fields calculated at the end of the ball retraction are then transferred to an implicit FE model to determine the settled residual stress in the component. This stage of the process; which is called spring back, is quasi-static in nature and therefore plastic material model at lower strain rate is required in the simulation. Thus the true stress and strain curves at strain rate of 1 sec^{-1} at room temperature, reported by et al. [89], has been implemented in form of isotropic plasticity in the FE model to carry out the spring back analysis. This isotropic plastic model was also used in the DCR simulation later to investigate the effect of the assumed plasticity model on the predicted residual stress profile.

3.3 Validation of the FE Model

In this study, the experimental results reported by Nalla et al. [3, 31] are used to validate the developed FE models of conventional DCR. In the experimental study, the deep rolling on Ti64 rod with the diameter of 7 mm was performed using a 6.6 mm diameter ball under rolling pressure of 150 bar (15 MPa) and constant feed of 0.1125 mm per revolution followed by annealing at 450˚C for 45 minutes. The X-ray diffraction (XRD) method was then used to measure the residual stress induced by DCR process and to measure the residual stress after the following thermal relaxation.

Lattice spacing variation is measured using Bragg law and compared to a strain-free reference specimen to calculate residual stress and strains in XRD technique. This method involves material layer removal which may cause inevitable relaxation and redistribution of the initial residual stress profile. Stresses in both directions tend to fall to zero after layer removal since all the volume where residual stresses balanced themselves are removed. Therefore, the measurement error increases with the depth from the surface. Additionally, measuring tensile residual stresses beneath the surface using XRD method is not possible due to this layer removal approach. The equilibrium of forces between the tensile region and compressive region must be maintained in each step and because of layer removal the compressive region either reduces or does not exist [25]. Also residual stress measurement techniques are more or less inefficient in measuring the residual stress in curved directions [52]. The residual stress in the rolling direction (axial) is considerably lower than that in perpendicular to the rolling direction (tangential). Therfore only the residual stresses measured in tangential directions have been reported [2, 3] and will be used here to validate the FE model.

Figure 3-4 shows the comparison of the tangential residual stress profile predicted by the developed FE model and the experimental measurements of Nalla et al. [3, 31]. Both JC and isotropic plastic models have been used as the materials constitute models in the developed FE model. As it can be realized predicted residual stress profile based on the JC model agrees very well with that obtained experimentally up to depth of 170μm. Specifically, the magnitude of the residual stress at the surface and also the maximum induced residual stress and its location beneath the surface have been accurately predicted. While FE model based on the isotropic plastic model was able to accurately predict the residual stress on the surface, it was not capable of capturing the location and magnitude of the maximum residual stress.

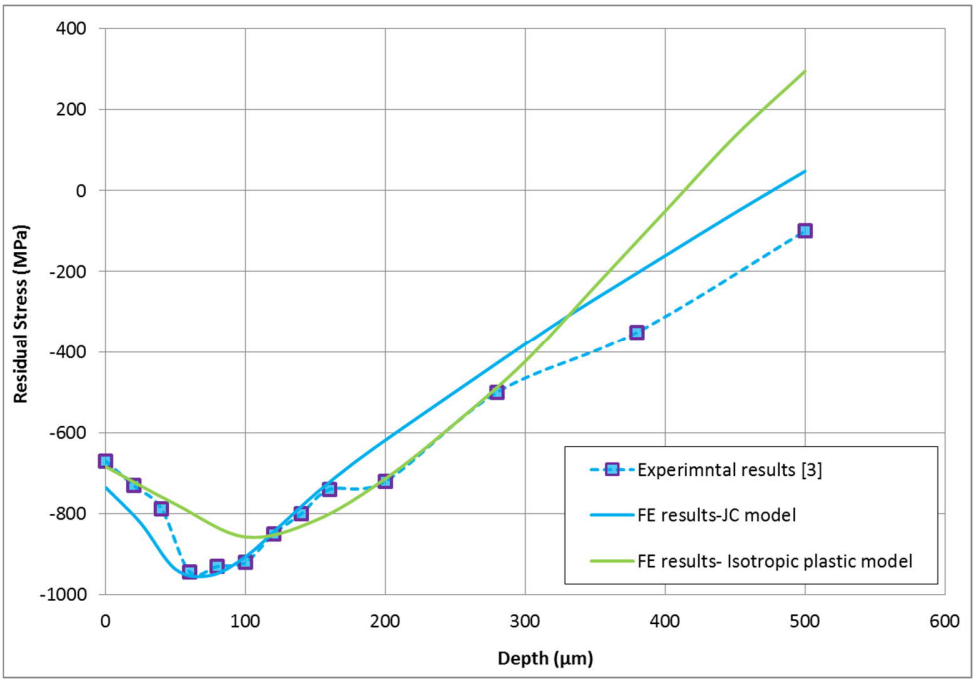

Figure 3-4: Comparing tangential residual stress profile through the depth obtained at room temperature using FE and experimental measurements of Nalla et al. [3, 31]

Next to further assure the validity of the developed FE model, the RS profile predicted by the FE model developed in the current study using the JC material model has been compared to a second XRD measurements reported by Tsuji et al. [2] which is presented in Figure 3-5. The deep rolling in the experimental study was performed in a lathe using a ball element with 6 mm diameter under the rolling force of 750 N, at a rotating speed of 750 rpm, and a feed 0.1 mm per revolution.

Results generally show that the simulation results based on the developed FE model agrees very well with those obtained experimentally. The difference between the simulation results for the residual stress and those reported experimentally at the deeper locations below the surface may be attributed to the fact that the residual stresses measured in the experiments have not been corrected to account for layer removals [2, 3, 31]. The residual stresses are self-equilibrating in surface treated components. As a result, by removing each layer of compressive residual stress in XRD processes the magnitude of the remaining compressive stresses must increase to satisfy the equilibrium with the intact tensile stress in deeper depth of the component. As it is has been presented in Figure 2-10, when the amount of measured compressive stresses is not corrected for the effect of the layer removal, the depth of the compressive layer and the measured compressive residual at each depth may be greater than their real values. Considering above, it can be concluded

the developed FE model is capable of predicting the residual stresses induced during the DCR process at the room temperature.

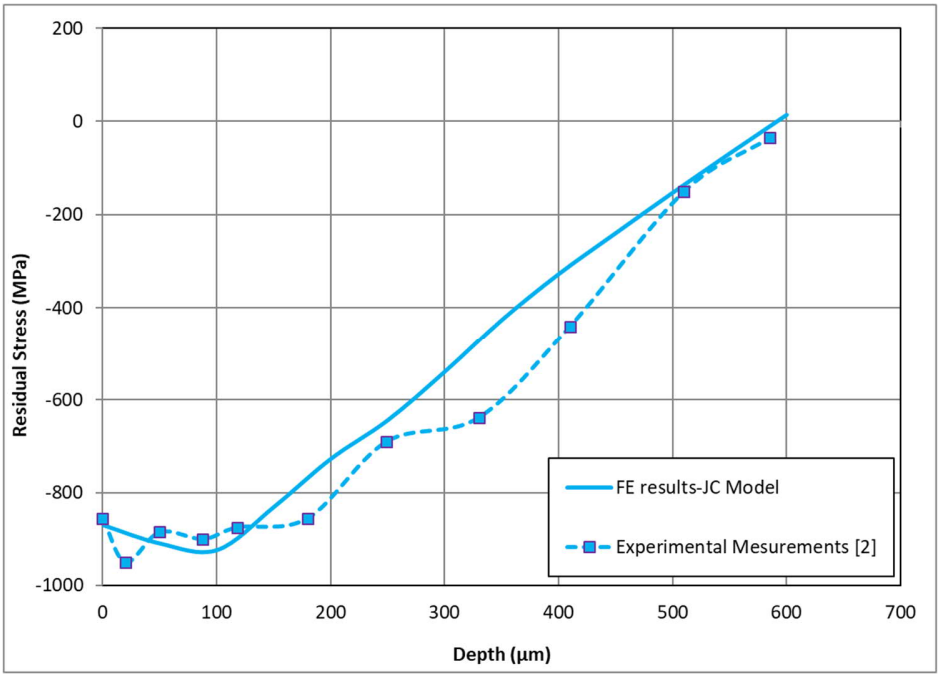

Figure 3-5: Comparing tangential residual stress profile through the depth at room temperature obtained using FE and experimental measurements of Tsuji et al. [2]

3.4 Effect of the Rolling Pass on the Residual Stress Distribution

Here the effect of rolling ball movement on the induced residual stress is investigated. The process paramerts are ball diameter of 6.6 mm, pressure of 150 bar (15 MPa), feed of 0.1125 mm and rolling speed of 700 mm/s which were taken from the experimantal study published by Nalla et al. [3, 31]. Figure 3-6 shows the displacement magnitude contours and material flow vectors after the first rolling pass. When the ball rolls, the flow of material in the *Z* direction is restrained by the surrounding material which forms lateral protrusions on each side of the created groove. As illustrated in the figure the heights of the protrusions on the sides of the groove are greater than the height of the front ridge which explained why the residual stress in tangential (z) direction is greater than the rolling (x) direction.

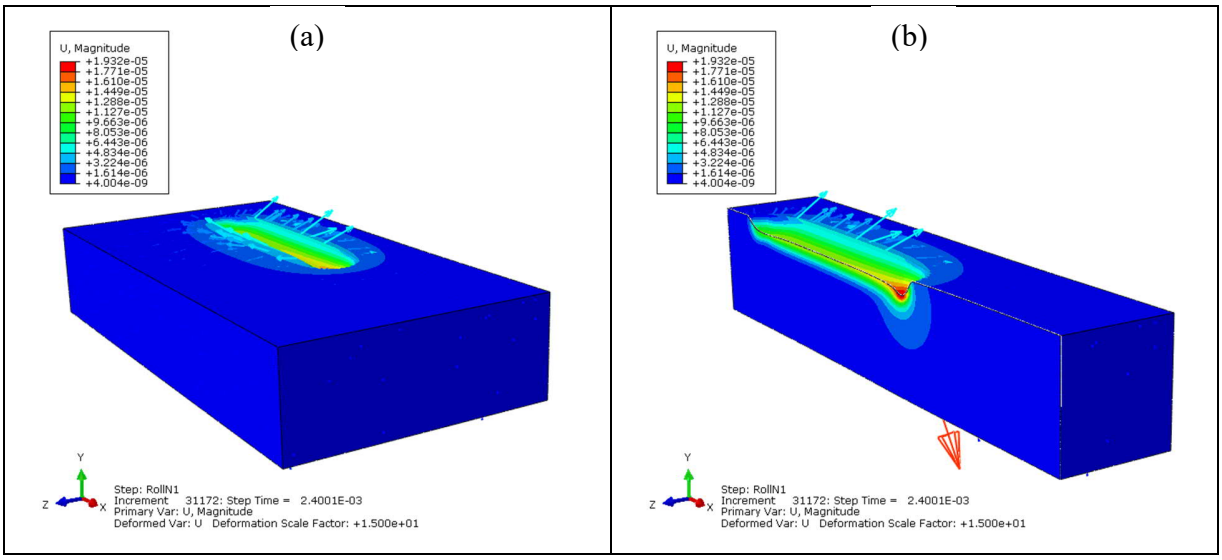

Figure 3-6: Displacement magnitude (*m*) with material flow vectors (a) and its sectioned view (b)

The lateral protrusions rising in the first rolling pass will interact with the ball movement during the next trajectory. In another word, the ball in the subsequent pass has to move over a surface deformed by the previous rolling pass which also inherits plastic hardening. Therefore, the generation of the lateral protrusions in the following trajectory is influenced by the already existing protrusions due to strain hardening and generated roughness in previous passes. The succeeding rolling also lifts up the bottom of the groove created by the previous passage. This can be easily observed from Figure 3-7 which shows the evolution of the surface profile in the first four rolling passes at the end of each cycle. It is noted that the deformed shapes are scaled by the factor of 20 for the sake of clarity.

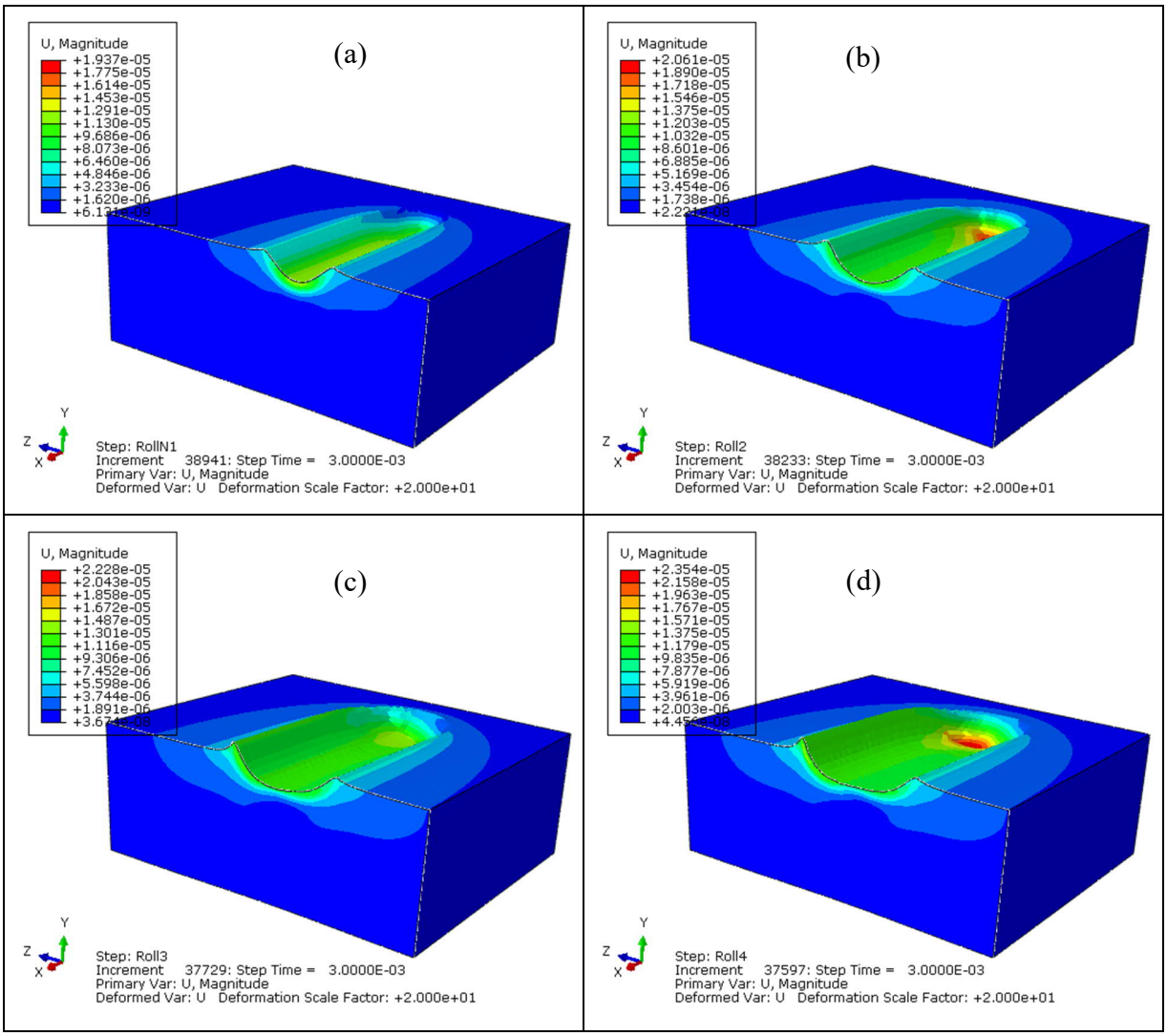

Figure 3-7: Resultant displacement (*m*) contour after one (a), two (b), three (c) and four (d) rolling pass

In order to investigate the saturation stage where the surface profile becomes stable and does not change by increasing the number of rolling passes, the displacements in mid span of the rolling trajectory were extracted in *y* direction (normal to the surface) in the *yz* plane. Figure 3-8 shows the line where the displacement in *y* direction has been investigated. The *y*-displacements of the nodes located on the entire mid-span line as shown in Figure 3-8 are analyzed after each rolling pass and results are presented in Figure 3-9. As it can be realized after six rolling passes, the displacements in the range between z= 500-1000 µm is nearly constant.

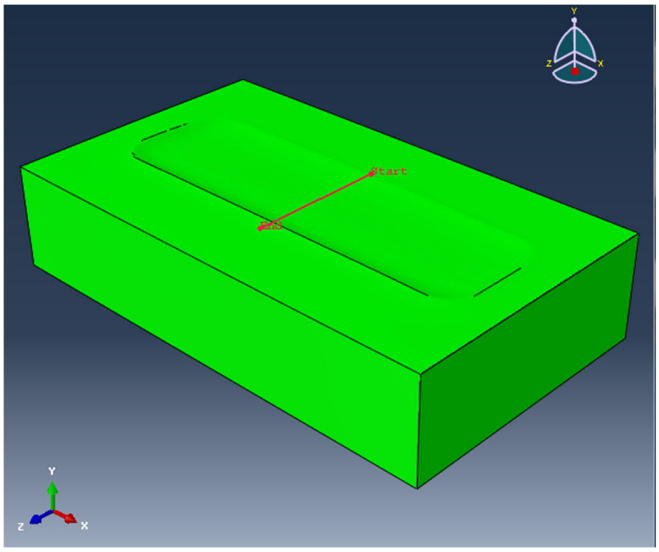

Figure 3-8: Mid-span line on which the displacement in y direction has been evaluated during each rolling pass

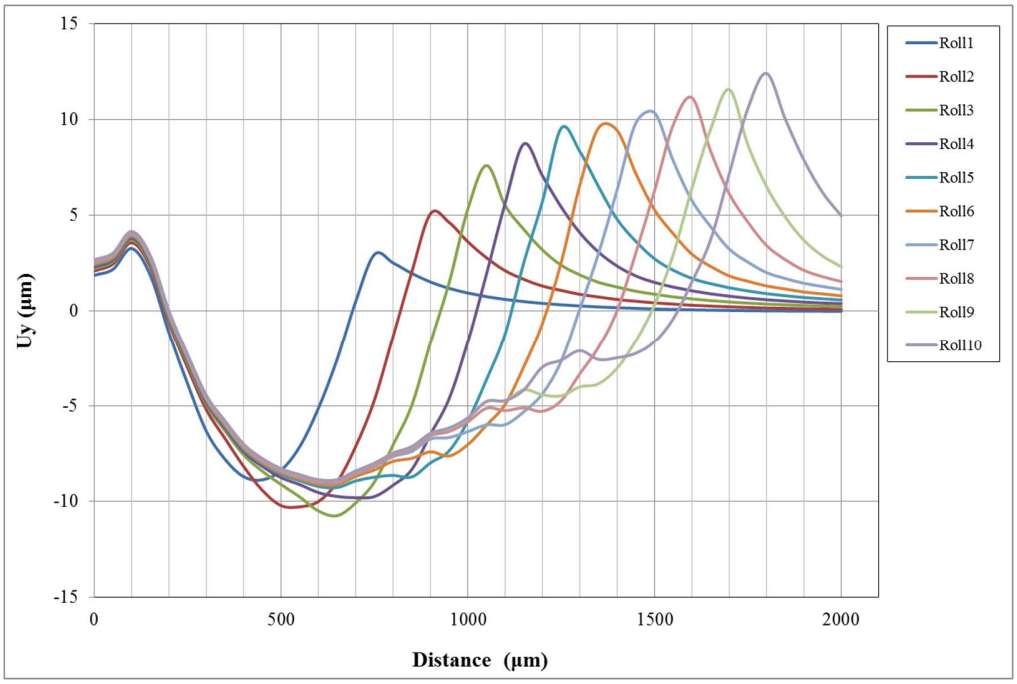

Figure 3-9: The evolution of surface profiles in *yz* plane (perpendicular to the work piece surface) at the mid span during each cycle of rolling

Further examination of Figure 3-9 also reveals that the displacement profile has evolutionary characteristics and strongly depends on the number of completed rolling passes. After several simulations, it has been observed that the displacements and subsequently induced residual stresses stabilize after around eight rolling passes.

3.5 Residual Stress Profiles

Figure 3-10 shows the residual stress in tangential direction (σ_{zz}) after spring back sectioned in the stabilized region; corresponding to z= 400-700 µm in Figure 3-9. Nine vertical lines (normal to the surface) are used to obtain the residual stress distribution through the thickness and the calculated average values are compared to experimental results as presented in Figure 3-4. It should be noted that due to very high numerical computation time, only 10 number of passes were considered in the simulation, which only covers a part of the surface but it is enough to develop a stabilized region to extract the results.

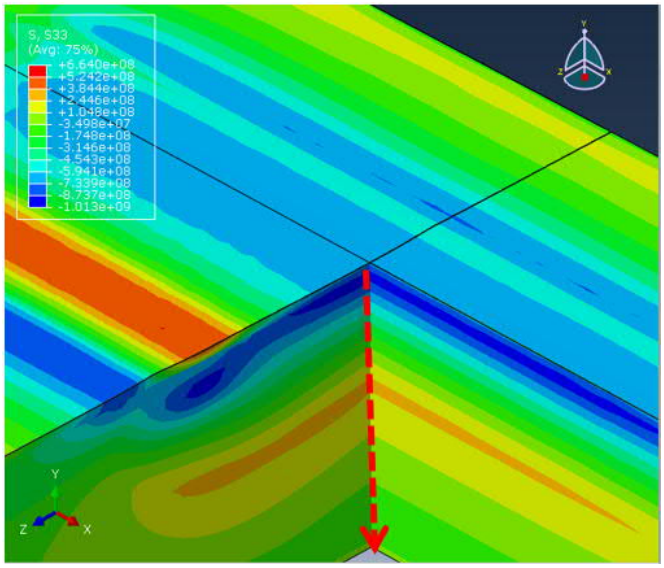

Figure 3-10: Residual stress (Pa) in tangential direction (σ_{zz}) after spring back sectioned in the stabilized region

The residual stress distribution in the axial (σ_{xx}) and tangential (σ_{zz}) directions in the stabilized region (seen in blue color in Figure 3-10) are shown in Figure 3-11. As it can be seen DCR process develops very different residual stress distribution through the depth along longitudinal and transverse directions.

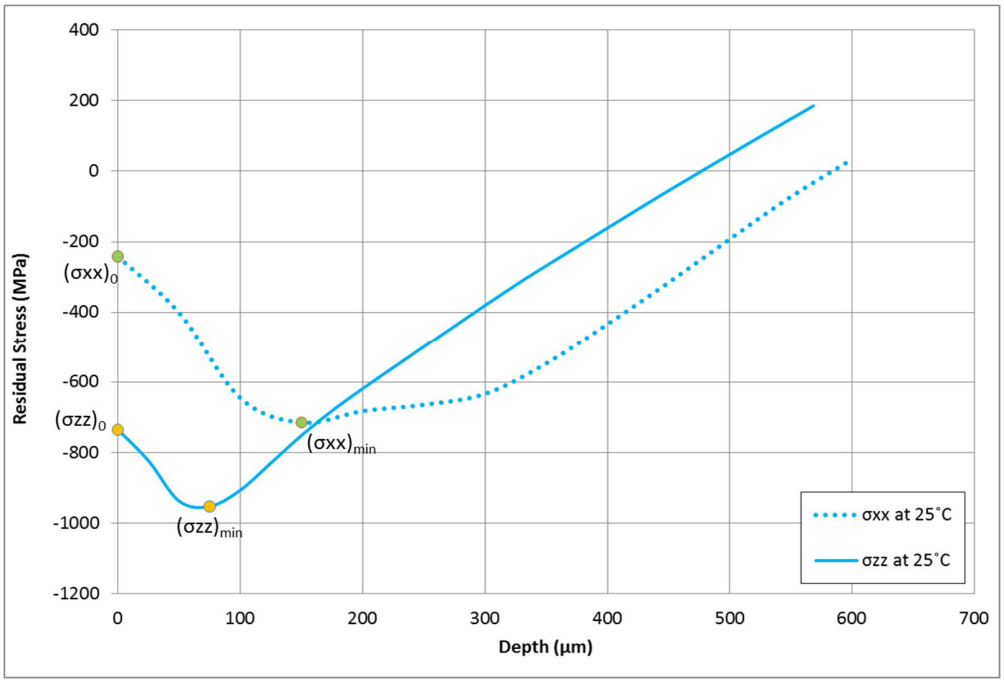

Figure 3-11: Residual stress profiles in axial and tangential direction at room temperature

The predicted residual stresses in axial and tangential directions illustrated in Figure 3-11 have been quantified using parameters defined in Figure 2-1(b) which are presented in Table 3-2. According to the presented results, the magnitude of the tangential residual stress is almost three times of the axial residual stress at the surface and the magnitude of $(\sigma_{min})_{zz}$ is approximately 35% higher than the magnitude of $(\sigma_{min})_{xx}$. This is in a very good agreement with experimental observations published by Liam et al. [59] where approximately 2.8 times and 35%, had been respectively reported. The comparison of Z_{min} and Z_0 values presented for tangential and axial directions shows that the axial residual stress is developed in a deeper depth compared with that of tangential residual stress.

Table 3-2: Characterization of residual stress depth profiles plotted in Figure 3-11

	Tangential (Z direction)	*Axial (X direction)*
σ_0 (MPa)	723	214
σ_{min} (MPa)	943	714
Z_{min} (µm)	75	150
Z_0 (µm)	480	580

It has also been observed that the amount of feed; which controls the overlap between the two following rolling passes, has a significant effect on the final state of the residual stress. To demonstrate this, the effect of feed on the residual stress profile has been investigated while the other process parameters were kept unchanged. The effect of the feed on tangential residual stresses σ_0 and σ_{min} is shown in Figures 3-12 and 3-13, respectively. Results show a parabolic relation between the introduced residual stresses and the feed.

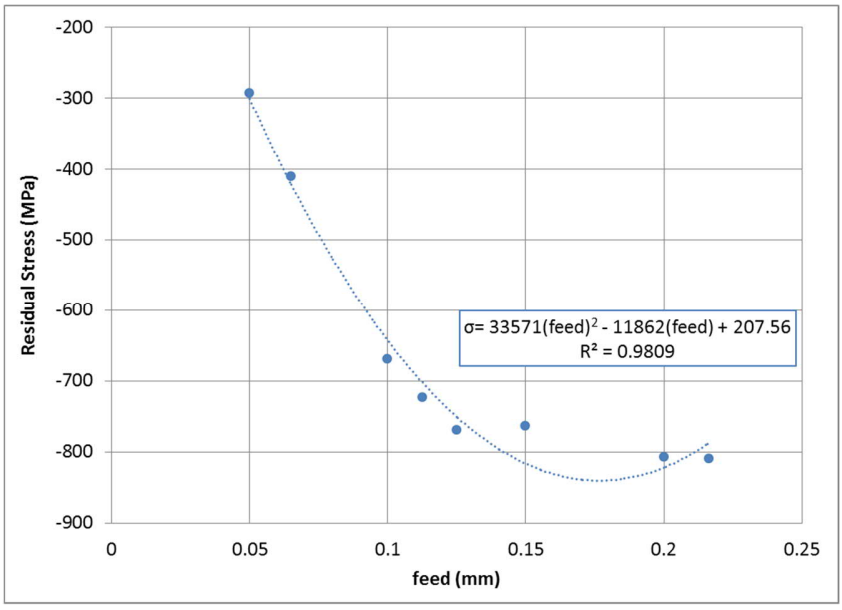

Figure 3-12: Effect of the feed on tangential residual stress on the surface (σ_0)

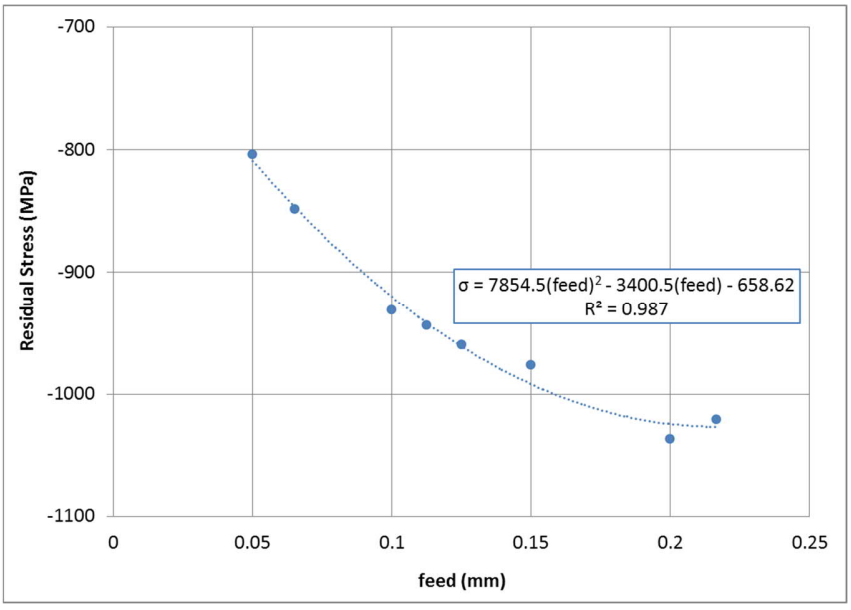

Figure 3-13: Effect of the feed on the tangential residual stress at Z_{min} (σ_{min})

Statistical analysis of the effect of feed on work hardening surface hardness in ball burnishing process shows that the surface hardness increases linearly by increasing the feed [90]. Prevéy has shown that a parabola function best fits the relation of measured residual stresses with respect to hardness measurements by the full width at half maximum (FWHM) distribution in LPB treated Ti64 [22]. Thus, one may conclude that a parabolic relationship can be established between the residual stresses with respect to the feed. Therefore, the developed FE model can describe the variation of the process parameters on the residual stress profile.

3.6 FE Model of Thermal Relaxation

The initial thermal relaxation is prompt and caused by the change in yield strengths and the Young's Modulus at elevated temperature. Decreasing the Young's Modulus leads to an elastic temporary relaxation. Also with the temperature increase, the yield stress decreases which can be lower than the high compressive residual stresses at room temperature which results in a local plastic deformation causing a permanent residual stress relaxation. It has been shown that the time dependent thermal relaxation can also be described by creep behaviour as shown experimentally for Ti64 [20, 24]. Correlation between time dependent plastic strains and mean residual stress are established in such approach [17].

The DCR process alters the microstructure of the surface layer and this change will result in a different material behaviour. Therefore, plasticity deformation mechanism combined with short term creep deformation needs to be adopted in the surface layer to model this high rate relaxation mechanism. Similar methodology has been successfully implemented before for FE modeling of thermal relaxation of shot peened Nickel-base supper alloy [91].

The residual stress and strain states at the end of spring back simulation are provided as initial condition for the subsequent thermal relaxation analysis conducted in ABAQUS/Standard. The FE analysis for thermal relaxation is a steady state thermo-mechanical analysis followed by a visco-plastic analysis to account for creep relaxation in the surface layer. An arbitrary time step was assigned to steady state analysis (here 10 sec) since the time has no role in the FE analysis at this stage. However, the step time is important for the creep analysis and it will be the same as annealing process (45 minutes at 450˚C) considered in experimental study of Nalla et.al. [3].

ABBAQUS/Standard employs a backward-difference scheme in the thermal-stress analysis to integrate temperatures, and the nonlinear coupled system of stress (displacement) and temperatures

are solved using Newton's method. The thermal loading is applied as the bulk metal temperature increases to 450 ºC and then remains constant for 45 minutes as illustrated in Figure 3-14.

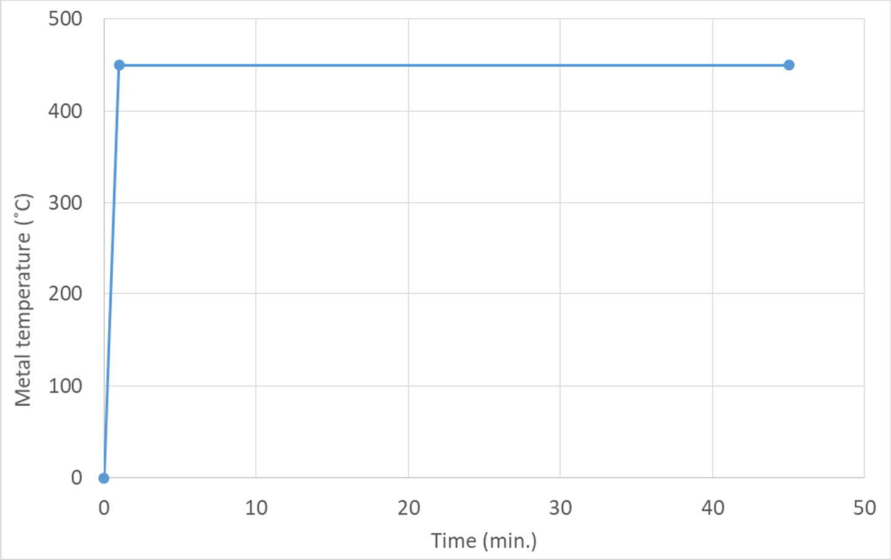

Figure 3-14: Time plot of metal temperature to be used in thermal relaxation simulation

As explained before, the JC model was used in the simulation of DCR process which involves a high strain rate deformation. The JC model parameters are obtained by fitting the model coefficients to plastic deformations under high strain rate regimes while the spring back and thermal relaxation processes occurs under a quasi-static or steady state condition. Therefore, JC model especially with original parameter values might not be a good representative of the plastic deformation of the material during thermal relaxation.

In an attempt to overcome this problem, Zhou et al. [23] recalibrated parameter *m* (which describes the thermal softening of yield stress) of their assumed JC model to analyze thermal relaxation of residual stress induced in laser shock peened Ti64 plate. However, this still is not representing the quasi-static nature of the thermal relaxation stage since the other JC parameters (i.e. *A, B* and *n*) had been extracted from high strain rate test data.

In the present study, temperature dependent quasi-static stress-strain curves in form of isotropic plasticity; based on true stress and strains measurements by Haight et al. [89] are utilized in the developed FE model. The true stress-strain data at strain rate of 1 sec^{-1} for Ti64 alloy at different temperatures are shown in Figure 3-15. The thermal relaxation stage is then performed using a

visco-plastic model which couples the creep and plasticity deformation mechanisms to predict the state of residual stresses at the elevated temperature.

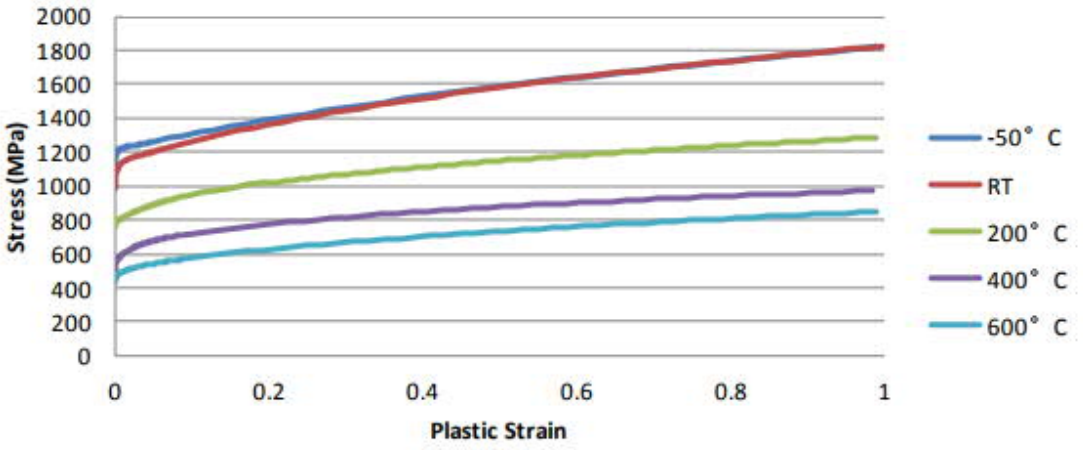

Figure 3-15: Temperature dependent plastic deformation of Ti64 at strain rate 1 sec^{-1} [89]

Norton and Hyperbolic-sine function are widely used creep laws and have been employed to describe the creep behaviour of Ti64 [20, 25]. Hyperbolic-sine creep model which has been found to be suitable for the primary creep can be described as:

$$\dot{\varepsilon}_c = A(sinhB\sigma)^n \exp(-\frac{\Delta H}{RT}) \tag{3-1}$$

where T is temperature [K]; ΔH is creep activation energy [kJ/(mol·K)]; R is gas constant, [kJ/mol]; A is material structure factor, [s^{-1}]; B is stress level factor, [MPa^{-1}]; n is stress exponent.

All the available creep models in the literatures have been developed either for long time deformations where the data have been fit to the secondary creep [20, 92] or at the temperatures above 450˚C [24]. The only short term creep strains and stresses available in the open source literatures were found in [92, 93] where the minimum reported dwell time is 1 hours.

Prevey et al [14] claimed that the thermal relaxation of residual stress induced by shot peening, gravity peening and laser shocking in Ti64 and IN718 materials shows strong correlation with the amount of induced cold work and the initial relaxation of compression residual stress appears to be time independent in both materials. Therefore it was assumed that the creep relaxation developed based on test data at 1 hour dwelling time is also applicable for 45 minutes. A new set of Hyperbolic creep law coefficients are constructed in the current study that has the best fit to

those experimental measurements data points available in [92, 93], in order to describe the primary creep at 450˚C and are presented in Table 3-3.

Table 3-3: Hyperbolic creep coefficients for 450˚C

A (s^{-1})	6.33034E-15
B (MPa^{-1})	0.0435
n	1.000504
H (kJ/(mol·K))	200

3.6.1 Validation of the FE model for Thermal Relaxation

The profile of residual stress in tangential direction; σ_{zz}, at elevated temperature was obtained using the developed FE model along the same lines where the stresses were acquired at room temperature. The results are shown in Figure 3-16 and compared to experimental measurements of Nalla et al [3].

As discussed in section 2.2, Zener-Wert-Avrami model described by Eq. (2-1) is an analytical function which describes the thermal relaxation of macro residual stresses and changes of work hardening states quantitatively and is applicable to a wide range of temperatures. Stanojevic et al. [20] determined the parameters of this model for axial and tangential stress relaxation in deep-rolled Ti64 as provided in Table 3-4.

Here Zener-Wert-Avrami model has also been considered in the present work to predict the profile of tangential residual stress after thermal relaxation for the sake of comparison with the FE results as shown in Figure 3-16. The results show the superiority of the developed FE to the analytical Zener-Wert-Avrami model as it agrees better with the experimental measurements.

Table 3-4: Zener-Wert-Avrami parameters in axial and tangential directions of deep-rolled Ti64 [20]

Parameter	Axial	Tangential
C [1/s]	3.96 E5	8.11 E4
ΔH_A [eV]	1.176	1.098
m [-]	0.2061	0.3132

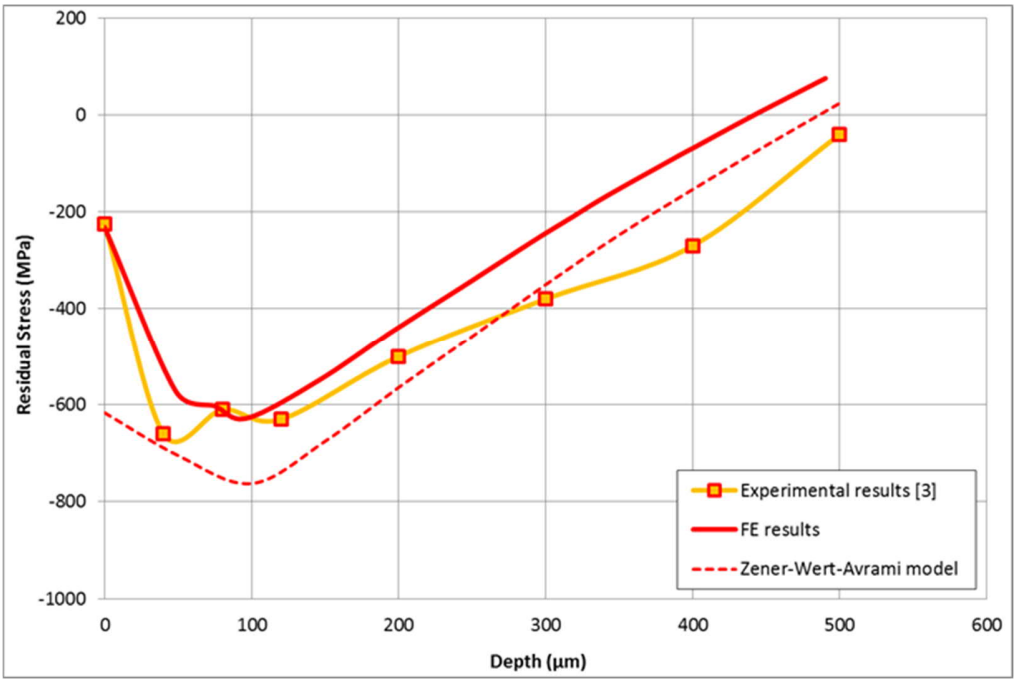

Figure 3-16: Residual stress profiles in tangential direction at 450˚C

The noticeable deviation between FE and experimental results in region above 200 µm depth in Figure 3-16 is mainly associated with the fact that the experimental measured residual stress has not been corrected to account for the effect of surface layer removals, standard deviation difference in creep behaviour of Ti-64 provided by different suppliers and also assumptions related to the material model. Results in Figure 3-16 also demonstrate that although the analytical model can predict the residual stress in a depth above 200 µm rather well, it fails to predict the magnitude of the residual stress on the surface layer and near subsurface layers. This may be attributed to the fact that the analytical model assumes constant activation energy and parameter C through the thickness. It is also noted that empirical models need to be recalibrated for each surface treatment process and associated control parameters. Moreover these models do not generally incorporate material microstructure, hardening behavior, plastic strain, and the underlying physical deformation mechanisms which have a significant role in the stress relaxation.

3.6.2 Effect of elevated temperature on the induced residual stress distribution

The distribution of residual stress in axial (σ_{xx}) and tangential (σ_{zz}) directions at room and elevated temperature 450˚C are shown in Figure 3-17 for the sake of comparison. The results clearly confirm that the thermal relaxation redistributes the residual stresses which leads to a more uniform

stress profiles through the depth and reduces the anisotropy of the residual stresses as the difference between σ_{xx} and σ_{zz} reduces at the elevated temperature.

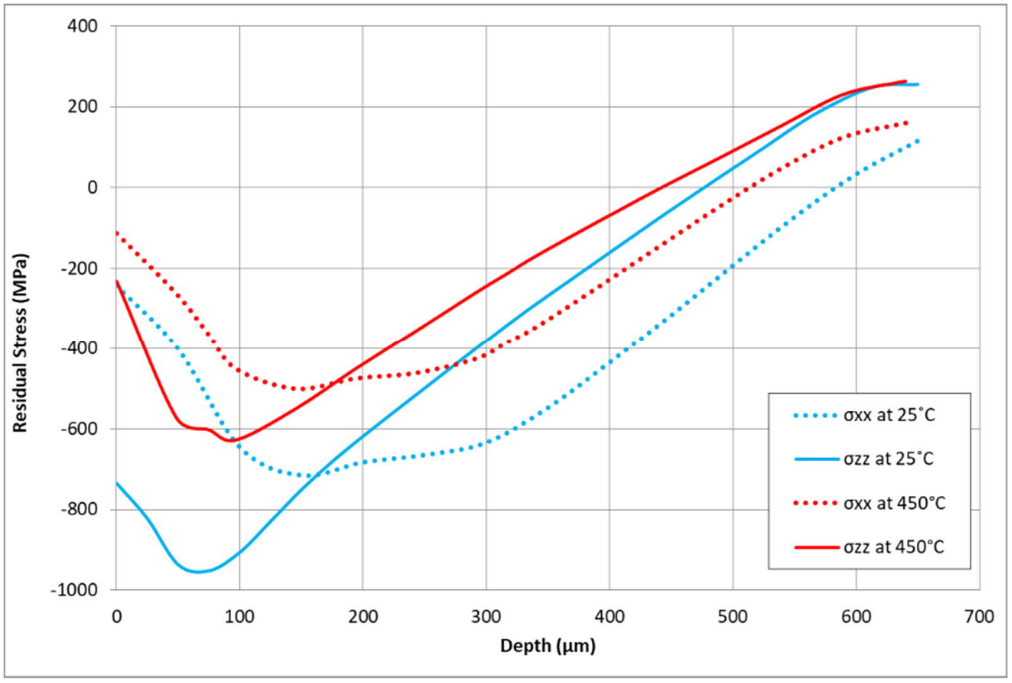

Figure 3-17: Residual stress profile in axial and tangential direction at 450°C

As it can be realized the induced residual stresses in DCR process substantially relaxes at the elevated temperature. This should be carefully taken into consideration as improper selection of process parameters may induce beneficial residual stresses which may be completely released at the elevated temperature and thus drastically reducing the fatigue life enhancement of the components. This suggests that any future design optimization on the selection of the optimal process parameters should be conducted based on the operating temperature.

3.7 Conclusion

A high-fidelity finite element (FE) model has been developed to predict the distribution of the residual stresses induced by the DCR process on Ti64 material at the room temperature and the subsequent thermal relaxation at elevated temperature. The results obtained from the developed FE model correlates well with the available experimental measurements. The FE model can accurately capture both the shape and magnitude of the residual stress profiles up to depth of 200µm from the surface. In deeper depth the numerical and experimental results deviate slightly mainly due to the layer removal involved in the experimental measurement.

It was discussed that deep rolling process changes the microstructure of the specimen in the surface layer which leads to change in mechanical behaviour of the material. In the current work a proper deformation mechanism was adopted based on dominating deformation mechanism associated to microstructure of the treated materials. At the surface layer where the dislocation density is high, the deformation is controlled by dislocation glide which results in primary creep deformation. However in deeper depths the main controlling relaxation mechanism is plastic deformation due to softening of the material at higher temperature. A hyperbolic-sine creep law used for primary creep deformation of Ti64 at 450˚C has been employed for thermal relaxation stage of the modeling. The conclusions and highlights of this chapter are summarised as follows:

1- A minimum number of rolling passes is required to reach the steady state of the residual stress field. The residual stress profile needs to be obtained in the steady state region where by further rolling the part, the residual stress state does not change.
2- The DCR process introduces an anisotropic residual stress in the material. The residual stress in the rolling direction (axial) is considerably lower than the stress component perpendicular to the rolling direction (tangential).
3- Under the same ball diameter and pressure level, increasing the feed raises the minimum and surface compressive residual stresses.
4- The developed FE model is able to predict the thermal relaxation of the residual stresses at the region of interest near to surface with a reasonable accuracy while Zener-Wert-Avrami analytical model fails to capture the magnitude and profile of the relaxed residual stress.
5- Thermal relaxation redistributes the residual stresses which leads to a more uniform stress profiles through the depth with less anisotropy of the residual stresses.

4 Design Optimization of Deep Cold Rolling of Ti-6Al-4V for Room and Elevated Temperature Operations

The main objective of this chapter is to identify the cold rolling process parameters on a Ti64 plate to achieve an optimum residual stress profile at room temperature as well as at the elevated temperature of 450 ˚C. As discussed before, the exposure to elevated temperature results in relaxation of the residual stresses induced at the room temperature during the process. In Chapter 3, high-fidelity finite element models have been developed to simulate the deep cold rolling (DCR) process and the residual stress redistribution due to such temperature increase. Conducting optimization directly on the developed high-fidelity finite element (FE) model is not practical due to high computational cost associated with nonlinear dynamic finite element models of DCR process. Here well-established machine learning principles are employed to develop and validate surrogate analytical models to replace the FE models. The developed analytical functions are smooth and explicit functions which can efficiently approximate the residual stress profiles with respect to the process parameters. This is also very beneficial for the formulation of the optimization problems, as responses from nonlinear dynamic finite element models; due to calculation at discrete design points, are typically noisy and render inaccurate optimum solution. A design optimization problem has then been formulated for multi-objective functions considering the fatigue property of the material. A hybrid optimization method, which combines genetic algorithm with sequential quadratic programming techniques, has been utilized to accurately obtain the global optimum solution. It has been shown that the optimal solution depends on the final resultant stress state in the component and operating temperature under the defined duty cycles.

4.1 Nonlinear Finite Element Model

It was discussed in the previous chapter that due to high level of nonlinearity associated with the rolling dynamic, friction contact and plasticity behavior of the material, the use of FE methods to predict the residual stresses introduced by DCR process is inevitable. In this research study, ABAQUS software has been used to develop high-fidelity nonlinear 3D FE models to simulate the DCR process and the subsequent thermal exposure. For the sake of clarity, Figure 3-1 is again repeated in Figure 4-1 which presents the sequence of simulations undertaken to model the DCR

process and the following thermal loading in order to calculate the induced residual stress and its subsequent relaxation during thermal exposure. Detailed information regarding FE modeling can be found in Chapter 3 and only a brief description is presented here.

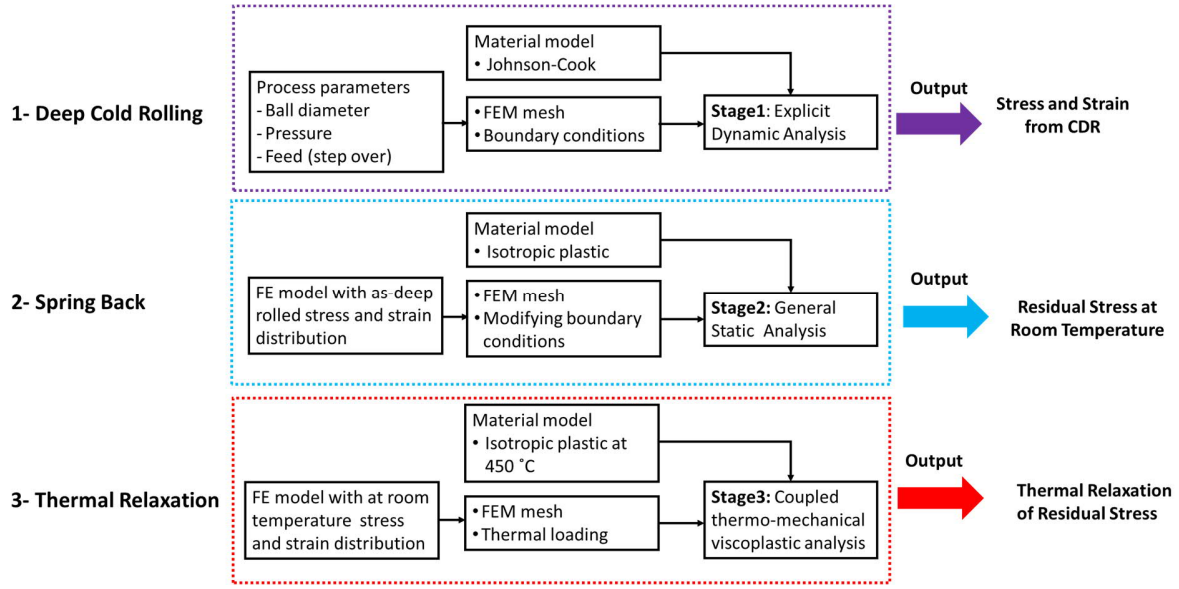

Figure 4-1: Flow chart for the DCR and thermal relaxation simulations.

Figure 4-2 shows the developed 3D FE model of the ball and the work piece in the ABAQUS environment. The workpiece is a Ti64 plate with 1 mm thickness and is meshed with 800,000 C3D8RT elements in the ABAQUS environment. This element is an 8-node thermally coupled brick element which accommodates temperature degree of freedom (DOF) in addition to translational displacement DOFs. Since the experimental measurements show that the DCR process can induce residual stresses with high gradient up to 600µm depth from the surface of the workpiece a very refined mesh (size of 25µm) has been assigned to the surface layer beneath the contact zone in order to achieve accurate results. Nevertheless, in the regions away from the contact zone, coarser elements were used to decrease the number of degrees of freedom and computational costs.

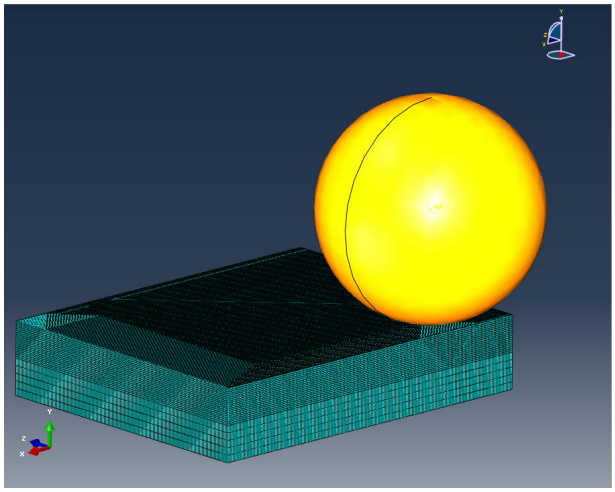

Figure 4-2: Geometric model and mesh of the workpiece in the 3D simulation

The DCR process is modeled in a series of simulation steps until a stable residual stress field is achieved in the contact zone. The roller is assumed to be rigid and its kinematics is defined in four steps by related boundary conditions, namely indentation, rolling, feed and retraction steps. In the indentation step a constant force is applied to the rigid ball to create a small indent on the surface of the specimen in –Y axis. The ball is then allowed to roll freely in the +X direction to complete a pass while the applied force is kept constant. This is followed by moving the ball in lateral direction (+Z) perpendicular to the rolling pass in the amount of feed and then again rolling the pressurized ball but now in –X direction. Based on the amount of feed, overlap would exist between successive rolling passes. Finally, the ball is retracted from the surface in the retraction step.

The residual stress and strain fields calculated at the end of the DCR process are then subsequently considered as initial conditions for the next simulation step which is the spring back analysis and it is modeled using isotropic plasticity behavior of the material at a low strain rate. The outcome of the spring back analysis is the initial state input for the thermal relaxation assessment. In this stage the evolution (relaxation and redistribution) of the residual stresses during the subsequent thermal exposure is modeled through the plastic softening mechanism.

ABAQUS/Explicit environment is used for modeling the DCR process because it can efficiently handle the nonlinearities due to the contact analysis, plastic behavior of the material, dynamic loading and large deformation. Since the spring back and thermal relaxation stages are rather quasi-

static processes, they are analyzed by ABAQUS/Standard package which uses implicit integration methods.

As it was demonstrated in Chapter 3, the residual stress state evolves by preforming each extra pass of the rolling and the state of residual stress (and the displacement) reaches a saturation in a stabilized region where further rolling the workpiece will not alter the residual stress. It was shown that 10 rolling passes; which covers a part of the surface, is enough to develop a stabilized region to extract the results while saving the numerical computation time.

The equivalent stress beneath the ball reaches the yield stress of the workpiece material under a substantial rolling force which results in plastic deformation. A detailed stress analysis of the process reveals a large area of vertical compressive stress directly beneath the rolling ball causing a vertical plastic compression, which leads to plastic extension in the surface of the workpiece. Because of the constant volume of the material, the extension of the surface of the material in one direction, leads to a transverse contraction of the material in the perpendicular directions on the surface as well as in the material beneath the surface layer. This results in lateral displacement of the material surrounding the contact zone and consequently developing residual stresses as a reaction to the plastic material displacements.

Residual stresses induced in the component during DCR process are the result of inhomogeneous plastic deformation. The resultant net material displacement defines the direction of reaction forces by the surrounding materials which indicates the nature (compressive or tensile) of the introduced residual stresses. The plastic deformation mechanism during the DCR process is the superposition of the material displacements in three simultaneous deformation mechanisms, namely the ball rolling (in x direction), the lateral movement of the ball (the feed in z direction) and the vertical movement of the ball (under the rolling force in y direction) in the treated zone.

The dominating plastic deformation direction dictates the material flow in the perpendicular directions. Therefore, under a certain rolling force with a given ball diameter, the sign of the residual stresses in axial and tangential directions can alter depending on the material flow caused by the different amount of feed.

Figures 4-3 and 4-4 respectively show the FE results for predicted residual stresses in axial (σ_{xx}) and tangential (σ_{zz}) directions in the stabilized region for the process parameters of $D=9\ mm$, $f=0.2\ mm$ and $P=20\ MPa$ at both room temperature and 450 ºC using the developed FE model. Figure

4-5 also shows the residual stress profile in axial and tangential directions through the thickness in the stabilized region. As it can be realized, DCR process at room temperature generates significantly different residual stress distribution through the depth in longitudinal and tangential directions and subsequent exposure to elevated temperature causes relaxation and redistribution of the residual stresses.

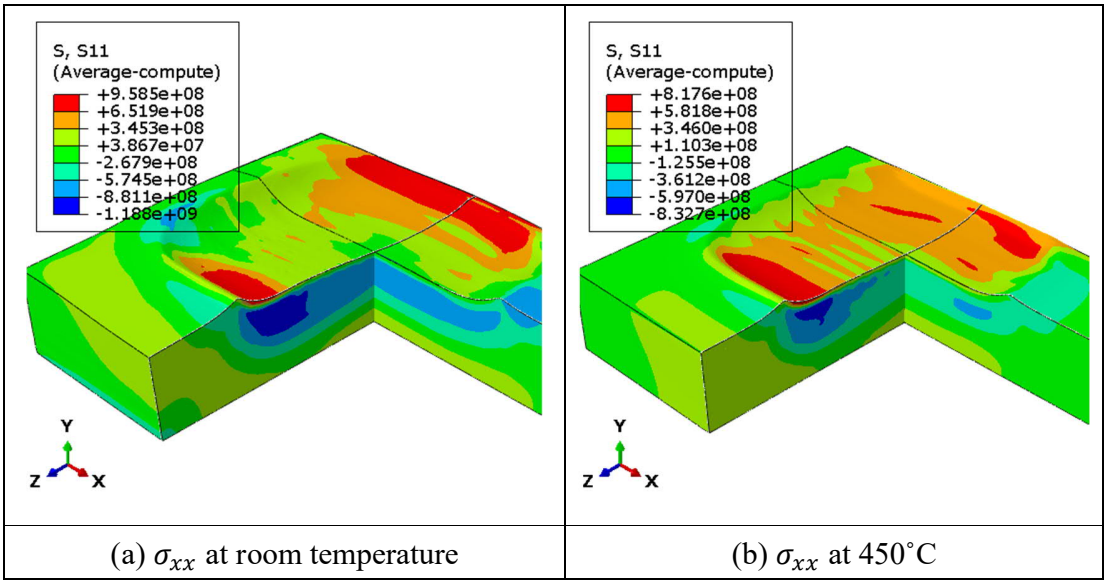

(a) σ_{xx} at room temperature | (b) σ_{xx} at 450˚C

Figure 4-3: Residual stress (Pa) in axial direction (σ_{xx}) sectioned in the stabilized region (a) after spring back at room temperature (b) after thermal relaxation at 450˚C

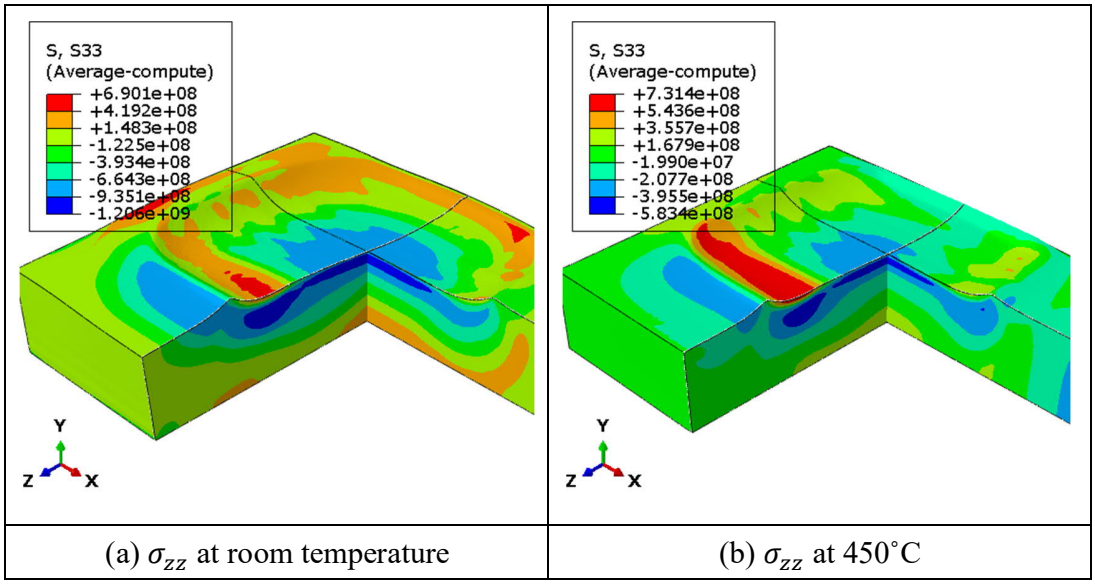

(a) σ_{zz} at room temperature | (b) σ_{zz} at 450˚C

Figure 4-4: Residual stress (Pa) in tangential direction (σ_{zz}) sectioned in the stabilized region (a) after spring back at room temperature (b) after thermal relaxation at 450˚C

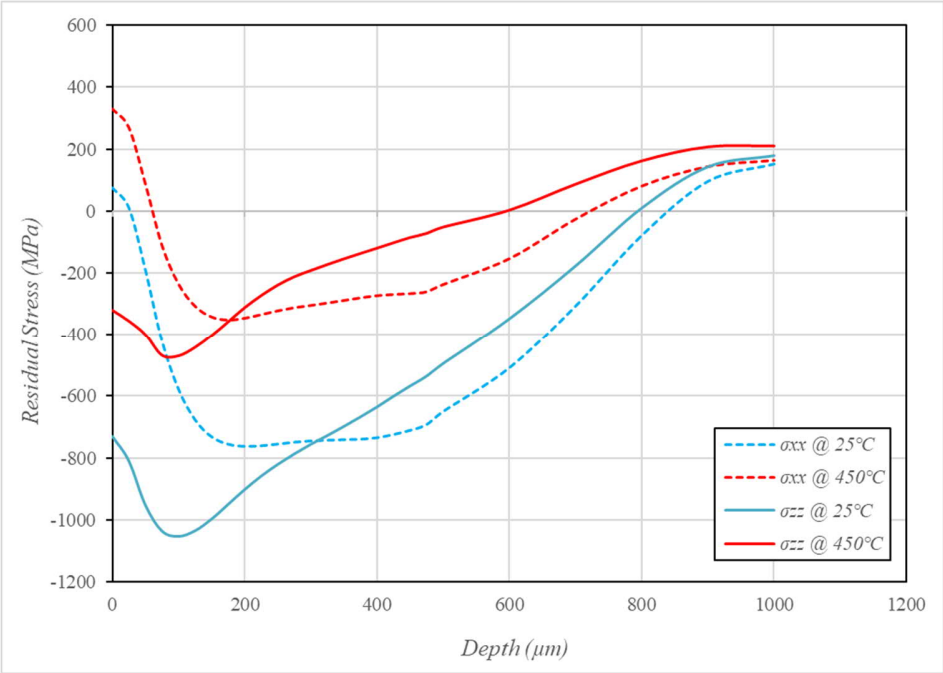

Figure 4-5: Residual stress profile in axial and tangential direction at 25 °C and 450 °C

Examination of Figure 4-5 also reveals that the conventional DCR process generates a large anisotropic biaxial residual stresses in surface layer constrained by balancing tensile stresses in deeper depth. However, the level of anisotropy diminishes by increasing the temperature. The level of anisotropy is rather higher in treatment of thin-walled components where the thickness of the specimen is comparable with the depth of residual stress profiles. The main material flow is attributed to rolling pressure (Y direction) and feed (Z direction), resulting in a significant material contraction in X direction which can lead to a detrimental tensile residual stress in the axial direction. Therefore, in order to benefit from the fatigue enhancement by introducing a deep residual stress in tangential direction, the rolling direction must be perpendicular to the direction of worst principle stress in the component due to external load.

4.2 Design of Experiments and Surrogate Models

The residual stress profile and the distribution of dislocation density induced by DCR highly depend upon the process parameters such as ball size, rolling pressure, feed and the rolling speed. As mentioned in Chapter 3, the previous experimental and numerical research works have unanimously confirmed that the impact of the rolling speed on the residual stress is negligible [9,

11, 52, 82]. Therefore, the ball diameter D (*6-12 mm*), feed f (*0.05-0.20 mm*) and fluid pressure P (*10-30 MPa*) are considered as design variables (design features) in this research study.

Simulation run time of each DCR process and the following spring back and thermal relaxation analysis took more than a week for about 197 hours to complete on a computer with four core i7 2.70 GHz CPU and 64 GB available RAM. As it can be realized, exploring the whole design space and more importantly performing design optimization of the process parameters on the residual stress profiles using FE simulation models is computationally very expensive and impractical.

Recent advances in machine learning techniques over the last decade have established a systematic framework for developing surrogate models [94]. This broad class of approaches, which includes regression-based response surface methods (RSM) [80, 81], neural networks (NN) and support vector machines (SVM) [95], is starting to have a wide industrial application in development of efficient and practical predictive tools based on FE simulation results.

Considering high computational cost associated with execution of full FE model and its utilization in design optimization problems, in this research study surrogate models have been developed based on results generated by the developed full FE on a sample of input design points identified by the DoE technique in the design space. The surrogate models can approximate the responses of interest to a certain level of accuracy with respect to the design variables, and they are significantly lower in order than a full-scale finite element simulation.

DoE generally refers to a collection of statistical techniques that maximizes the knowledge gained from the minimum number of simulations by identifying the best positions of the design points in the design domain to run the FE analysis [80, 81]. Central Composite Design (CCD) and Box–Behnken are the main DoE techniques implemented in Mintab© software to perform RSM. Optimal design such as A-optimal, D-optimal, V- optimal and G-optimal can also be used to reduce the number of design points if the original design contains more points than feasible to conduct the experiments (or simulations) [96].

Regression-based behavioral models are developed in the current study, to approximate residual stress profiles induced by DCR process after the spring back at the room temperature and after thermal relaxation due to the following exposure to elevated temperature. Multiple surrogate models have been trained on results obtained from the 3D non-linear FE models, to develop low-order predictive models. The accurate and low-order surrogate models represent a suitable

substitute for the FE modeling, enabling rapid residual stress computation outside the ABAQUS environment to investigate the effect of several process parameters simultaneously and incorporation into a design optimization scheme.

The advantage of the proposed methodology is twofold. First it allows to efficiently investigate the effect of several process parameters on induced residual stresses simultaneously without the need to run computationally very expensive high-fidelity FE model; and second, the developed surrogate response functions can be effectively and efficiently utilized to formulate a formal design optimization problem to identify the optimal process parameters without the need to execute the FE model during each optimization iteration. Using the full high-fidelity nonlinear dynamic FE model in optimization formulation is computationally very expensive as during each optimization iteration the FE model may be called many times to evaluate the objective function and design constraints. Besides the nonlinear FE model itself requires many iterations to converge to an accurate solution due to associated high material and geometrical nonlinearity. Moreover, direct responses from nonlinear dynamic FE results are typically noisy as they are calculated at discrete points over the design space. Thus, calculating the derivatives of the objective functions or design constraints which are required for gradient based optimization algorithms can be erroneous if not impossible.

RSM is one of the mathematically proven regression techniques to establish surrogate models, which describes the statistical relationship between the measured or simulated response variables and input design parameters. This method finds the best analytical function based on a given training data set to approximate the response of a system. The input data set for the finite element analysis has been identified using Design of Experiments (DoE) which intelligently selects design points (in other word training data set) in the design domain.

The design variables in the current study as discussed before are the ball diameter D (*6-12 mm*), the feed f (0.0*5-0.20 mm*) and the fluid pressure P (*10-30 MPa*). Here full CCD technique has been utilized to identify the 15 optimally located design points in the design space. Table 4-1 presents the identified design points and associated desired responses predicted by the FE model at both room and elevated temperature of 450 ºC.

As provided in Table 4-1, the desired output responses are the summation of the area under residual stress profile in tangential direction, i.e. $Area = A_{(-)} + A_{(+)}$ as shown in Figure 2-1 in Chapter

2, equivalent plastic strain in the material (PEEQ, ε_{eq}) on the surface, the tangential residual stresses (σ_{0zz}) and ($\sigma_{Max\,zz}$) evaluated on the surface and in (Y_{Max}), respectively.

Table 4-1: Design points (training data set) and the FE results

D *(mm)*	*f* *(mm)*	*P* *(MPa)*	$(\sigma_{0zz})_{RT}$ *(MPa)*	$(\sigma_{Max\,zz})_{RT}$ *(MPa)*	$(Area)_{RT}$ *(MPa.m)*	$(\sigma_{0zz})_{450}$ *(MPa)*	$(\sigma_{Max\,zz})_{450}$ *(MPa)*	$(Area)_{450}$ *(MPa.m)*	(ε_{eq}) *(μm/μm)*
6	0.050	10	186	371	0.0237	318	326	0.1063	0.04463
6	0.200	10	-363	173	-0.1472	-306	94	-0.1106	0.03442
6	0.050	30	-94	294	-0.1693	201	282	0.0330	0.15444
6	0.200	30	-924	189	-0.4596	-568	144	-0.2503	0.23832
6	0.125	20	-718	317	-0.1365	-334	276	0.0304	0.11701
9	0.050	20	56	186	-0.3202	309	229	-0.0630	0.13080
9	0.200	20	-731	180	-0.5462	-320	210	-0.3280	0.16830
9	0.125	10	-142	270	-0.1511	126	248	0.0231	0.05387
9	0.125	30	-525	103	-0.3467	-228	216	-0.0843	0.19184
9	0.125	20	-479	257	-0.2851	-120	253	-0.0337	0.12894
12	0.050	10	198	251	-0.2976	370	219	-0.1008	0.07859
12	0.200	10	-250	132	-0.5009	-81	83	-0.3006	0.07269
12	0.050	30	-163	-110	-0.6164	85	103	-0.3022	0.26652
12	0.200	30	-432	-119	-0.6887	-170	130	-0.3467	0.28210
12	0.125	20	-295	45	-0.3154	-17	268	0.0032	0.15718

These output responses are explained below:

- *Area* is the summation of the total area under the tangential residual stress profile through the thickness of the component and calculated using both negative and positive areas of the stress components throughout the thickness in *z* direction. In other words, according to Figure 2-1(b) in Chapter 2, $Area = \left[\left(A_{(+)} + A_{(-)}\right)_{\sigma_{zz}}\right]$. $(Area)_{RT}$ and $(Area)_{450}$ basically represent the area associated with room temperature and 450 °C, respectively. The objective is to minimize $(Area)_{RT}$ for room temperature and minimize $(Area)_{450}$ for elevated temperature applications. It is noted that since this response variable is the summation of negative and positive areas, minimizing it will make negative part (compressive) larger and the positive part (tensile) smaller.

- The tangential residual stress components on the surface of the workpiece which is represented by $(\sigma_{0zz})_{RT}$ at room temperature and $(\sigma_{0zz})_{450}$ at 450˚C. The objective is also to minimize these residual stresses on the surface.
- The maximum residual stress σ_{max} located at $Y = Y_{max}$ in tangential direction and represented by $(\sigma_{Max\ zz})_{RT}$ and $(\sigma_{Max\ zz})_{450}$ at room temperature and 450℃, respectively. The balancing tensile stress will be maintained below a certain limit defined based on the high cycle fatigue (HCF) endurance of the material.
- The Equivalent Plastic Strain (ε_{eq}) on the surface will maintain below a certain limit defined by the low cycle fatigue (LCF) strength of the material at 10,000 cycles. This will ensure that the induced residual stress will not deteriorate the LCF life.

As mentioned before, RSM combined with DoE is utilized to develop approximate surrogate models by minimizing the error of the approximation between full finite element model and surrogate functions in the design space. The RSM-based responses are smooth and explicit functions with respect to selected design variables, so they can be efficiently analyzed and employed in any gradient-based and derivative-free optimization algorithms [80]. The RSM-based approximate response can be written as:

$$\widehat{\boldsymbol{y}} = \boldsymbol{X}\,\boldsymbol{\beta} \tag{4-1}$$

where X is the design matrix with the size of $n \times m$, in which the n is the number of training examples (here finite element runs) and m is the number of unknown coefficient parameters of the model, β. The approximate response, $\hat{y}$, differs from the exact response, y, (the direct results of the finite element model) which can be expressed as:

$$y = \hat{y}(x_1, x_2, \dots\dots, x_n) + \varepsilon \tag{4-2}$$

where x_i are the identified design variables (design feature) and ε represents the error between the exact response y and its approximation $\hat{y}$. The polynomial functions are generally utilized to establish the RSM regression model as [97]:

$$\hat{y} = \beta_0 + \sum_{i=1}^{n} \beta_i x_i + \sum_{i=1}^{n} \sum_{j=i+1}^{n} \beta_{ij}\, x_i\, x_j + \sum_{i=1}^{n} \beta_{ii} x_i^2 + \cdots \tag{4-3}$$

The problem can be basically formulated as a structured supervised machine learning problem, where a regression model can be trained and validated using the experimental or simulation data. The coefficients of approximate polynomial response function in Eq. (4-3) can be identified using the least square technique aiming at minimize the summation of the square error between approximate and known exact responses obtained from the RSM response and FE simulation, respectively over the entire training set. The accuracy of the developed approximate analytical models is examined by R^2 (i.e. R-Squared) which is also known as the coefficient of determination, or the coefficient of multiple determination for multiple regression. R^2 is a statistical measure of how close the simulation or experimental data are to the fitted regression models and is always between 0 and 100%. In general, a model with a higher R^2 better fits the data and 100% indicates that the model explains all the variability of the response data around its mean over the entire design space. The coefficient of determination, R^2, can be presented as:

$$R^2 = 1 - \frac{SSE}{SST} \quad where$$
$$SSE = \sum_{i=1}^{n} (y_i - \hat{y}_i)^2, \qquad SST = \sum_{i=1}^{n} (y_i - \bar{y})^2 \tag{4-4}$$

It can be realized from Eq.(4-3) that a number of different types of polynomial such as the linear, quadratic and cubic functions can be utilized to develop the approximate models. In this research study, a full quadratic model was considered for the response surface functions as R^2 value over 90% can be achieved without overfitting the training data set by higher order polynomials.

The obtained quadratic response surface functions for the desired output responses are presented in Eqs.(4-5) to (4-11). Table 4-2 also summarizes the R^2 values of the developed surrogate models which show the high accuracy of the models to approximate the responses of interest.

$$(\sigma_{0zz})_{RT} = 1355 + 27 * D - 13236 * f - 85.1 * P - 3.61 * D * D + 24312 * f^2 + 1.407 * P^2 + 368 * D * f + 1.24 * D * P \tag{4-5}$$

$$(\sigma_{Max\,zz})_{RT} = 160 + 85 * D - 2127 * f + 8.12 * P - 4.96 * D^2 + 97.1 * D * f - 2.299 * D * P \tag{4-6}$$

$$(Area)_{RT} = 0.554 - 0.0882 + 1.363 * f - 0.01942 * P + 0.00310 * D^2 - 9.59 * f^2 + 0.000301 * P^2 - 0.000364 * D * P \quad (4\text{-}7)$$

$$(\sigma_{0zz})_{450} = 1174 - 18.6 * D - 9709 * f - 41.1 * P + 9832 * f^2 + 0.750 * D^2 + 382 * D * f \quad (4\text{-}8)$$

$$(\sigma_{Max\ zz})_{450} = 696 - 78.3 * D + 1147 * f - 6.31 * D + 2.76 * D^2 - 16576 * f^2 + 144.6 * D * f + 42.9 * f * P \quad (4\text{-}9)$$

$$(Area)_{450} = 0.0796 - 0.00802 * D + 1.684 * f + 0.00037 * P - 11.14 * f^2 - 0.000505 * D * P \quad (4\text{-}10)$$

$$(\varepsilon_{eq}) = 0.0182 + 0.00197 * D - 0.994 * f + 0.00295 * P + 3.08 * f^2 + 0.000348 * D * P + 0.01926 * f * P \quad (4\text{-}11)$$

Table 4-2: R^2 values of the developed surrogate models

$(\sigma_{0zz})_{RT}$	$(\sigma_{Max\ zz})_{RT}$	$(Area)_{RT}$	$(\sigma_{0zz})_{450}$	$(\sigma_{Max\ zz})_{450}$	$(Area)_{450}$	(ε_{eq})
94.3%	96.0%	98.2%	94.5%	95.7%	92.8%	97.4%

The sensitivity analysis of output responses with respect to variation in input design variables using the above developed response functions is discussed in the following section.

4.3 Parametric Study

Figure 4-6 (a) shows the variation of the $(\sigma_{0zz})_{RT}$ with respect to rolling pressure and feed for the given ball diameter *D=6 mm*. It can be realized that at any given ball diameter, the effect of the feed on $(\sigma_{0zz})_{RT}$ is more significant than the pressure which is mainly due to the dominating impact of feed on plastic deformation and thus the residual stress in the tangential direction. The most compressive tangential residual stress occurs at the upper boundary of the variables. A similar parabolic behavior of $(\sigma_{0zz})_{RT}$ with respect to feed under a given ball diameter and rolling pressure, has also been previously reported for conventional deep rolling of Ti64 [7, 22] and AISI1045 [90].

The effect of the thermal relaxation on σ_{0zz} is shown in Figure 4-6 (b) where the variation of $(\sigma_{0zz})_{450}$ is presented. The most compressive tangential residuals stress is achieved at the upper

bound of the feed and rolling pressure variables which is similar to the behavior observed at room temperature. Comparing the surface plots of $(\sigma_{0zz})_{RT}$ and $(\sigma_{0zz})_{450}$ reveals that by increasing the design variables the level of thermal relaxation increases which is due to higher dislocation. This is in agreement with the experimental findings where surface layers with medium dislocation density show a better thermal stability of residual stresses compared with surface layers with extremely high dislocation densities [14, 22]. Further examination of the results also reveals that due to thermal relaxation, the residual stress can alter from compressive to tensile at lower feed as the plastic deformation in tangential direction is not high enough to maintain a compressive residual stress at elevated temperature.

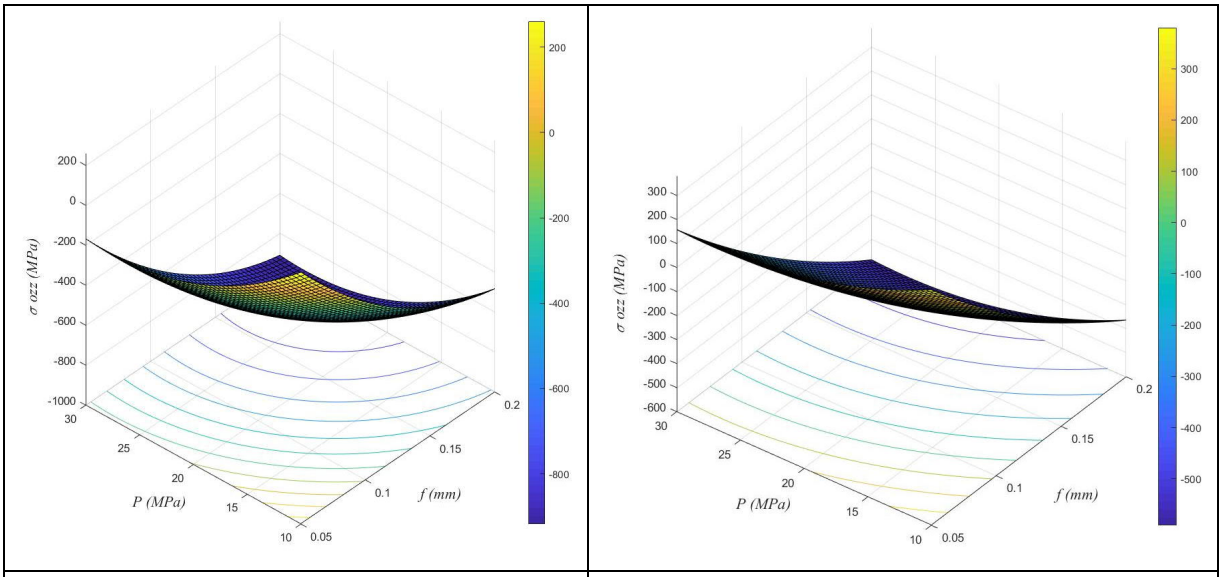

(a) (b)

Figure 4-6: Effect of the rolling pressure and feed on the surface residual stress in tangential direction (σ_{0zz}) for *D=6mm* (a) at room temperature 25°C, and (b) at elevated temperature 450 °C

Figure 4-7 shows the surface plot of $(\sigma_{\max})_{zz}$ at room temperature (a) and elevated temperature (b), with respect to rolling pressure and ball diameter for the given feed *f=0.125 mm*. A small ball diameter generates a high localized plastic deformation resulting in compressive residual stress closer to the surface. The plastic deformation, however, decays faster through the depth resulting in a smaller Y_{min} , Y_0 and Y_{max} (shown in Figure 2-1) and thus creating a higher balancing tensile stress as it can be observed in Figure 4-7(a). Moreover as it can be realized, at lower bound of ball diameter where the induced localized compressive residual stress on the surface does not influence over the complete thickness and $(\sigma_{min})_{zz}$ occurs closer to the surface, increasing the rolling

pressure increases the balancing tensile stress which agrees with understanding from Hertzian contact stress. On the other hand, deep rolling a thin plate with larger ball diameters creates a lower compressive residual but deeper in the thickness and as a result the balancing residual stress decreases when higher rolling pressure is applied.

Redistribution and rebalancing of the residual stress beside softening of the material is clearly observed in Figure 4-7(b) depending on the ball size. The material softening is more dominant at medium size ball where the compressive residual stress is neither high nor deep. While in the lower and upper bounds, redistribution and rebalancing the stresses are more significant which is due to thermal relaxation of a high but shallow compressive residual stress in small ball diameter; and low but deep compressive residual stress due to large ball size.

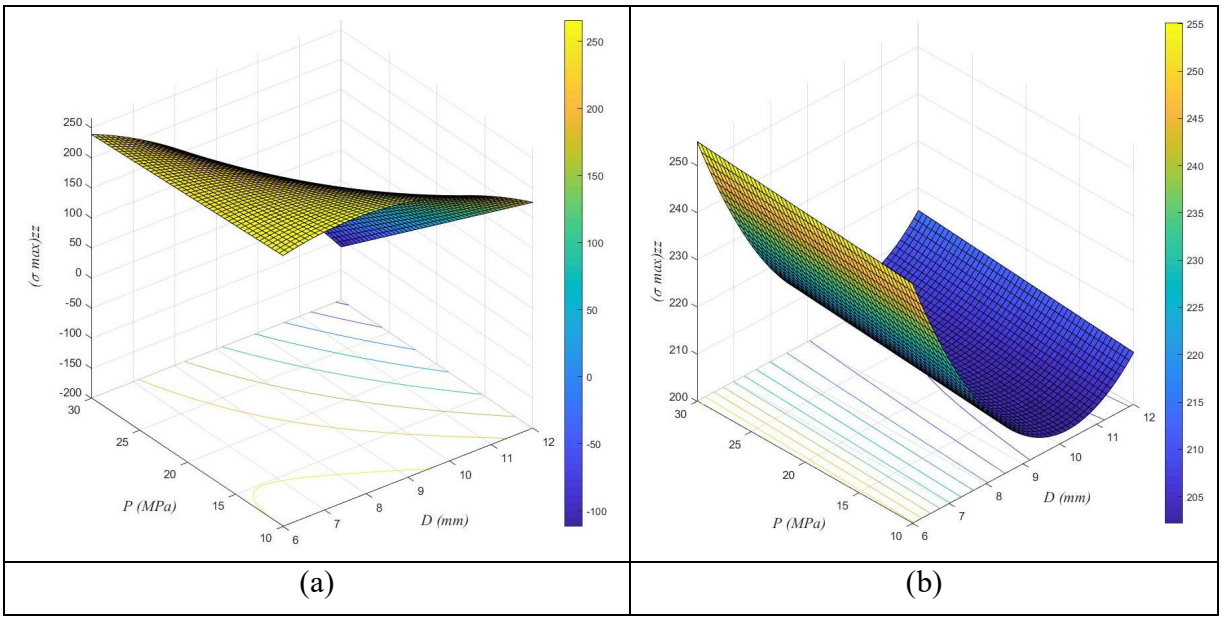

Figure 4-7: Effect of the rolling pressure and ball diameter on the balancing residual stress in tangential direction $(\sigma_{\max})_{zz}$ for *f=0.125 mm* (a) at room temperature 25°C, and (b) at elevated temperature 450 °C

The effects of ball diameter and rolling pressure on total area of the residual stress profile given feed of *f=0.125 mm* are shown in Figure 4-8(a) and (b) for room and 450 ℃ temperature, respectively. As the surface plots show the most negative total area occur at the higher bound of the ball diameter and rolling pressure variables for both room and elevated temperature. When the process is performed using lower bound of the variables, the induced compressive residual stress is not deep nor high enough and thus exposure to the elevated temperature leads to relaxation of

the compressive residual stresses which can be observed as very low positive values of $(Area)_{450}$ in Figure 4-8(b).

The effect of ball diameter and rolling pressure on (ε_{eq}) has been investigated for the given feed of *0.125 mm* and presented in Figure 4-9(a). Results clearly show that for the given feed, increasing the rolling pressue and ball diameter increases the plastic deformation on the surface and the effcet of pressure is more significant than the ball diameter. The effect of rolling pressure and feed on the equivalent palstic deformation on the surface for the given ball diameter of 6 mm is also demonstrated in Figure 4-9(b). As expected, results show that the maxium plastic deformation on the surface is achieved at the upper bound of pressure and feed design variables. As it can be realized the effect of feed becomes more dominant at higher pressure level.

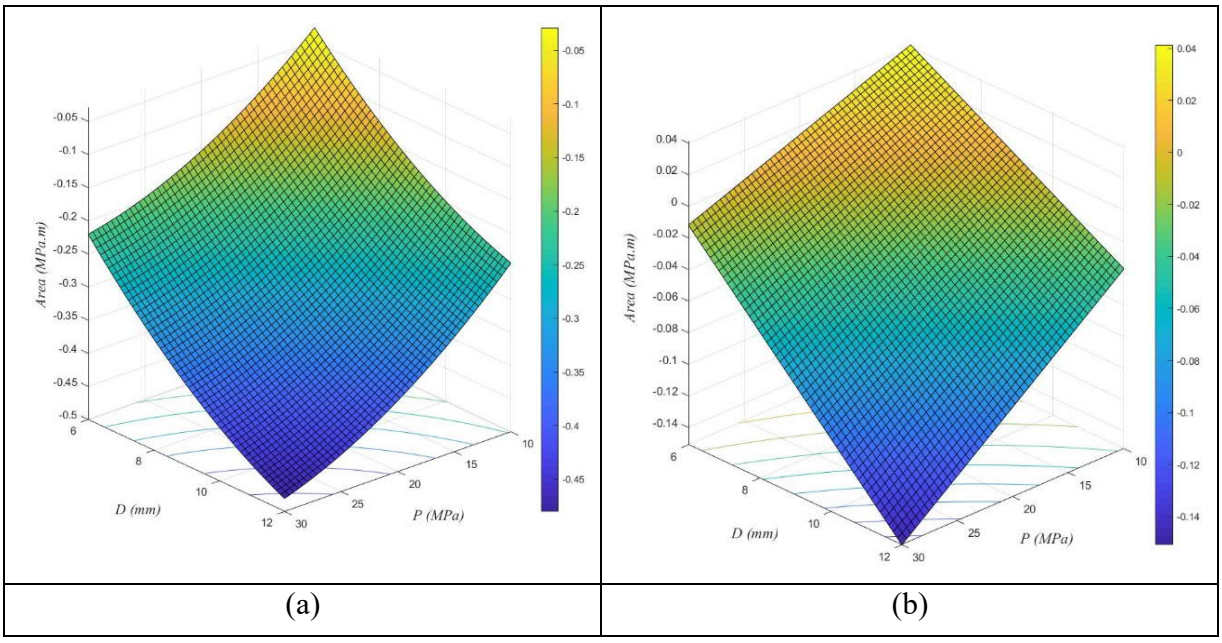

(a) (b)

Figure 4-8: Effect of the rolling pressure and ball diameter on total area of the residual stress profile *(Area)* for *f=0.125 mm* (a) at room temperature 25°C, and (b) at elevated temperature 450 °C

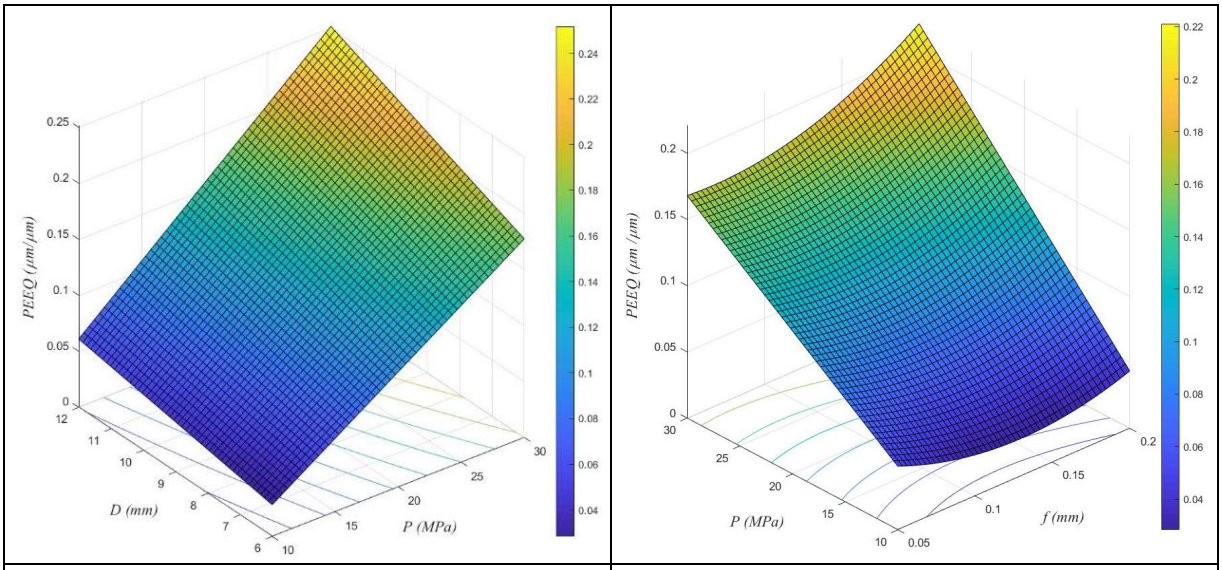

(a) (b)

Figure 4-9: Response surface of equivalent plastic deformation (ε_{eq}) with respect to process parameters (a) for constant feed *0.125 mm*, and (b) for constant ball diameter *6 mm*.

4.4 Optimization Problem

The ultimate objective of DCR is to improve fatigue life of a component by creating a deep compressive residual stress and plastic hardening in the surface layer of the component at the room temperature. The experimental results show that the affected depth of the surface treatment (i,e, the depth of compressive residual stresses and strain hardening) has a significant effect on the fatigue enhancement of the treated component [3]. However, the optimal profile of the induced residual stress strongly depends on the state of stress distribution due to the applied external load. A deep residual stress is more essential in components subjected to a push-pull loading than in parts under bending or torsional loads with high stress gradients where a more comprehensive stress on the surface layer is beneficial [19].

As discussed before, optimal selections of the process parameters in thin-walled components where the depth of the residual stress is comparable with the thickness of the component is more crucial as the process can easily result in a tensile residual stress in the surface layer [11]. In addition, the exposure of the deep cold rolled components to elevated temperature relaxes and redistributes the residual stress induced by the DCR process at the room temperature [3, 7, 16]. Therefore, identifying optimal process parameters to achieve an optimal residual stress profile at the room temperature does not necessarily result in the most optimum solution for operations at

elevated temperatures. The fatigue enhancement is a mandated process requirement that should not be compromised because of maltreatment of the component. Therefore, the impact of the process parameters on the fatigue life of Ti64 needs to be considered in formulating the optimization problem.

It was discussed in section 2.3 that crack nucleation in deep-rolled Ti64 specimens in the HCF regime occurs in regions of peak tensile residual stress. Thus, appropriate constraints based on fatigue endurance of the material needs to be considered in the DCR process in order to mitigate the detrimental effect of tensile residual stress on HCF life. Since Ti64 also shows Anomalous Mean stress Sensitivities (AMSS), the effect of mean stress; including the balancing tensile residual stress caused by DCR, on the fatigue life cannot be explained by the conventional fatigue life approaches [98]. As an alternative approach, Smith, Watson and Topper (SWT) and Manson-Coffin techniques will be respectively implemented to describe the HCF and LCF strength of the deep-rolled Ti64.

SWT is a well-used strain based fatigue assessment method in which a single stress-strain function is used to combine the effects of mean stress and alternating strain as [98]:

$$\sqrt{\sigma_{max}\varepsilon_a E} = constant \tag{4-12}$$

where σ_{max}, ε_a and E are maximum stress, alternating strain and module of elasticity of the material, respectively. Also one can write:

$$\sqrt{\sigma_{max}\sigma_a} = S_e \tag{4-13}$$

where S_e is the fatigue endurance of the material and σ_a is the alternating stress. Thus, the Eq. (4-13) can be rewritten as:

$$(\sigma_{mean} + \sigma_{Residual} + \sigma_a) * \sigma_a = (S_e)^2 \tag{4-14}$$

where σ_{mean} and σ_a represent the mean and alternating stresses due to repeated external loading , and $\sigma_{Residual}$ is the induced residual stress during the process. The fatigue endurance of untreated Ti64 under fully reversed axial load ($\sigma_{mean} = 0$) , S_e, at 25°C and 450°C has been reported to be 380 MPa [8] and 200 MPa [99] , respectively. In the current study, the maximum balancing residual stress generated by the process is limited to the half of the fatigue endurance i.e. 190 MPa and 100 MPa for operation at room temperature and 450°C, respectively.

As mentioned before the LCF life of deep-rolled Ti64 shows a strong correlation with the accumulated plastic strain during the cycles, and the cracks are initiated on the surface and propagates toward the interior. On the other hand, the residual stresses are the result of substantial plastic deformation caused by the process in the surface layer. However, the level of plastic strain induced by the process needs to be controlled to prevent over consumption of accumulated plastic strain and introducing unnecessary cumulative damage due to the process. Therefore, the amount of plastic strain based on fatigue properties of the component is considered as another constraint function in the current study in order to prevent compromising the LCF life.

Based on Coffin-Manson model, damage of material under LCF is correlated to cyclic plastic strain amplitude [8, 100]. Manson-Coffin relates the plastic strain amplitude as a function of the number of cycles to failure in LCF-regime as given by Eq. (4-15)

$$\varepsilon_P = aN^b \tag{4-15}$$

where ε_P and N represent the amount of equivalent plastic strain and the number of cycles to failure, respectively. It is noted that $\log(\varepsilon_P) = \log(a) + b\log(N)$ which is a linear line used to evaluate parameters a and b using experimental data provided in log-log scale. Figure 4-10 shows the experimental data together with linear line models in log-log plot of the plastic strain amplitude with respect to number of cycles to failure for treated and deep-rolled Ti64 at different ambient temperatures published by Altenberger et. al [8]. The values of a and b have been obtained by least-square minimization and provided for deep-rolled Ti64 alloys which are presented in Table 4-3.

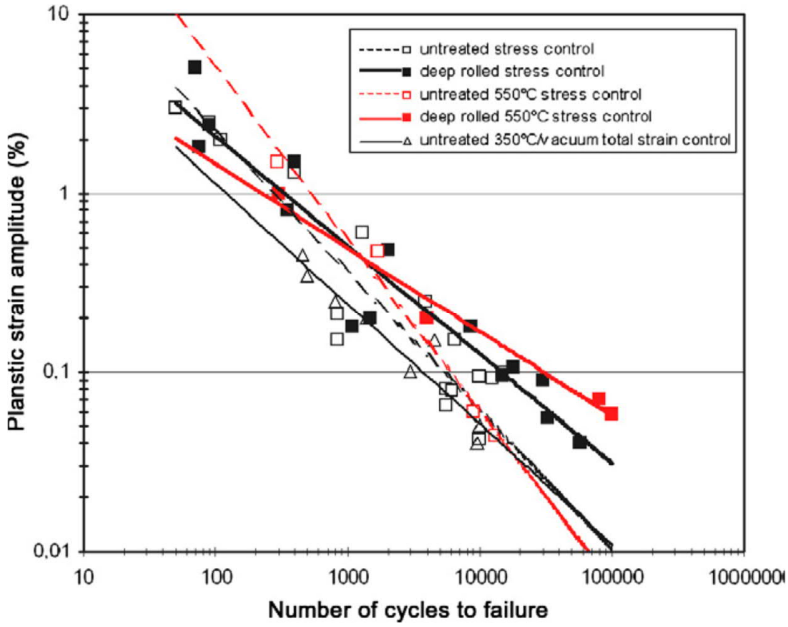

Figure 4-10: Manson-Coffin-plot for deep-rolled and untreated Ti–6Al–4V at room temperature and elevated temperature [8]

Table 4-3: Manson-Coffin coefficients [8]

Temperature (°C)	a	b
22	34.47	-0.61
550	12.67	-0.47

Although the coefficients have been provided only at 550°C, based on the authors' arguments in the same reference [8], the coefficients at 450°C should be very similar to what has been presented for 550 °C. Considering Table 4-3 and Eq. (4-15), the cumulative plastic deformation to failure at 10,000 cycles (here defined by ε_f') at 25 and 450°C are found to be 0.125 and 0.167 (µm/µm), respectively.

Using the constraint functions established based on the fatigue properties of Ti64, a design optimization strategy has been proposed here to find the optimum process parameters to achieve an optimum residual stress distribution not only at the room temperature but also at elevated temperature considering the impacts on the fatigue life, which to the best of our knowledge has not been previously addressed. The optimal solutions obtained at each of the ambient temperatures are then compared.

The depth and magnitude of the residual stress profile is optimized by minimizing a multi-objective function which considers surface residual stress in tangential direction and the

summation of the area of induced compressive and tensile residual stresses throughout the thickness of the workpiece. The tangential residual stress at $Y = Y_{max}$ and plastic strain on the surface will be considered as constraint functions to prevent undesirable impact of the DCR process on fatigue strength of the material. It is assumed that the component is under a uniaxial external loading imposing a maximum principle stress in the Z direction.

The proposed multi-objective design optimization problem can be formally formulated as:

$$\begin{aligned} &minimize\ the\ function && w_1\ Area + w_2(\sigma_0)_{zz} \\ &Subject\ to\ the\ constarint && (\sigma_{max})_{zz} \leq 0.5\ S_e \\ & && (\varepsilon_p)_0 \leq 0.08\ \mu m/\mu m \\ & && 6\ mm \leq D \leq 12\ mm \\ & && 0.05\ mm \leq f \leq 0.2\ mm \\ & && 10\ MPa \leq P \leq 30\ MPa \end{aligned} \tag{4-16}$$

where S_e as explained before is the fatigue endurance of Ti64 which will be adopted according to the operating temperature considered in the optimization problem. The constraint functions prevent the over utilization of the fatigue endurance in HCF regime due to high levels of tensile $(\sigma_{max})_{zz}$ and over consumption of ε_f' due to high level of plastic deformation induced by the process on the surface of the component i.e.$(\varepsilon_p)_0$. The proposed objective function can be tailored based on the stress distribution in the plate due to the external applied loading and temperature. Based on the fundamentals of mechanics of material, the weighting factors presented in Table 4-4 could be considered in the optimization problem according to the expected stress distribution due to external loads. The impact of the tangential residual stress in the final state is pronounced by assigning high weighting factor, in applications where a high gradient unidirectional stress distribution (bending) is expected.

Table 4-4: Assigned weighting factors in the optimization problem

Type of loading	w_1	w_2
Bending	0	1
Uniform axial	1	0
Combined	$w_1 > 0$	$1 - w_1$

It should be noted that the developed analytical response functions given in Eqs. (4-5)-(4-11) can be effectively used to establish the objective and constrain functions presented in Eq. (4-16) analytically and explicitly with respect to the design variables at both 25 ºC and 450 ºC operating temperatures. Considering this, the optimization problem formulated in Eq. (4-16) can be efficiently solved using gradient based optimization algorithms.

The sequential quadratic programming (SQP) technique is a powerful nonlinear mathematical programming technique which is capable of capturing a local optimum solution accurately. SQP is a local optimizer without any mechanism to search for global solution. Executing SQP with different initial points may generally result in different local optimum solution in a multimodal nonconvex problem. Here first SQP algorithm in the MATLAB optimization toolbox has been utilized to solve the optimization problem. To catch the global optimum solution, a computer code was written to generate random initial points across the design domain and then the optimization problem was executed for each randomly generated initial point. The optimal objective functions, obtained from each initial point, are then compared in a loop and a minimum value with the corresponding design variables are reported as the solution of the optimization problem.

As number of random points increases the chance to catch the global optimal solution increases. Thus, a sensitivity analysis was performed on the impact of the numbers of random points on the identified global optimum solution. It is found that results for the number of random points above 1000 were identical in all cases.

Next to assure the optimum solution captured by SQP is a true global optimum solution, genetic algorithm (GA), which is a widely used and popular stochastic-based global optimizer has been utilized in combination with SQP algorithm. In this hybrid method, instead of providing large number of random initial points for SQP, the optimal solutions from GA which is in neighborhood of the true global optimum solution are forwarded as the initial points to the SQP method in order to accurately capture the global optimal solutions. This method has been successfully employed in design optimization of multiphysics problem where finding a global solution was not analytically guaranteed [80]. Figure 4-11 shows the flowchart of the proposed design optimization process.

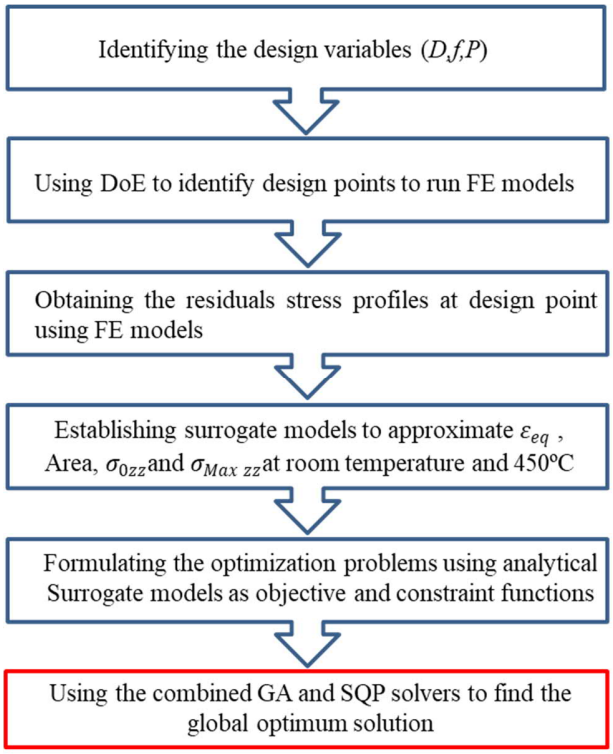

Figure 4-11: Design optimization procedure

4.5 Results and Discussion

Design optimization problem formulated in the previous section has been used to obtain the optimum set of design variables (i.e. ball diameter, rolling pressure, and rolling feed) in order to achieve an optimal residual stress profile at room and at elevated temperature of 450°C. The optimization problems were solved first by SQP using the 1000 randomly generated initial points and then using GA combined with SQP method. Optimum results found to be identical for all cases. The optimization results are presented in Table 4-5 for different weighting factors, at ambient temperature of 25°C.

Table 4-5: Optimization results at 25 °C based on constraint functions $(\sigma_{\max})_{zz} < 190\ MPa$ and $\varepsilon_{eq} < 0.08$

w_1	w_2	D *(mm)*	f *(mm)*	P *(MPa)*	$(\sigma_{0zz})_{RT}$ *(MPa)*	$(Area)_{RT}$ *(MPa.m)*	$(\sigma_{max\ zz})_{RT}$ *(MPa)*	ε_{eq} *(μm/μm)*
1	0	12.00	0.200	10.36	-209	-0.3832	141	0.08
0	1	10.22	0.188	11.82	-327	-0.3377	190	0.08
0.5	0.5	9.96	0.200	11.47	-326	-0.3526	190	0.08

As it can be realized the optimal set of parameters depends on the specific duty cycle defined for the component. The optimization results also show that when the objective is to reach a high compressive tangential stress on the surface (larger weighting factor, w_2) selecting a correct optimal rolling pressure is important which is somewhere between lower and upper bounds and not on the boundary. Based on the understandings from the fundamentals of contact mechanics it is expected to achieve the maximum depth of the residual stress with higher rolling pressure which does not agree with the results provided in Table 4-5. However, as the constraint functions are active in considered loading conditions, it appears that the allowable level of rolling pressure is limited by the constraints. To demonstrate this fact, the optimization problem was solved without constraint functions and optimal results are presented in Table 4-6. As it can be realized rolling pressure reaches the upper limit when the constraint on the plastic strain is removed. However, as it can be realized for all cases the level of ε_{eq} is very high.

Table 4-6: Unconstrained optimization results at 25 °C

w_1	w_2	D *(mm)*	f *(mm)*	P *(MPa)*	$(\sigma_{0zz})_{RT}$ *(MPa)*	$(Area)_{RT}$ *(MPa.m)*	$(\sigma_{maxzz})_{RT}$ *(MPa)*	ε_{eq} *(μm/μm)*
1	0	12.00	0.200	30.00	-473	-0.6117	-110	0.2956
0	1	6.00	0.200	27.60	-918	-0.3416	211	0.1998
0.5	0.5	7.64	0.200	29.41	-769	-0.4427	162	0.2360

The optimization problem was then solved for elevated temperature 450℃ using the relevant objective and constraint functions provided in Section 4.2 and the results are presented in Table 4-7. Comparing results in Table 4-7 with those in Table 4-5, it can be realized that the service temperature changes the optimal design variables. For further clarification, the desired output responses at 450℃ have been evaluated using the optimal design process parameters (optimal *D, f* and *P*) obtained at room temperature and compared with those optimal values obtained at 450 ℃ and results are provided in Table 4-8. As it can be realized optimal results obtained at room temperature while provides optimal distribution of residual stress at room temperature, it generates a residual stress distribution at the elevated temperature of 450 ℃ which might not be the most optimal solution. For example, the optimization for bending load (i.e. $w_1 = 0$) solved at room temperature results in $(\sigma_{0zz})_{450}$ of -141 MPa which is significantly lower than -459 MPa achieved by optimization at elevated temperature.

Table 4-7: Optimization results at 450 ºC based on constraint function $(\sigma_{\max})_{zz} < 100\ MPa$ and $\varepsilon_{eq} < 0.08$

w_1	w_2	D *(mm)*	f *(mm)*	P *(MPa)*	$(\sigma_{0zz})_{450}$ *(MPa)*	$(Area)_{450}$ *(MPa.m)*	$(\sigma_{max\ zz})_{450}$ *(MPa)*	ε_{eq} *(μm/μm)*
1	0	12.00	0.200	10.36	-26	-0.1844	91	0.08
0	1	6.00	0.200	14.13	-459	-0.1149	98	0.08
0.5	0.5	6.00	0.200	14.13	-459	-0.1149	98	0.08

Table 4-8: Output results at 450 ºC using optimal design variables obtained at room temperature versus at elevated temperature

weighting factors		*Optimized at room temperature*			*Optimized at elevated temperature*		
w_1	w_2	$(\sigma_{0zz})_{450}$ *(MPa)*	$(Area)_{450}$ *(MPa.m)*	$(\sigma_{max\ zz})_{450}$ *(MPa)*	$(\sigma_{0zz})_{450}$ *(MPa)*	$(Area)_{450}$ *(MPa.m)*	$(\sigma_{max\ zz})_{450}$ *(MPa)*
1	0	-26	-0.1844	91	-26	-0.1844	91
0	1	-141	-0.1361	113	-459	-0.1149	98
0.5	0.5	-172	-0.1625	70	-459	-0.1149	98

The influence of the constraint function is more significant at the room temperature as the achievable optimum solutions are more affected. Comparing Table 4-5 and Table 4-6 shows that more compressive $(\sigma_{0zz})_{\mathrm{RT}}$ can be achieved after relaxing the constraint function. Therefore, there is a trade-off between achieving the most negative $(\sigma_{0zz})_{\mathrm{RT}}$ and the balancing residual stress which can only be decided based on the knowledge of external load. Solving the optimization problem without any behavior constraint for the 25°C-case resulted in very high plastic strain on the surface which was deemed to be unacceptable and confirming that the assumed constrained function is important and required. Results reveal that the impact of the service temperature on the achieved optimal process parameters is substantial and cannot be ignored in the optimization of the process parameters.

4.6 Conclusion

A high-fidelity 3D nonlinear finite element model has been devolved to model the DCR process on a 1mm thick Ti64 plate and then to predict the resultant residual stress profile after relaxation at an elevated operating temperature of 450ºC.

Efficient analytical surrogate models have been derived to approximate the residual stress profiles, using developed 3D non-linear thermo-mechanical finite element simulation executed on a set of design points optimally located by the DoE technique in the design domain. It was shown that the developed surrogate models with full quadratic polynomial form can accurately predict the response of the system in the given design domain and thus replacing computationally expensive full-scale FE model.

The developed analytical functions have then been effectively used for systematic parametric study to investigate the impact of key process parameters on the profile of the residual stress components at the two operating temperatures of 25°C and 450°C. Moreover, they have been utilized to formulate design optimization problems to identify the optimal processing parameters to maximize the induced compressive residual stress profile in DCR process. Combined GA and SQP algorithms were used to accurately catch the true optimum solution in the proposed optimization problems.

Using the developed optimization methodology, a clear knowledge of the correlation between process parameters and the induced residual stress profiles at both room (25°C) and elevated (450ºC) operating temperatures can be established. This knowledge can be used as a guideline in early stage of a design to determine optimal process parameters for a given duty cycle. The main conclusions driven in this chapter can be summarized as follow:

1. The thickness of the component has a significant impact on the profile of the residual stresses induced by the process.
2. HCF crack initiation of deep-rolled component is observed in deeper depth of the component where the tensile balancing stress region exist. Therefore, the process parameters optimization is required to maximizing the compressive residual stress on the surface while limiting the unavoidable tensile balancing stress.
3. The exposure to the elevated temperature relaxes and redistributes the residual stresses which are induced by DCR process at room temperature. Therefore, consideration of the operating temperature is important in developing the optimal process parameters.
4. The optimal design variables achieved at the room temperature will not guarantee an optimal solution at the elevated temperature and in some cases even creates undesirable stress profiles for elevated temperature applications.

5. Conventional DCR of thin plate can result in unfavorable tensile residual stresses on the untreated side of the components. Double-sided deep rolling can be considered as an alternative solution as it treats the both sides simultaneously and can be efficiently employed to introduce compressive residual stress on both side of the thin-walled components.

5 Analysis and Design Optimization of Double-Sided Deep Cold Rolling Process of a Ti-6Al-4V Blade

In this chapter, a high-fidelity non-linear finite element model is first developed to simulate the double-sided DCR process on thin Ti64 plate to predict the residual stress profile introduced by the process and after thermal relaxation due to subsequent exposure to high temperature. The accuracy of the developed finite element model is validated by comparison with the experimental measurement available in the literature. Well-established machine learning principles have then been carried out on data generated by the high-fidelity FE model to develop predictive analytical models to approximate residual stresses induced by the double-sided DCR process. The developed analytical functions are considerably lower in order than a full-scale finite element simulation and thus can efficiently replace FE models to perform sensitivity analysis and design optimization of process parameters. Load distribution at high stress areas of a generic compressor blade is considered to formulate a design optimization problem of double-sided DCR process in order to achieve optimal residual stress distributions at room temperature and after thermal relaxation at elevated temperature of 450°C.

5.1 Double-sided DCR

As mentioned before, Ti64 is a titanium alloy with a high strength-to-weight ratio and excellent corrosion resistance making it an excellent material for gas turbine applications. The main usage of Ti64 is in compressor blades which their lives are mainly limited by fatigue. Therefore, improving the fatigue life to enhance durability and reliability of the blades while maintaining their airfoil shape is of paramount importance. DCR is a promising mechanical surface treatment which can be effectively used to improve the fatigue life of components by introducing deep and high beneficial compressive residual stresses on the surface and sub-surface layers. However, the application of conventional DCR on thin walled geometries such as compressor blades can be very challenging and has some short falls outlined as follow:

1. Bending and damaging the component during the process.
2. Creating tensile stress in the untreated side of the component.
3. Developing asymmetrical strain and stress states which can cause the thermal distortion of the treated part at elevated temperature.

As discussed in section 2.1, a special tool which has been illustrated schematically in Figure 2-4, has been designed to simultaneously perform the DCR process on both sides of the part in order to address this issue. Double-sided deep rolling on thin-walled components has been proven to be a viable alternative solution as both side of the component are treated simultaneously which thus decreases the risk of component distortion.

The FE simulation of conventional DCR (burnishing on one side) process on a thick component as well as on a thin plate Ti64 have been presented in the previous chapters and the FE model was validated comparing to XRD measurements. However, the distribution of residual stresses in thin geometries is considerably different from bulk geometries. Bulk geometries are only affected in the surface layer while thin-walled geometries are influenced over their entire thickness. The simultaneously developed RS from both sides of the part interact with each other through the thickness and this interaction determines the final state of induced residual stress which needs to be captured in the FE model.

5.2 Finite Element Simulation and Validation of Results

It was discussed earlier that DCR process inherits high level of nonlinearity due to rolling dynamic, friction contact and plasticity behavior of the material. Thus, the prediction of the residual stresses introduced by the process requires FE simulation. The level of nonlinearity is even higher on the double-sided DCR process of thin walled geometries as both sides of the component are treated simultaneously and the induced plastic deformation (and thus the strain hardening) from one side affects the process of the other side and as a result the introduced residual stresses.

ABAQUS software has been utilized to develop the nonlinear 3D FE models to simulate the double-sided DCR process on a thin Ti64 plate and then the subsequent short-time thermal exposure to 450°C. The steps for conducting the FE analysis are similar to those provided previously in Figure 4-1 where the sequence and pertinent details of each step are also presented. The predicted residual stress profile after spring back analysis using the developed FE model has been compared with experimental measurement reported by Klocke et al [53] for the purpose of validation. The thermal relaxation analysis has been subsequently conducted using the validated finite element methodology.

The FE model to simulate the DCR process has been developed in the ABAQUS/Explicit environment as it can handle the high nonlinearities due to friction contact, plastic deformation

and dynamic loading efficiently and accurately. However, the spring back and thermal relaxation analysis steps are quasi-static in nature and thus have been modeled in ABAQUS/Standard environment which employs implicit integration methodology. The simulation sequences presented in Figure 4-1 have been followed to model the process and the following thermal relaxation in order to predict the residuals stresses at room temperature and after thermal relaxation at 450°C .

The workpiece is made of titanium alloy, Ti64 with a 1 mm thickness. It has been reported that the effect of friction coefficient on the simulation is negligible as long as the friction is nonzero as any level of friction will allow the ball to be in a pure rotating state of motion [59]. Considering a frictions coefficient above 0.2 seems unrealistic as the pressurized fluid acts as the coolant and lubricant in the process and the burnishing ball is hydrostatically suspended and free to rotate within the tool holder. Isotropic Coulomb friction model with friction coefficient of 5×10^{-3} has been considered in this study to model the interaction between the workpiece and ball.

The double-sided DCR process; which is schematically demonstrated in Figure 5-1 (a), is symmetry with respect to X-Z plane. Thus only half of the workpiece is modeled and the YSYMM symmetry boundary condition (BC) in ABAQUS is applied on the midface (symmetry plane). The process induces residual stresses with high gradient in the neighborhood of contact region which demands a very fine mesh to obtain an accurate stress prediction. Therefore, the surface layer beneath the contact zone has been discretized with a very fine mesh with the size of 25µm. Since the model benefits from the defined symmetry BC to reduce the computational cost, it was possible to mesh the whole symmetric geometry uniformly using 640,000 C3D8RT elements in ABAQUS environment as presented in Figure 5-1 (b). This element is as discussed before is an 8-node thermally coupled brick element accommodating temperature degree of freedom (DOF) in addition to translational displacement DOFs.

The DCR process can be applied under either force control or displacement control of the rolling ball. While the force control mode ensures that a constant load (pressure) is applied to the ball during the process, under displacement control mode the process is performed under a defined displacement which is prescribed at the end of ball indentation step. Although the reference experimental study reported by Klocke et al [53] was conducted under load control, in this study

the FE simulation will be conducted under both displacement and force control procedures for the sake of comparison.

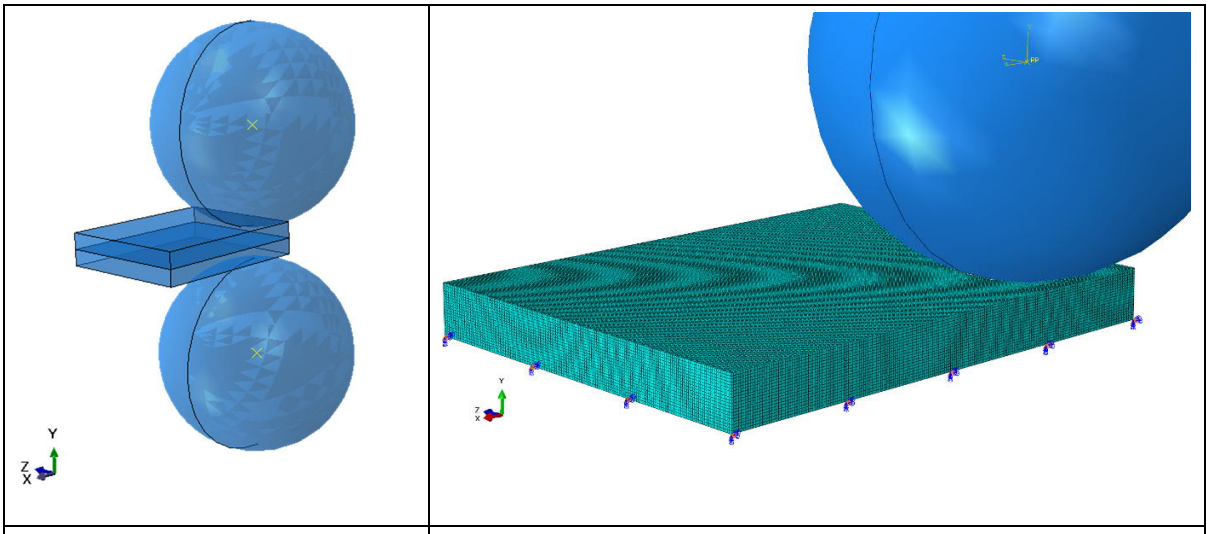

(a) (b)

Figure 5-1: (a) Geometric model and (b) FE BC and mesh of the workpiece in the 3D simulation

The DCR process is modeled as a sequence of analysis steps until a stable residual stress field is achieved in the contact zone. The rolling ball has been modeled as an analytical rigid component and its kinematics is described in four steps namely indentation, rolling, feed and retraction [7]. In the indentation step the rolling ball is forced normally into the top surface in –Y axis until it reaches the full load. Then the ball rolls freely in the +X direction to complete one rolling pass while either the applied force (force control) or Y displacement of the ball (displacement control) is kept constant. In the feed step, the ball is moved in lateral direction (+Z) perpendicular to the rolling pass with the amount of feed and then again rolling back the ball but now in –X direction. Based on the amount of feed, overlap exists between successive rolling passes. Finally, the ball is withdrawn from the surface in the retraction step. The Johnson-Cook material model presented in Table 3-1 has been used to describe the material behavior in the simulation of cold rolling processes.

As discussed before in Chapter 3, the residual stress state changes by preforming each rolling pass until it reaches to a saturation state in a stabilized region where further rolling the workpiece will not alter the residual stress. It has been previously shown that 10 rolling passes; which covers a part of the surface, is sufficient to achieve a stabilized region in order to extract the results while

saving the numerical computation time. Twelve vertical line normal to the treated surface and through the component thickness has been considered in the stabilized region to extract the FE results and calculating the average value at each depth (y-coordinate from the top surface).

The residual stress and strain fields evaluated at the end of the DCR process are then imported as initial conditions to the spring back analysis which is modeled using isotropic plasticity behavior of the material at a low strain rate. The relaxation and redistribution of the residual stresses during the following short-term thermal exposure to temperature of 450 °C is then modeled through the plastic softening mechanism where the outcome of the spring back analysis is considered as the initial state input for the analysis. Since the thermal relaxation is quasi-static, the plastic material model at lower strain rate is required for the analysis. Temperature dependent quasi-static stress-strain curves at the strain rate of 1 sec^{-1} presented by Haight et al. [89] had been successfully adapted in form of isotropic plasticity to simulate the thermal relaxation of DCR-induced residual stresses in Ti64.

The double-sided DCR process treats both sides of the component simultaneously which results in a different material flow and plastic hardening and deformation compared with conventional DCR process. In this study, both processes have been simulated on a plate with a 1 mm thickness with process parameters of ball diameter 9 mm, feed 0.200 mm and rolling pressure 20 MPa under load control mode. The results for tangential residual stress (z-direction) through the thickness are presented in Figure 5-2.

As it can be realized that the residual stress profile induced by double-sided DCR process is significantly different than that induced by the conventional DCR process performed on the same workpiece under identical processing parameters. Under simultaneous deep rolling process of the two sides of a thin walled component, the strain hardening induced from one side is deep enough to interact with the rolling process on the opposite side which consequently lowers the plastic deformation imposed from the opposite side and subsequently the induced residual stress through the thickness. However, as it can be seen the double-sided DCR process creates a more uniform RS profile which is compressive on both sides of the component which can be very beneficial for fatigue enhancement under some applications.

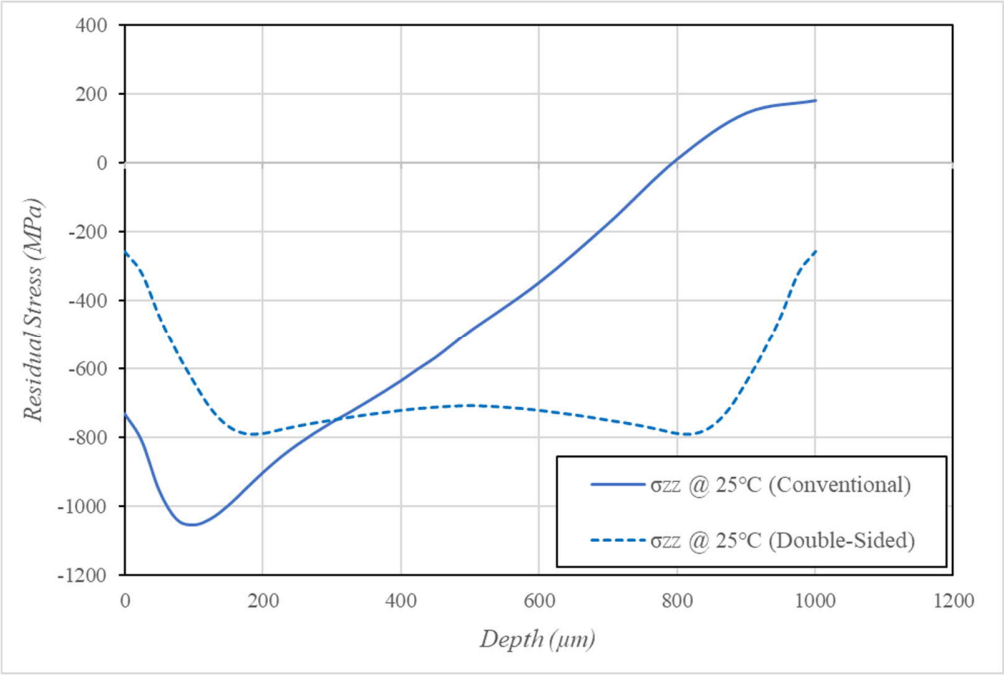

Figure 5-2: Residual stress profile in tangential direction conventional versus double-sided DCR

5.2.1 Double-sided DCR process under force control

The simulation and results of double-sided DCR process under force control is explained in this section. The results have been compared with simulation and experimental results reported by Klocke et al [53] where double-sided DCR treatment of a 1 mm thick Ti64 plate was performed using ball diameter of 6 mm, rolling pressure of 150 bar, rolling velocity of 10 mm/s and coverage of 60% . Since the amount of the lateral movement of the rolling ball in Z-direction (feed) was not explicitly mentioned in the reference [53], the simulation was first run for only one rolling pass to obtain the track width and then the feed was evaluated using the given coverage. The DCR process was then continued considering the calculated feed of 0.240 mm for the next nine subsequent rolling passes until a stabilized region is achieved.

Figures 5-3 and 5-4, respectively show the material flows and plastic deformation in the stabilized region for the process parameters of *D=6 mm*, *f=0.240 mm* and *P=150 bar* (*15 MPa*) using the developed FE model. It is noted that to reduce the computational cost, the simulation was conducted only on half of the thickness due to the symmetry about the X-Z plane. The deflection scale has been set to 6 and the component has been sectioned using cutting plane for the sake of better visualization.

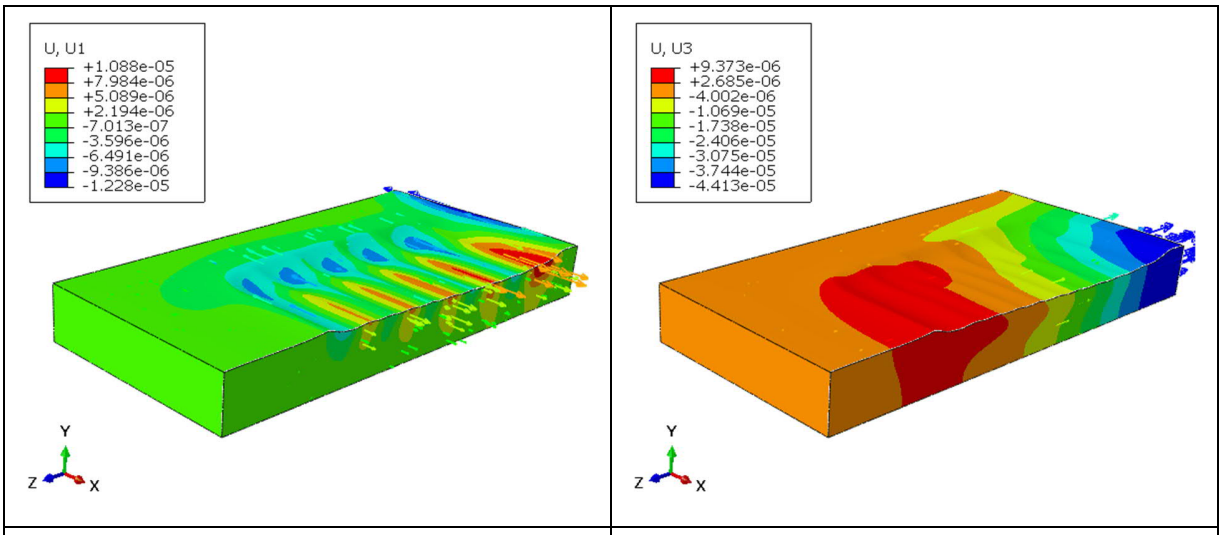

(a) U_x at room temperature | (b) U_z at room temperature

Figure 5-3: Material displacement after spring back at room temperature in the stabilized region (a) in axial direction and (b) in tangential direction, under force control DCR

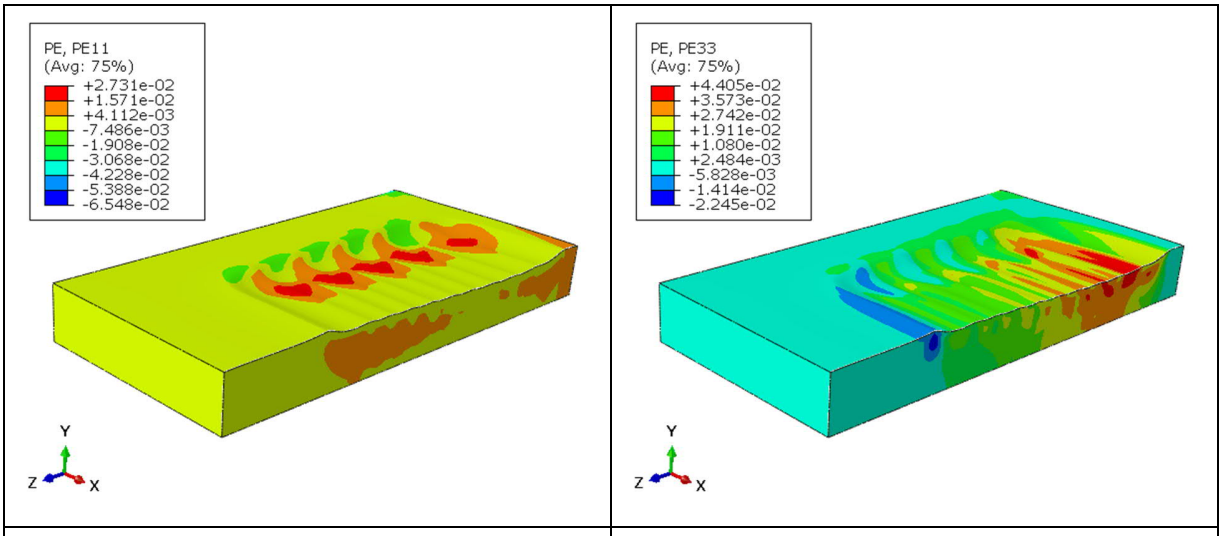

(a) ε_{xxp} at room temperature | (b) ε_{zzp} at room temperature

Figure 5-4: Plastic strain after spring back at room temperature in the stabilized region (a) in axial direction (ε_{xxp}) and (b) in tangential direction (ε_{zzp}), under force control DCR

Residual stresses are the result of inhomogeneous plastic deformation generated in component during DCR process. The final state of the material flow defines the direction of reaction forces by the surrounding materials which subsequently defines the nature (compressive or tensile) of the introduced residual stresses. In another words, under a certain rolling force with a given ball

diameter, the sign of the residual stresses in axial and tangential directions can alter depending on the net material flow caused by the different amount of feed.

It has been demonstrated that the residual stress distribution can be explained by the net material flow and the resulting plastic strain [59]. The plastic deformation mechanism during the DCR process is the superposition of the material displacements in the treated zone attributed to three simultaneous deformation mechanisms, namely as the ball rolling (in x direction), the lateral movement of the ball (the feed in z direction) and the vertical movement of the ball (under the rolling force in y direction) which interact with each other during the whole process.

The equivalent stress beneath the ball reaches the yield stress of the workpiece material under a substantial rolling force which results in plastic deformation. A detailed stress analysis of the process reveals a large area of vertical compressive stress directly beneath the rolling ball causing a vertical plastic compression, which leads to plastic extension in the surface of the workpiece. Because of the constant volume of the material, the extension of the surface of the material in one direction, leads to a transverse contraction of the material in the perpendicular directions on the surface as well as in the material beneath the surface layer. This results in lateral displacement of the material surrounding the contact zone and consequently developing residual stresses as a reaction to this plastic material displacements.

Figures 5-5 and 5-6 respectively show the residual stresses in axial and tangential directions in the stabilized region at both room temperature and 450 ^{o}C predicted by the developed FE model. As it can be realized the process introduces anisotropic residual stress fields which are significantly different in the axial and tangential directions. The thermal relaxation causes material softening and the subsequent material flow and plastic deformation which redistributes the residual stresses. Developing residual stresses in the treated area results in a compensatory residual stress in the surrounding material which plays an important role in the final state of the residual stress field in the treated region after thermal relaxation.

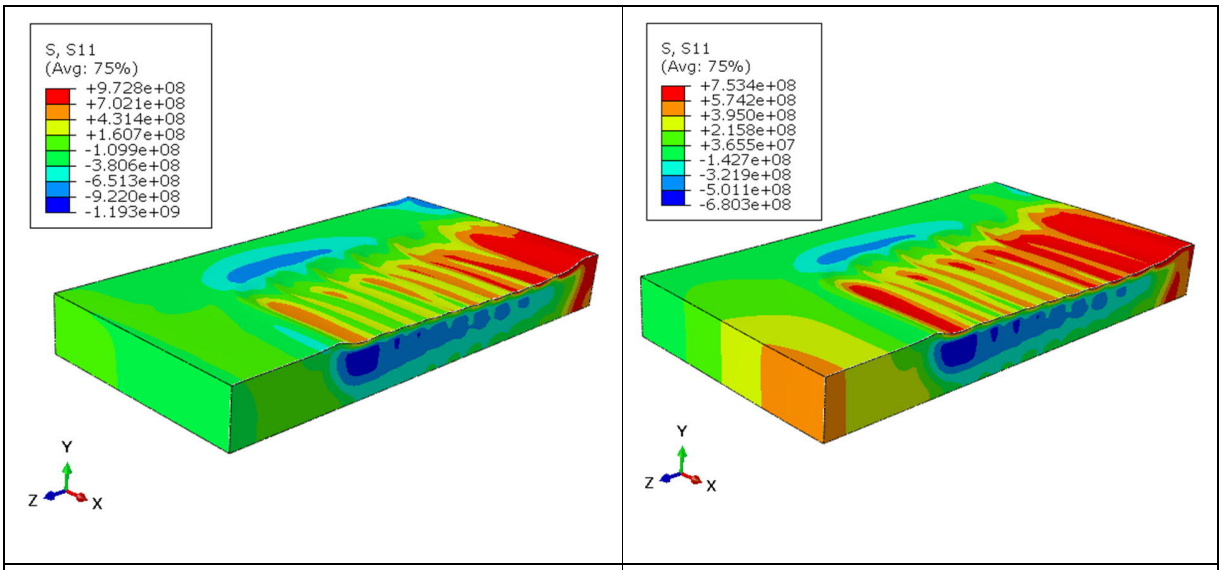

(a) σ_{xx} at room temperature	(b) σ_{xx} at 450˚C

Figure 5-5: Residual stress (Pa) in axial direction (σ_{xx}) sectioned in the stabilized region (a) after spring back at room temperature (b) after thermal relaxation at 450˚C, under force control DCR

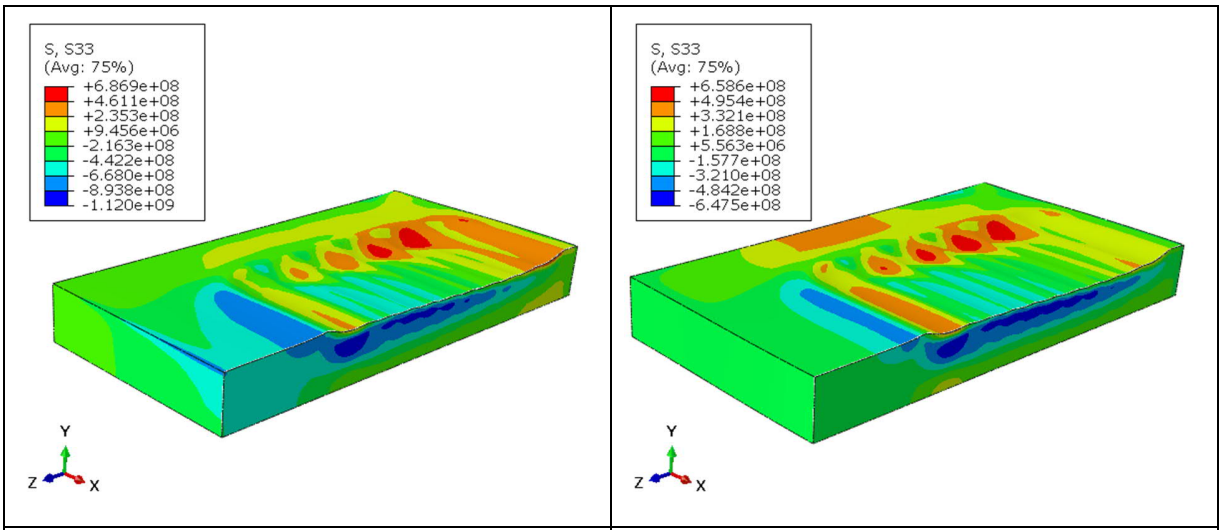

(a) σ_{zz} at room temperature	(b) σ_{zz} at 450˚C

Figure 5-6: Residual stress (Pa) in tangential direction (σ_{zz}) sectioned in the stabilized region (a) after spring back at room temperature (b) after thermal relaxation at 450˚C, under force control DCR

The tangential residual stress values (σ_{zz}) through the depth of the components were extracted along twelve lines in Y-direction spread over the stabilized region and the average values were calculated and compared with the experimental measurements. Figure 5-7 shows the results of the tangential residual stress through the thickness predicted using the developed FE model in the

present study and comparison with those of experimental measurements and the simulation results reported by Klocke et al [53]. As it can be seen the developed FE model in the current study can accurately predict the trend and behaviour of the residual stress profile and is in better agreement with experimental results compared with those reported by Klocke et al [53].

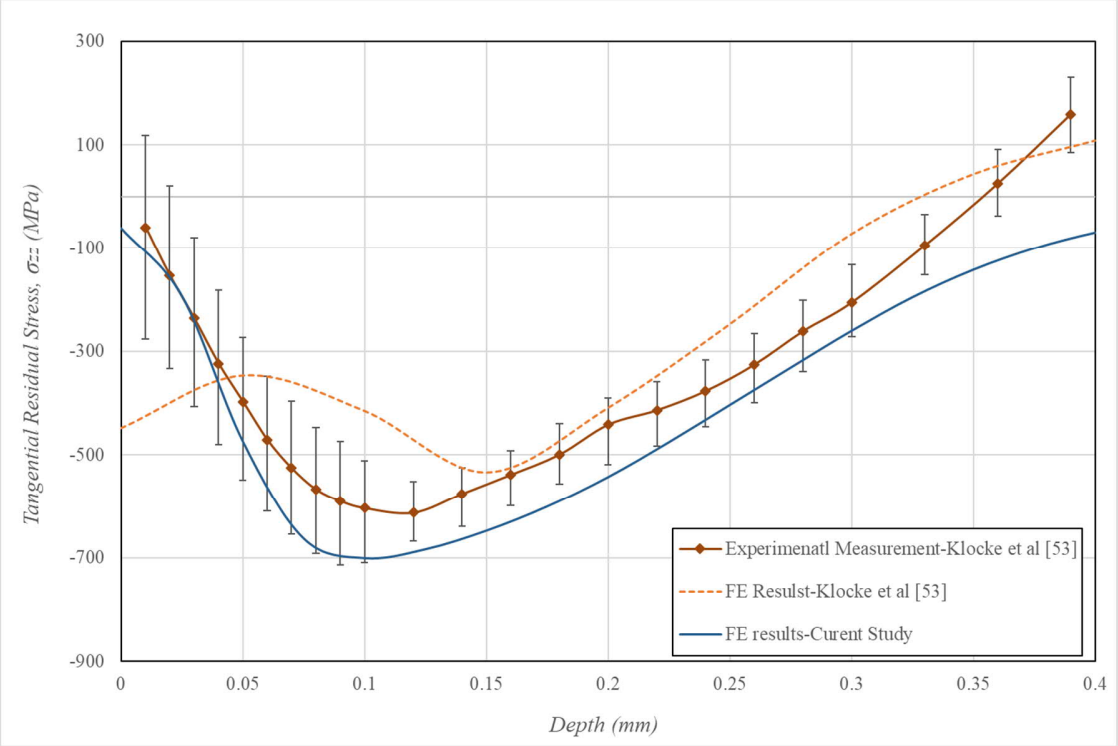

Figure 5-7: Comparing tangential residual stress profile through the depth obtained using FE and experiment at room temperature

Compared with the current simulation results, experimental results mainly underpredicts the residual stress. It should be noted that the residual stress measurement involves material removals which causes inevitable relaxation and redistribution of the initial residual stress profile. The equilibrium of forces between the tensile region and compressive region must maintain after each step of layer removal resulting in reduction or even elimination of the compressive stress region [25]. The relaxation can be greater for thin walled specimen as the volume of the treated region is less in compared with thick components. The inevitable stress relaxation caused by the material removal in electro polishing was not basically considered in the measurements reported by Klocke et al [53] which may result in slight under prediction of the residual stress beneath the surface. Considering the measurement errors and assumptions involved in the FE simulation including the assumed material model and ignoring the impact of initial surface roughness and residual stress of

the component prior to the deep rolling, the results of the FE models developed in the current study are generally in a very good agreement with the experimental measurements and thus the model can be confidently utilized to simulate the double-sided DCR process.

Figures 5-8 and 5-9 show induced residual stress distribution in axial (σ_{xx}) and tangential (σ_{zz}) directions through half the thickness, respectively at both room and temperature 450 ºC. As it can be realized, the double-sided DCR process generates significantly different residual stress distribution in axial and tangential directions at the room temperature and the subsequent exposure to elevated temperature causes relaxation and redistribution of the stresses. As it was discussed before, the anisotropy of the developed residual stresses at the room temperature can be explained by the plastic deformation caused during the process.

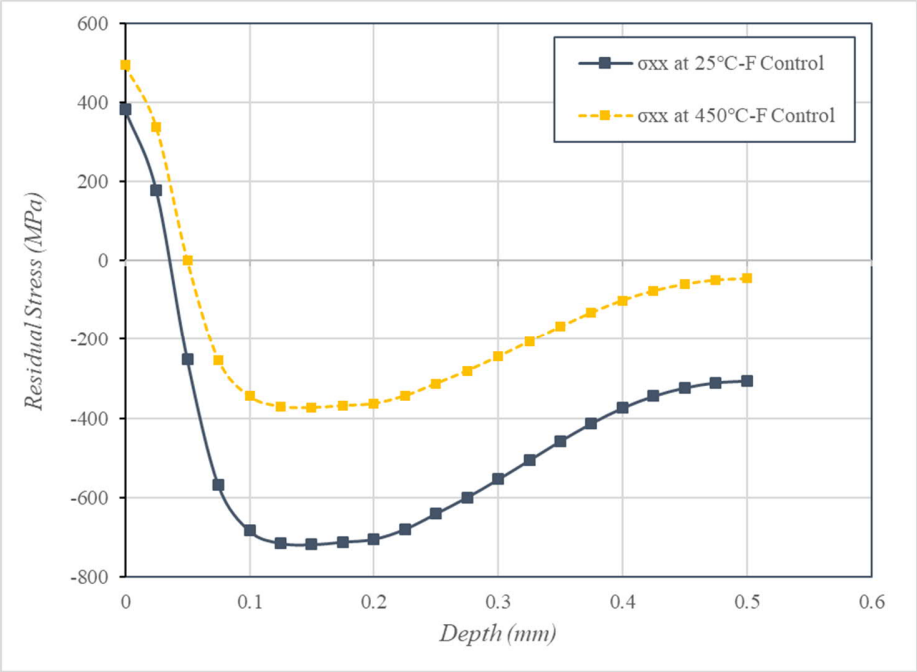

Figure 5-8: Residual stress profile in axial direction at 25 °C and 450 °C

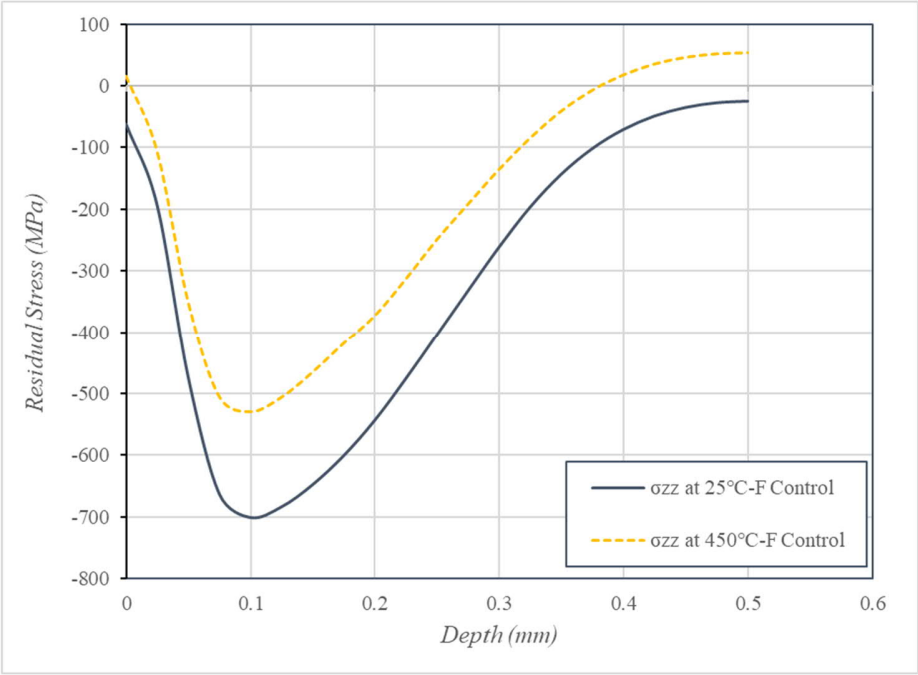

Figure 5-9: Residual stress profile in tangential direction at 25 °C and 450 °C

5.2.2 Double-sided DCR process under displacement control of the rolling ball

One may prefer applying DCR process under displacement control mode as programming displacements for Computer Numerical Control (CNC) machines are usually easier than controlling the fluid pressure during the process. However, the residual stress profiles achieved by the two methods are quite different and thus should be carefully examined. The simulation results for double-sided DCR process under displacement control of the rolling ball and their comparison with those under force control mode are discussed in this section. The process is performed under the prescribed displacement of the ball reaching at the end of the indentation step.

Figures 5-10 and 5-11 demonstrate the time history of the rolling force and normal displacement of the rolling ball for both force and displacement control methods, respectively. Results show that when one of the controlling parameters is fixed the other one must change to compensate the plastic deformation and effect of the strain hardening on the dynamic movement of the rolling ball. As it can be realized from Figure 5-12, the material displacement in Y-direction is quite different under the two processes and significantly higher when the process is performed under force control mode which ultimately results in a different plastic deformation and residuals stress in the perpendicular directions (X and Z).

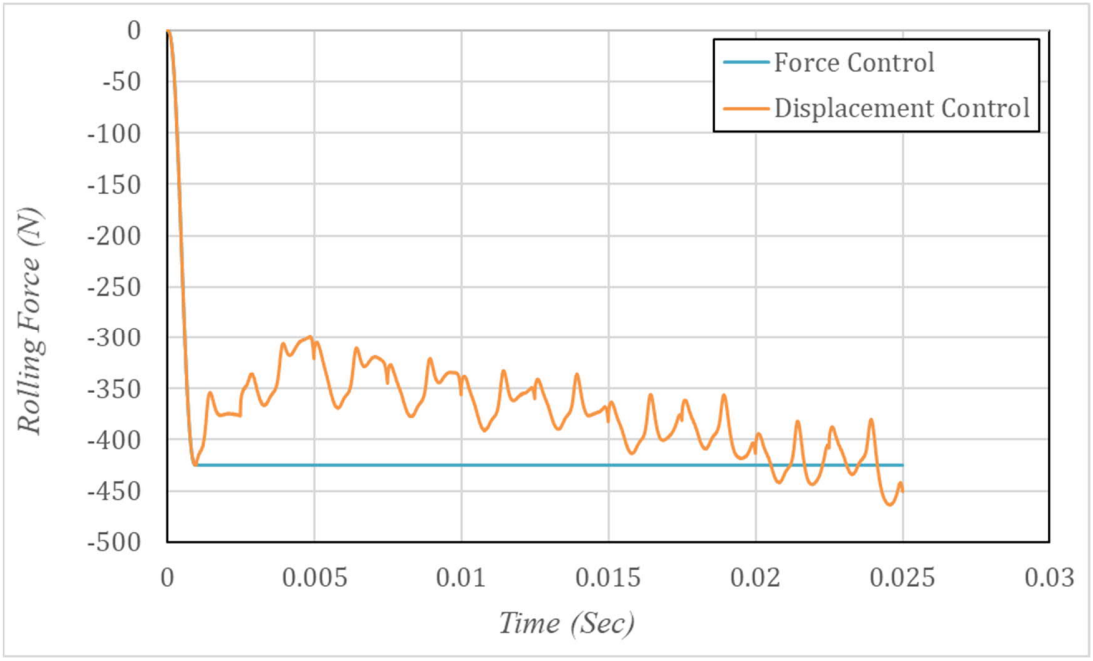

Figure 5-10: Variation of rolling force versus time

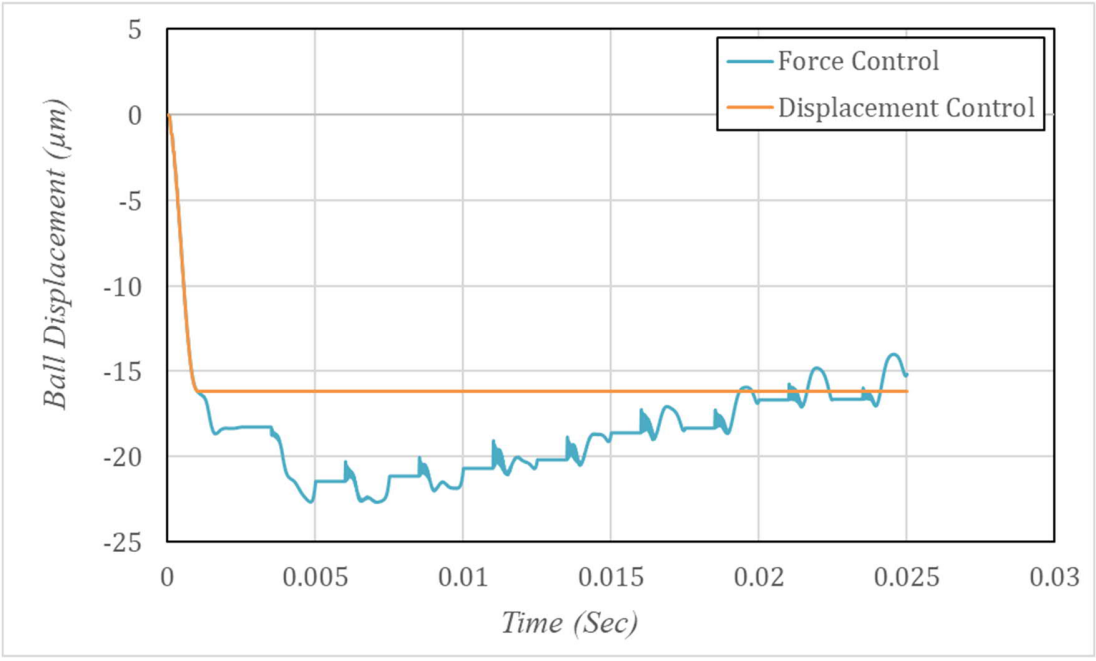

Figure 5-11: Normal displacement of the rolling ball (*Uy*) versus time

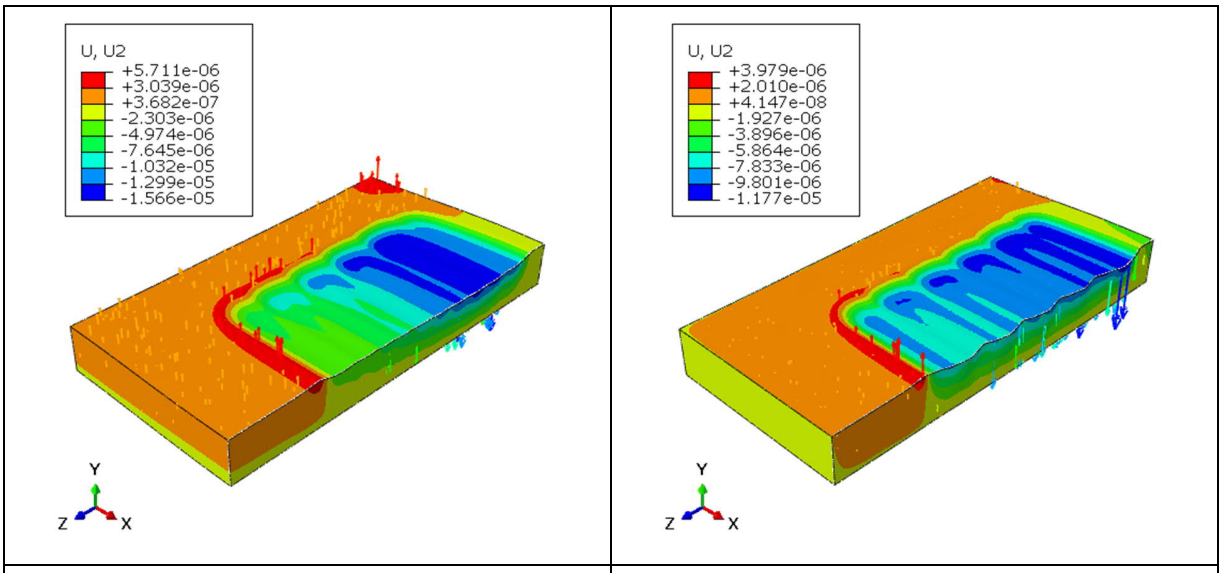

(a) force controlled DCR	(a) displacement controlled DCR

Figure 5-12: Comparison of material displacement in Y-direction after spring back at room temperature in (a) force controlled DCR (b) displacement controlled DCR

The material flow in x and z direction under displacement control mode has been shown in Figure 5-13 (a) and (b) respectively. Comparing Figure 5-3 and Figure 5-13 shows that although the net material flows closer to the surface can be similar for force and displacement control modes, they deviate by increasing the depth and material displacement in X and Z directions are higher under force control which is attributed to deeper indentation of the rolling ball as it can be observed in Figure 5-12. Figure 5-14 also shows the plastic strain distribution in the axial and tangential direction under displacement-controlled process which again differ with those for force control mode shown in Figure 5-4.

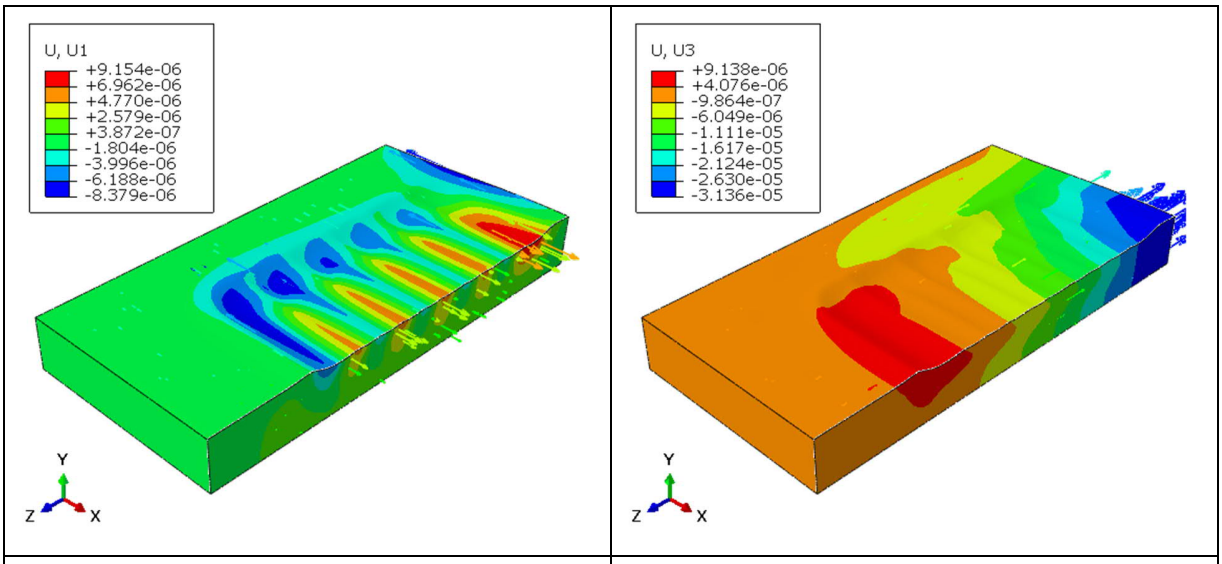

(a) U_x at room temperature | (b) U_z at room temperature

Figure 5-13: Material displacement after spring back at room temperature in the stabilized region (a) in axial direction and (b) in tangential direction, under displacement control DCR

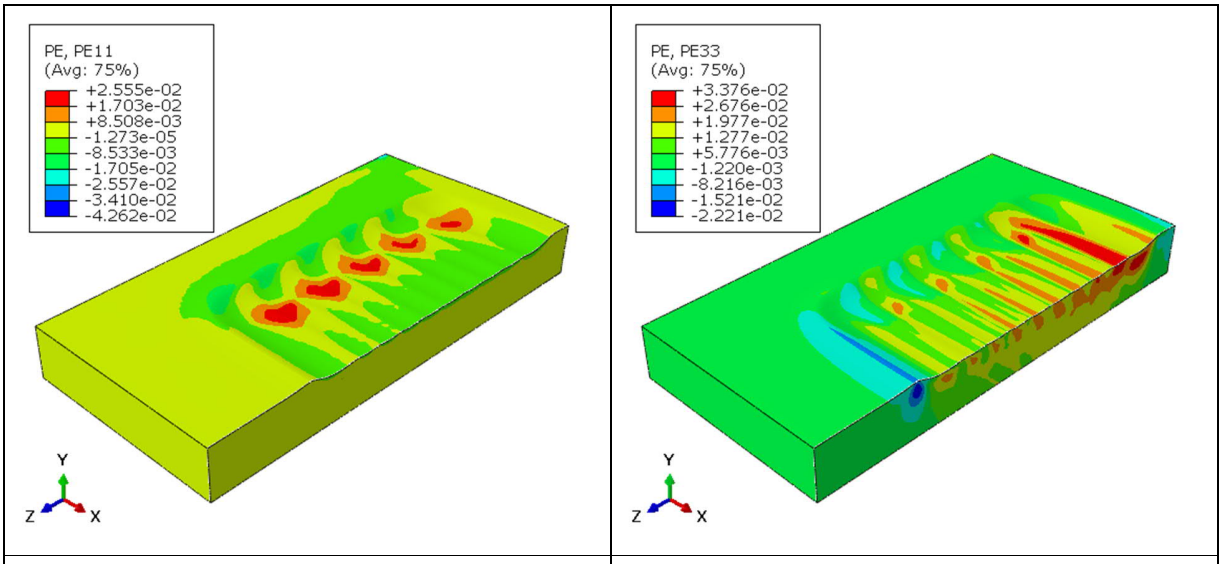

(a) ε_{xxp} at room temperature | (b) ε_{zzp} at room temperature

Figure 5-14: Plastic strain after spring back at room temperature in the stabilized region (a) in axial direction (ε_{xxp}) and (b) in tangential direction (ε_{zzp}), under displacement control DCR

Figures 5-15 and 5-16 , respectively show the predicted residual stresses in axial and tangential directions in the stabilized region at both room temperature and 450 ºC under displacement control mode. By comparing Figures 5-15 and 5-16 with Figures 5-5 and 5-6 for force control mode, one

can realize the differences in material displacements and plastic strains developed by the two modes have resulted in different level of residual stresses.

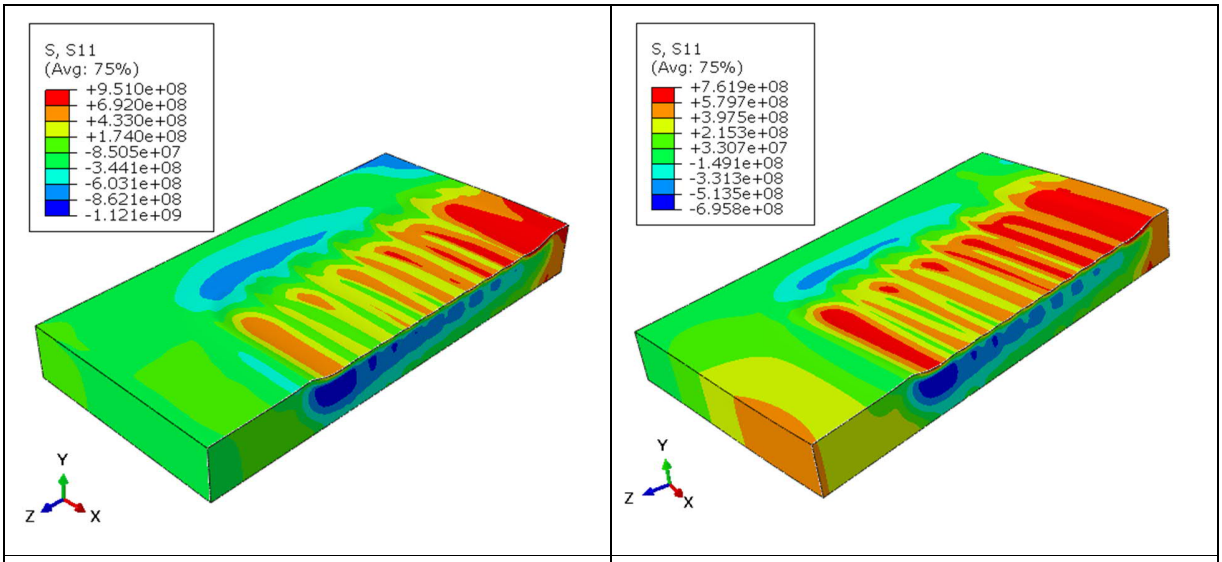

(a) σ_{xx} at room temperature | (b) σ_{xx} at 450˚C

Figure 5-15: Residual stress (Pa) in axial direction (σ_{xx}) sectioned in the stabilized region (a) after spring back at room temperature (b) after thermal relaxation at 450˚C, under displacement control DCR

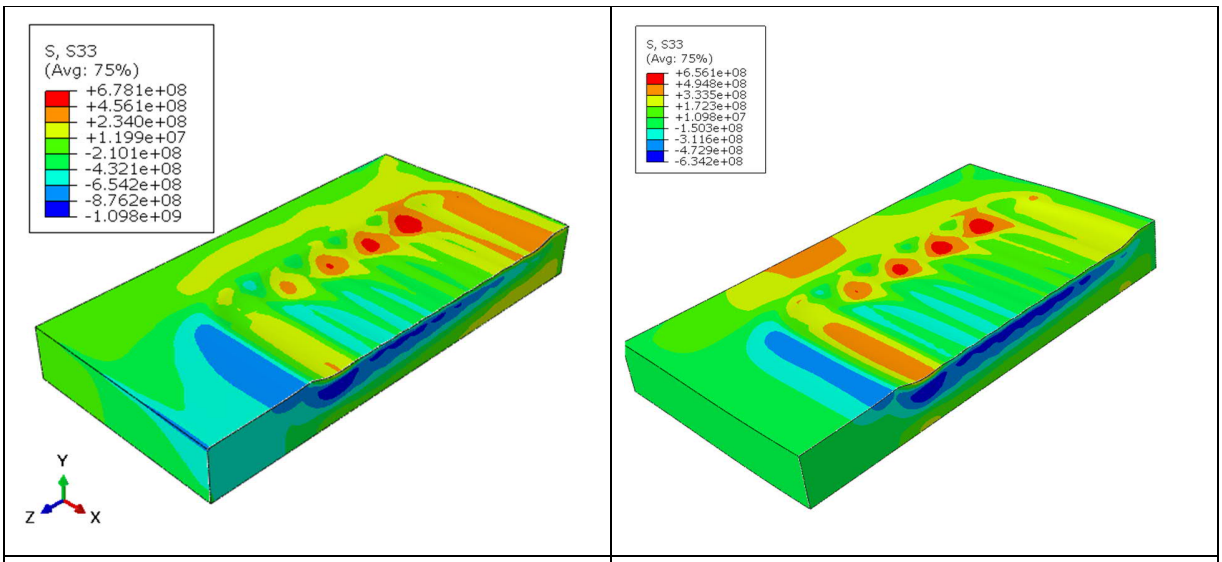

(a) σ_{zz} at room temperature | (b) σ_{zz} at 450˚C

Figure 5-16: Residual stress (Pa) in tangential direction (σ_{zz}) sectioned in the stabilized region (a) after spring back at room temperature (b) after thermal relaxation at 450˚C, under displacement control DCR

To better realize the difference in induced residual stresses under displacement and force control modes, the residual stress profiles through the thickness have been extracted for the force and displacement controlled DCR and the results at 250°C and 450°C are presented in Figures 5-17 and 5-18, respectively. The two methods introduce a very similar pattern for residual stress profile through the thickness. Results for residual stresses based on both approaches are fairly close in regions near to the surface layer while they deviate for deeper layers which is attributed to a different material flow. When the process is performed under the displacement control mode, the imposed net material flow is lower in Y direction; which means will be lower in the perpendicular directions (X and Z), thus resulting in a lower compressive residual stress in tangential and axial directions compared with force-controlled process.

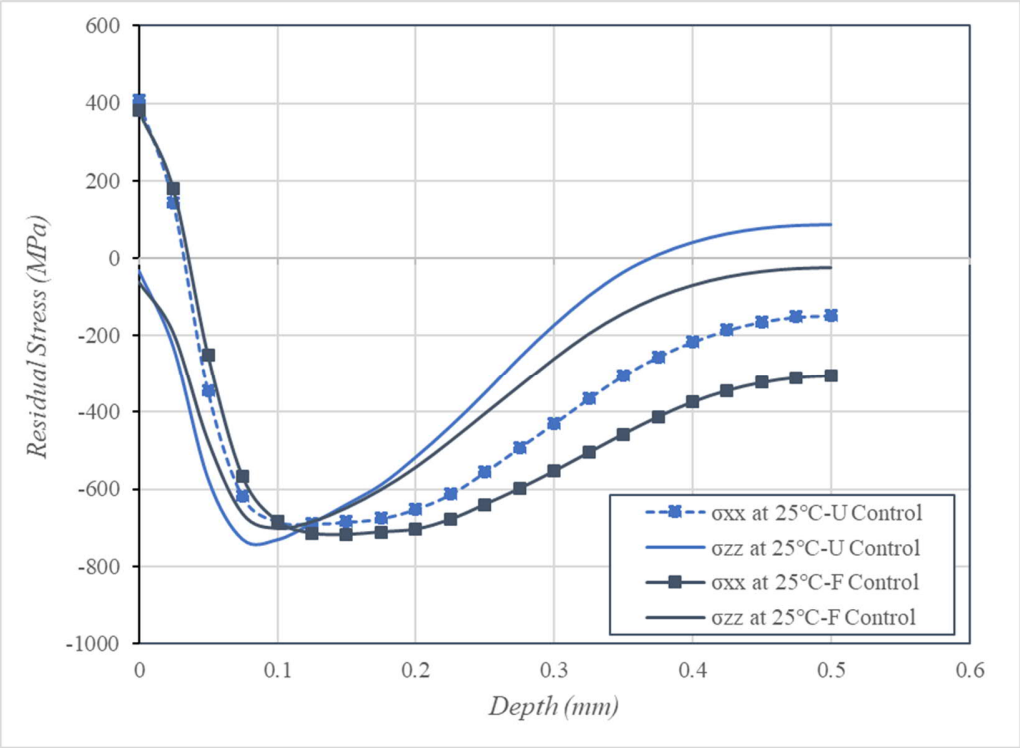

Figure 5-17: Residual stress profiles induced by force and displacement control DCR processes at room temperature 25°C

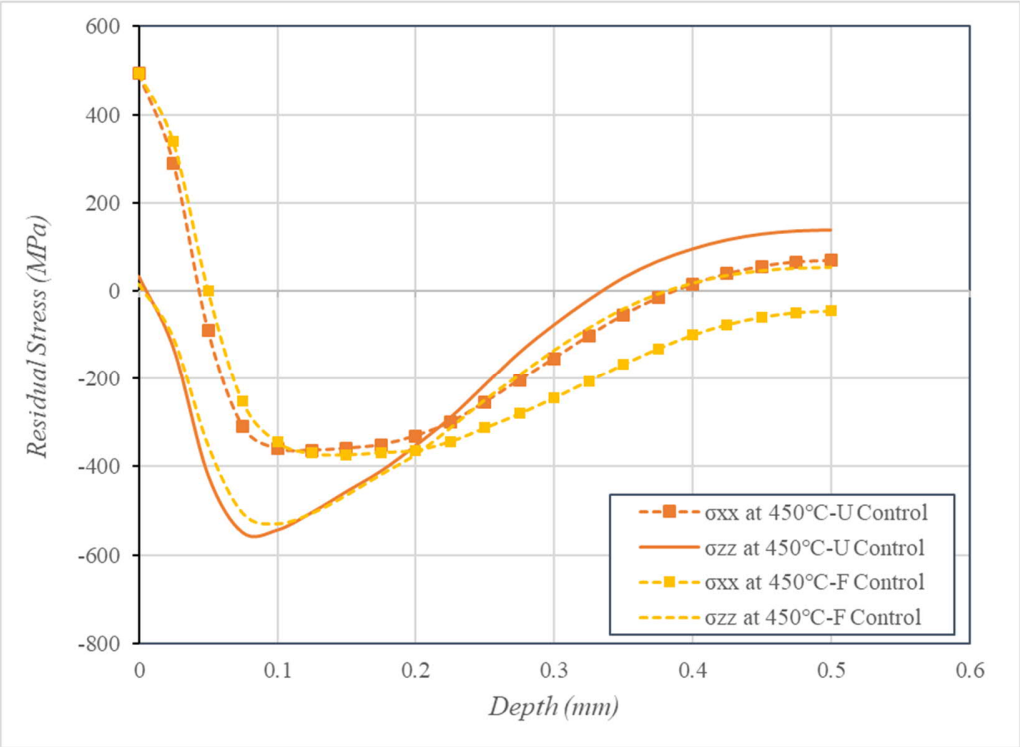

Figure 5-18: Residual stress profiles induced by force and displacement control DCR processes at 450°C .

5.3 Design of Experiments and Response Surface method

Each simulation run of the DCR process and the following spring back and thermal relaxation analysis took about 188 hours on a computer with four core i7 2.70 GHz CPU and 64 GB available RAM. As it can be realized performing sensitivity analysis, design optimization or assessing uncertainty of the process parameters on the residual stress profiles using FE simulation models is computationally expensive and impractical.

The development of an efficient methodology to establish an explicit correlation between process parameters and the induced residual stress profiles (at both room temperature and 450°C) for double-sided DCR process are discussed in this section. The depth of the created compressive layer and the distribution of dislocation density caused by cold working of the surface layers depend upon the process parameters such as ball size, rolling pressure, feed and the rolling speed. As discussed before in Chapter 4, the previous experimental and numerical research works have unanimously confirmed that the impact of the rolling speed on the residual stress is negligible [9, 11, 52, 82]. Therefore like one-sided DCR process, ball diameter D (*6-12 mm*), the feed f (*0.05-*

0.20 mm) and the fluid pressure *P* (*10-30 MPa*) are considered as design variables (design features) in the current study.

The results presented in the previous section confirmed that the residuals stress profiles achieved under force or displacement control of the rolling ball are not significantly different on the surface and the variance is mainly observed in deeper depth from the surface. Thus, without loss of generality, it was decided to consider force controlled DCR process for further investigation.

Design of experiments (DoE) has been employed to discretize the design domain at intelligently selected sampling points named design points. The design points are the most representative input configurations for simulation or physical experiments in a given design domain. DoE refers to a collection of statistical techniques that provides a frame work to maximize the knowledge sought over a design domain with minimum number of required simulations (or experiments) performed at the design points [80, 81].

Ten output response have been considered in the current study which can effectively describe the residual stress profile.

- The summation of the total area of the residual stress calculated using both negative and positive areas of the stress components throughout the thickness in *x* and *z* directions, i.e. $[Area\ \sigma_{xx} + Area\ \sigma_{zz}]$ which represents the depth of the residual stress. This will be represented by $(Area)_{RT}$ and $(Area)_{450}$ for room temperature and 450 °C, respectively.
- The residual stress components (parallel and perpendicular to the rolling direction) on the surface of the workpiece which are represented by $(\sigma_{0xx})_{RT}$ and $(\sigma_{0zz})_{RT}$ at room temperature, and $(\sigma_{0xx})_{450}$ and $(\sigma_{0zz})_{450}$ at 450˚C.
- The residual stress components in the depth of 500µm (mid thickness of the workpiece) which are represented by $(\sigma_{500xx})_{RT}$ and $(\sigma_{500zz})_{RT}$ at room temperature, and $(\sigma_{500xx})_{450}$ and $(\sigma_{500zz})_{450}$ at 450˚C.

Central Composite Design (CCD) method available in Mintab© software was used to design the experiments and identify the design points. The developed high-fidelity FE model has then been executed at each design point to evaluate the desired output responses described above. Table 5-1 and 5-2 summarize the design points and their associated desired responses at room and elevated temperature of 450 ºC, respectively.

Table 5-1: Design points and the FE results (training data set) at room temperature

D (mm)	f (mm)	P (MPa)	$(\sigma_{0xx})_{RT}$ (MPa)	$(\sigma_{0zz})_{RT}$ (MPa)	$(\sigma_{500xx})_{RT}$ (MPa)	$(\sigma_{500zz})_{RT}$ (MPa)	$(Area)_{RT}$ (MPa.m)
6	0.050	10	-44	-80	156	575	-0.4907
6	0.200	10	285	-144	-71	233	-0.6530
6	0.050	30	314	244	-822	56	-1.1037
6	0.200	30	216	-504	-446	-550	-1.2341
6	0.125	20	153	54	-651	-326	-1.1461
9	0.050	20	-132	200	-947	-141	-1.1846
9	0.200	20	110	-257	-522	-706	-1.2258
9	0.125	10	126	327	-749	-247	-1.1546
9	0.125	30	-210	162	-822	-782	-1.4541
9	0.125	20	-82	123	-861	-674	-1.3957
12	0.050	10	-118	115	-947	1	-1.0802
12	0.200	10	110	-73	-660	-716	-1.2613
12	0.050	30	-594	44	-1105	-544	-1.4769
12	0.200	30	-402	-169	-536	-688	-1.2911
12	0.125	20	-333	174	-814	-781	-1.4047

Table 5-2: Design points and the FE results (training data set) at 450°C

D (mm)	f (mm)	P (MPa)	$(\sigma_{0xx})_{450}$ (MPa)	$(\sigma_{0zz})_{450}$ (MPa)	$(\sigma_{500xx})_{450}$ (MPa)	$(\sigma_{500zz})_{450}$ (MPa)	$(Area)_{450}$ (MPa.m)
6	0.050	10	21	-48	458	196	-0.3180
6	0.200	10	328	-79	226	69	-0.3615
6	0.050	30	430	246	92	-473	-0.6403
6	0.200	30	266	-203	-259	-267	-0.7068
6	0.125	20	252	144	-326	-394	-0.6946
9	0.050	20	100	249	-49	-582	-0.6874
9	0.200	20	180	-5	-350	-315	-0.6669
9	0.125	10	235	353	-114	-468	-0.7060
9	0.125	30	-40	295	-440	-522	-0.8531
9	0.125	20	64	240	-408	-575	-0.8609
12	0.050	10	96	163	55	-534	-0.5959
12	0.200	10	193	142	-377	-422	-0.7011
12	0.050	30	-228	138	-356	-647	-0.8542
12	0.200	30	-156	106	-347	-282	-0.6629
12	0.125	20	-97	320	-461	-508	-0.8090

Response Surface Methodology based on well-stablished regression-based machine learning technique has been utilized to train and validate the best polynomial approximate to the responses of interest (residual stress profile in this study), by minimizing the error of the approximation. As mentioned in Chapter 4, the accuracy of the developed surrogate models is usually examined by R^2 (i.e. R-Squared) which is also known as the coefficient of determination. R^2 is a statistical measure of how close the data are to the fitted regression models and is always between 0 and 100% in which a model with a higher R^2 better fits the training data. The coefficient of determination, R^2, has been presentenced by Eq. (4-4) in Chapter 4.

It can be realized from Eq.(4-3) that several types of polynomial such as the linear, quadratic and cubic functions can be considered for the surrogate models. In this research study, a quadratic model was considered for the response surface functions as R^2 value over 85% can be achieved without overfitting the training data set by higher order polynomials. The derived quadratic response surface functions for the desired output responses are presented in Eqs. (5-1) to (5-10) and the R^2 values of each developed surrogate model is presented beside it in a bracket which generally demonstrates the high accuracy of the developed models to approximate the responses of interest.

$$(\sigma_{0xx})_{RT} = -362 + 31.0 * D + 793 * f + 47.22 * P + 7764 * f^2 - 5.322 * D * P - 77.2 * f * P\ ,\ (R^2 = 95.88\%) \quad (5\text{-}1)$$

$$(\sigma_{0zz})_{RT} = -780 + 113 * D + 7173 * f + 11.17 * P - 6.94 * D^2 - 36425 * f^2 + 230 * D * f - 118.4 * f * P,\ (R^2 = 87.63\%) \quad (5\text{-}2)$$

$$(\sigma_{500xx})_{RT} = 3316 - 470 * D - 9733 * f - 108.6 * P + 13.1 * D^2 + 20617 * f^2 + 0.651 * P^2 + 392 * D * P + 5.5 * D * P + 147.7 * f * P,\ (R^2 = 93.31\%) \quad (5\text{-}3)$$

$$(\sigma_{500zz})_{RT} = 2976 - 155.9 * D - 14294 * f - 116.6 * P + 44511 * f^2 + 1.591 * P^2 + 3.27 * D * P,\ (R^2 = 94.48\%) \quad (5\text{-}4)$$

$$(Area)_{RT} = 1.774 - 0.3278 * D - 9.36 * f - 0.0563 * P + 0.0116 * D^2 + 30.34 * f^2 + 0.003198 * D * P + 0.0664 * f * P,\ (R^2 = 95.46\%) \quad (5\text{-}5)$$

$$(\sigma_{0xx})_{450} = -396 + 67.4 * D + 96 * f + 42.63 * P - 1.77 * D^2 + 8339 * f^2 - 4.255 * D * P - 82.8 * f * P,\ (R^2 = 91.25\%) \quad (5\text{-}6)$$

$$(\sigma_{0zz})_{450} = -974 + 146.6 * D + 5925 * f + 18.24 * P - 7.24 * D^2 - 31135 * f^2 + 245 * D * f - 1.029 * D * P - 68.9 * f * P,\ (R^2 = 89.88\%) \quad (5\text{-}7)$$

$$(\sigma_{500xx})_{450} = 2212 - 95.1 * D - 12035 * f - 91.7 * P + 36874 * f^2 + 1.295 * P^2 + 1.96 * D * P + 53.7 * f * P,\ (R^2 = 93.61\%) \quad (5\text{-}8)$$

$$(\sigma_{500zz})_{450} = 2647 - 400 * D - 8200 * f - 61.2 * P + 13.09 * D^2 + 21402 * f^2 + 222 * D * f + 4.30 * D * P + 97.6 * f * P,\ (R^2 = 93.19\%) \quad (5\text{-}9)$$

$$(Area)_{450} = -1.086 - 0.1966 * D - 7.108 * f - 0.03282 * P + 0.00718 * D^2 + 24.76 * f^2 + 0.00186 * D * P + 0.0458 * f * P,\ (R^2 = 92.20\%) \quad (5\text{-}10)$$

5.4 Parametric Study- Double Sided DCR process

Figure 5-19 (a) and (b) respectively show the response surfaces of $(\sigma_{0xx})_{RT}$ and $(\sigma_{oxx})_{450}$ with respect to ball diameter and rolling pressure for the given feed of *f=0.125 mm*. As it can be seen for the given feed, increasing the rolling pressure at smaller ball diameter increases $(\sigma_{0xx})_{RT}$ toward tensile region while at larger ball diameter decreases more toward the compressive region. Therefore, the impact of the rolling pressure on the axial residual stress highly depends on ball diameter. The similar trend can also be observed for $(\sigma_{oxx})_{450}$ in which increasing the rolling pressure increases $(\sigma_{oxx})_{450}$ toward the tensile region for the smaller ball diameter while decreases $(\sigma_{oxx})_{450}$ toward compressive region for the larger ball diameters. Comparing the surface plot of $(\sigma_{oxx})_{450}$ with its counterpart at room temperature shows that the thermal relaxation significantly reduces the magnitude of the compressive axial residual stress on the surface and the level of relaxation is significantly higher at the upper bound of the parameters where the plastic deformation is higher.

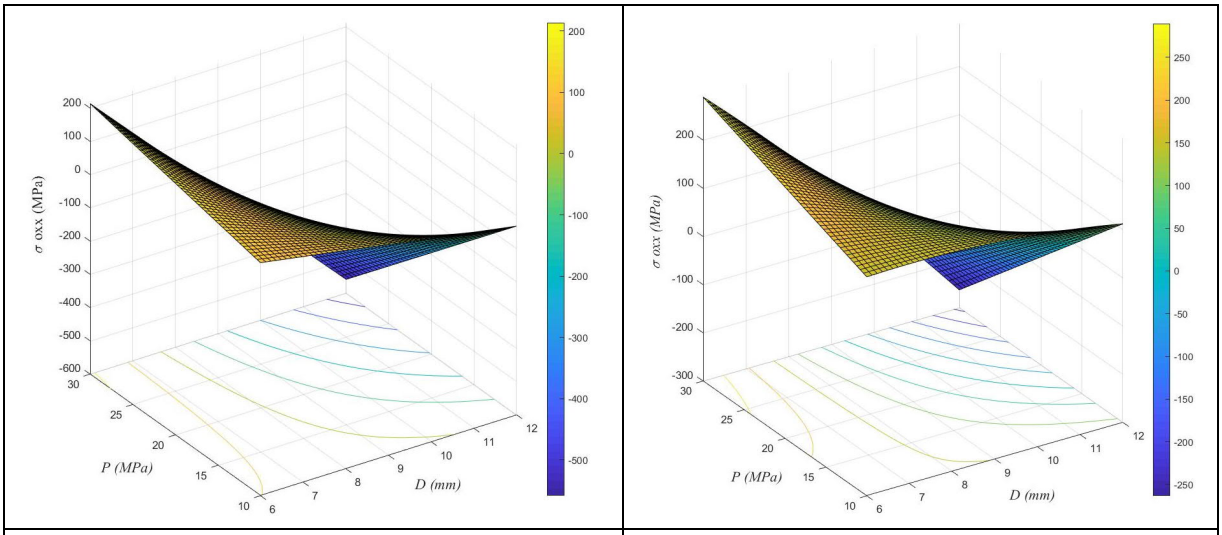

(a) (b)

Figure 5-19: Effect of ball diameter and rolling pressure on σ_{0xx} for *f=0.125 mm* (a) at room temperature 25℃, and (b) at elevated temperature 450 ℃

Figure 5-20 (a) and (b) also show the surface plot of $(\sigma_{0zz})_{RT}$ and $(\sigma_{0zz})_{450}$ with respect to ball diameter and feed for rolling pressure of *20MPa*, respectively. Results clearly show the dominant effect of feed on the responses. For $(\sigma_{0zz})_{RT}$, a higher value of feed is required to guarantee a compressive surface residual stress in tangential direction. It can be concluded from the results that the desirable compressive residual stress for $(\sigma_{0zz})_{RT}$ is only achievable at higher feed values. As it can be realized, results show a parabolic relation between the introduced tangential residual stresses and the feed. It is noted that similar parabolic behavior has been previously reported for conventional deep rolling of Ti-6Al-4V [7, 22] and AISI1045 [90]. With respect to $(\sigma_{0zz})_{450}$, one can realize that a high level of feed is required to maintain a compressive residual stress in tangential direction, particularly for small ball diameters. Moreover, comparing Figure 5-20 (a) and (b) show that the thermal relaxation decreases the magnitude of the compressive tangential residual stress on the surface at a higher rate compared with tensile tangential residual stresses. This is mainly attributed to thermal softening and net material movement of the surrounding material (untreated regions) and therefore imposing a less restrain on the treated region with compressive residual stress.

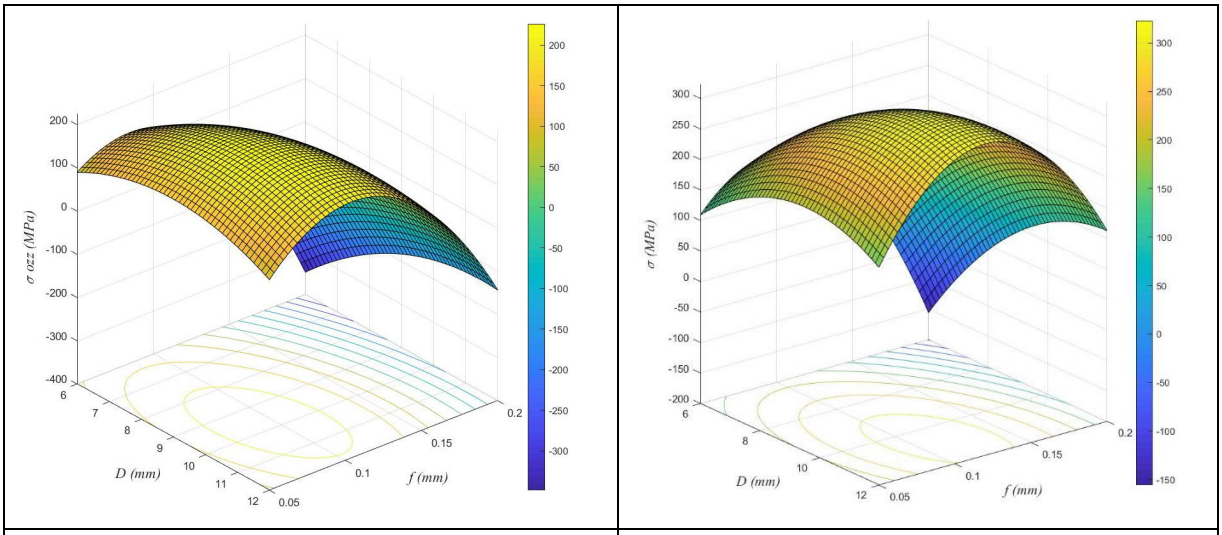

(a) (b)

Figure 5-20: Effect of feed and ball diameter on σ_{0zz} for *P=20 MPa* (a) at room temperature 25℃, and (b) at elevated temperature 450 ℃

The results presented in Figures 5-19 and 5-20, show the thermal relaxation of residual stresses on surface are higher when they are induced by higher rolling pressure and feeds (upper bounds of the design variables). This agrees with the experimental findings [14, 22], where surface layers with medium dislocation density show a better thermal stability of residual stresses compared with surface layers with extremely high dislocation densities. Nevertheless, it can be realized the residual stress can alter from compressive to tensile at lower feed as the plastic deformation in tangential direction is not high enough to maintain a compressive residual stress at elevated temperature.

The response surfaces for $(Area)_{RT}$ and $(Area)_{450}$ with respect to rolling pressure and feed for the given ball diameter of *6 mm* are presented in Figure 5-21 (a) and (b), respectively. As it can be realized both $(Area)_{RT}$ and $(Area)_{450}$ are more dominated by the rolling pressure and for the assumed ball diameter, increasing the rolling pressure creates a deeper residual stress profile at any given feed. However, comparing Figure 5-21 (a) and (b), one can conclude that the exposure to the elevated temperature leads to decreasing the depth of the residual stress profiles induced at the room temperature. It is noted that feed has more significant effect on the residual stress closer to the surface layer while the profile of the residual stresses through the depth of the component is more affected by the rolling pressure. The stress relaxation is basically more dependent on the

level of rolling pressure than the feed and the residual stress profile relaxes more when the process is performed under higher rolling pressure.

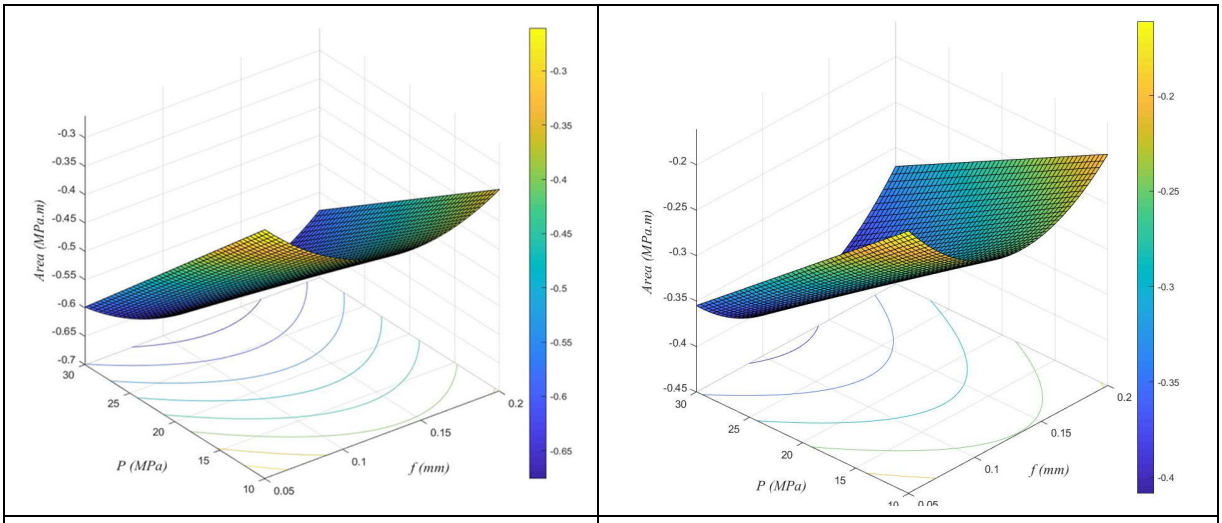

(a) (b)

Figure 5-21: Effect of feed and ball diameter on the stress $Area$ for D=6 mm (a) at room temperature 25℃, and (b) at elevated temperature 450 ℃

Figures 5-22 and 5-23 respectively show the surface plots of (σ_{500xx}) and (σ_{500zz}), with respect to ball diameters and rolling pressure for feed f =0.125mm at both room and 450 ℃ temperature. The output responses show a very similar behavior with respect to the design variables. As it can be realized the effect of the rolling pressure is more significant at smaller ball diameter where increasing the rolling pressure leads to a more compressive residual stress. However, at higher ball diameters a parabolic behavior is observed which may be attributed to deep strain hardening introduced due to process applied from both sides which interact around mid surface of the component. The thermal relaxation especially at higher ball diameter is mainly dominated by material softening as the plastic strains are developed through the whole thickness.

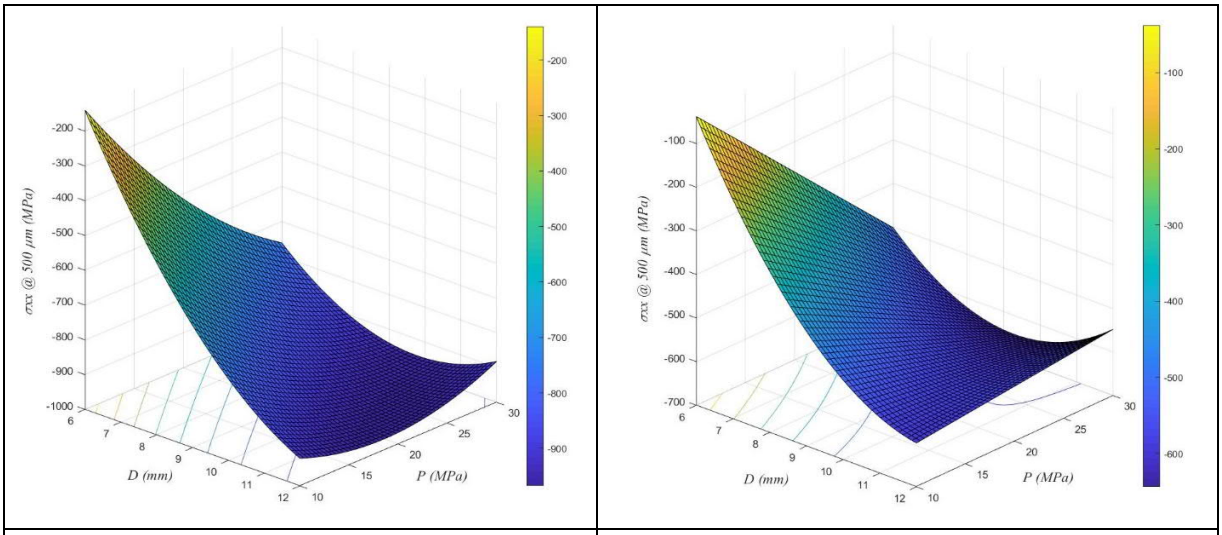

(a) (b)

Figure 5-22: Effect of rolling pressure and ball diameter on σ_{500xx} for *f=0.125 mm* (a) at room temperature 25℃, and (b) at elevated temperature 450 ℃

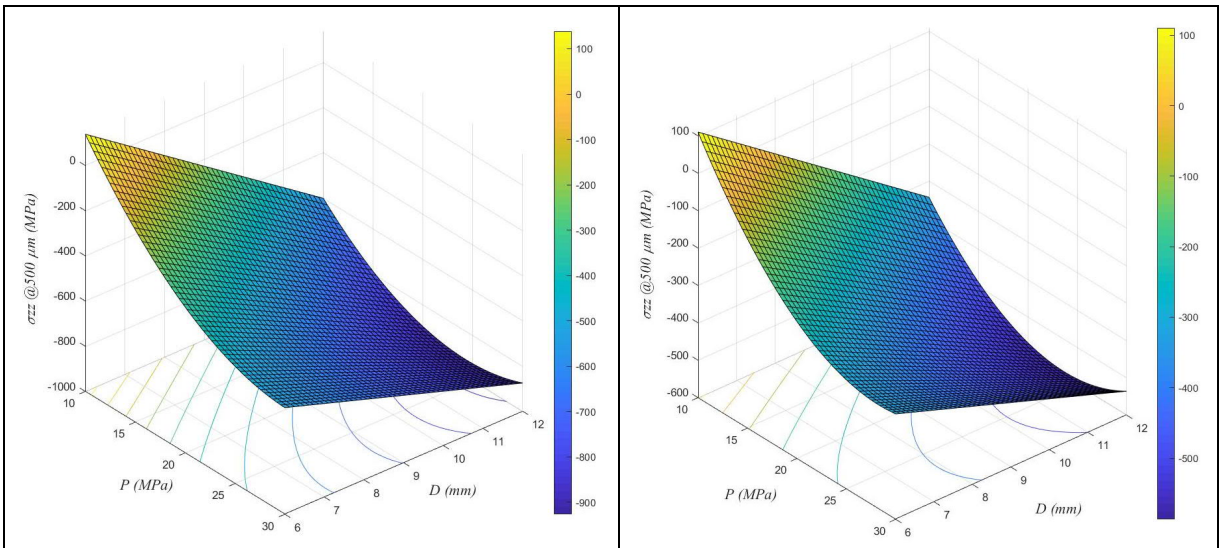

(a) (b)

Figure 5-23: Effect of rolling pressure and ball diameter on σ_{500zz} for *f=0.125 mm* (a) at room temperature 25℃, and (b) at elevated temperature 450 ℃

5.5 Optimization

As it was explained and shown in the previous sections, the double-sided DCR process also induces anisotropic residual stress profiles which are significantly different in axial and tangential direction. Therefore, the process parameters need to be tailored according to the stresses imposed

by the external loading. Double-sided deep rolling of a compressor blade of a gas turbine which is schematically presented in Figure 5-24 was considered in the current study for the optimization problem. The external loads on the blades are centrifugal (CF) load due to the shaft rotation and pressure load imposed by the hot gas. These load result in significant radial stress in Z' direction and moments around X' axis ($M_{X'}$) at the inner platform zone highlighted in blue. The aerodynamic definition of the airfoil also results in a very thin trailing edge (zone highlighted in red) which results in high radial stress in this region. Therefore, the surface treatment can be efficiently employed to enhance the fatigue life of the part by introducing a compressive residual stress in the highlighted zones without any design change.

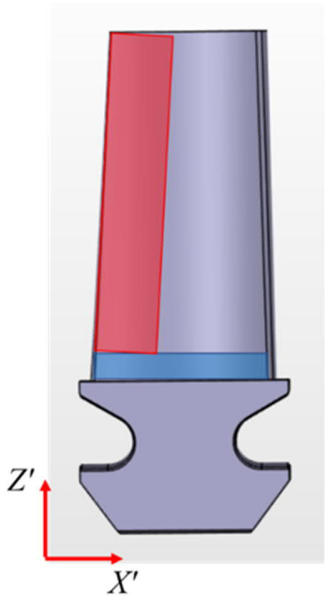

Figure 5-24: Schematic of a compressor blade and the treated areas

The application of the double-sided DCR process in the highlighted zones of the blade is constrained by the rolling direction imposed by the geometry. As it can be realized, the double-sided DCR in blue and red zones can be practically performed only in global *X'* and *Z'* directions, respectively. Therefore, while the objective in the blue zone is to achieve the most compressive residual stress perpendicular to the rolling direction (σ_{0zz}) (note that rolling direction, x in blue region, coincides with global X'), the objective in the red zone is to achieve the most compressive stress in the rolling direction (σ_{0xx}), (note that rolling direction, x in red region, coincides with global Z').

The proposed multi-objective design optimization problem can be formally formulated as:

$$
\begin{aligned}
&minimize\ the\ function && 0.5\ Area + w_1(\sigma_0)_{zz} + w_2(\sigma_0)_{xx} \\
&Subject\ to\ the\ constarint && w_1(\sigma_{500})_{zz} + w_2(\sigma_{500})_{xx} < -100MPa \\
& && 6\ mm \leq D \leq 12\ mm \\
& && 0.05\ mm \leq f \leq 0.2\ mm \\
& && 10\ MPa \leq P \leq 30\ MPa
\end{aligned}
\tag{5-11}
$$

The defined constraint function will guarantee sufficient compressive residual stress is introduced throughout the thickness while avoiding a tensile balancing stress at the mid thickness of the workpiece. The proposed objective function can be tailored based on the stress distribution in the blade due to the external applied load using the weighting factors provided in Table 5-3.

Table 5-3: Assigned weighting factors in the optimization problem

Treated area	w_1	w_2
Inner platform zone (Blue zone)	0.5	0
Trailing edge zone (Red zone)	0	0.5

The developed analytical response functions provided in Eqs. (5-1)- (5-10) can now be effectively used to establish the objective and constraint functions formulated in Eq. (5-11) with respect to the design variables at both 25ºC and 450 ºC operating temperatures. Considering this the optimization problem formulated in Eq. (5-11) can be efficiently solved using optimization algorithms.

A combination of sequential quadratic programming (SQP) and genetic algorithm (GA) techniques is employed in the current study to solve the optimization problem. As mentioned before, SQP is a local optimizer without any mechanism to search for global solution but it is a powerful nonlinear mathematical programming technique which can capture a local optimum solution accurately. On the other hand, genetic algorithm (GA) is a widely used and popular stochastic-based global optimizer. In this hybrid optimization method, the optimal solutions from GA which are in neighborhood of the true global optimum solution are forwarded as the initial points to the SQP solver in order to accurately capture the global optimal solutions. This method has been successfully employed in design optimization of multiphysics problem where finding a global solution was not analytically guaranteed [80].

5.6 Results and Discussions

Design optimization problem formulated in the previous section has been used to obtain the optimum set of design variables (i.e. ball diameter, rolling pressure, and rolling feed) in order to achieve an optimal residual stress profile at room and at elevated temperature of 450℃. The optimization problems were solved using the proposed GA combined with SQP method.

Tables 5-4 and 5-5 present the process parameters to achieve optimal residual stress profiles at the identified critical areas at 25℃ and 450 ℃, respectively. As it can be realized from comparing Tables 5-4 and 5-5, the operating temperature slightly changes the optimal design variables for surface treatment of the trailing edge. For further clarification, the desired output responses at 450℃ have been evaluated using the optimal design process parameters (optimal *D, f* and *P*) obtained at room temperature and compared with those optimal values obtained at 450 ℃ and the results are provided in Table 5-6. The optimal results obtained for double-sided DCR is less sensitive to the operating temperature compared with those obtained for conventional DCR. This is mainly attributed to the more uniform residual stress distribution through the thickness induced by the double-sided process.

Table 5-4: Optimization results at 25 ℃

	Inner platform zone	Trailing edge zone
w_1	0.5	0
w_2	0	0.5
D (mm)	6.00	12.00
f (mm)	0.200	0.112
P (MPa)	30.00	30.00
$(\sigma_{0xx})_{RT}$ *(MPa)*	289	-563
$(\sigma_{0zz})_{RT}$ *(MPa)*	-474	170
$(Area)_{RT}$ *(MPa.m)*	-1.1644	-1.5347
$(\sigma_{500xx})_{RT}$ *(MPa)*	-515	-825
$(\sigma_{500zz})_{RT}$ *(MPa)*	-480	-940

Table 5-5: Optimization results at 450 ℃

	Inner platform zone	Trailing edge zone
w_1	0.5	0
w_2	0	0.5
D (mm)	6.00	12.00
f (mm)	0.200	0.129
P (MPa)	30	30
$(\sigma_{0xx})_{450}$ *(MPa)*	314	-264
$(\sigma_{0zz})_{450}$ *(MPa)*	-173	279
$(Area)_{450}$ *(MPa.m)*	-0.6413	-0.8823
$(\sigma_{500xx})_{450}$ *(MPa)*	-201	-540
$(\sigma_{500zz})_{450}$ *(MPa)*	-276	-538

Table 5-6: Output results at 450 ℃ using optimal design variables obtained at room temperature versus at elevated temperature for the trailing edge zone

	Optimized at 25℃	Optimized at 450℃
D (mm)	12.00	12.00
f (mm)	0.112	0.129
P (MPa)	30.00	30.00
$(\sigma_{0xx})_{450}$ *(MPa)*	-258	-264
$(\sigma_{0zz})_{450}$ *(MPa)*	290	279
$(Area)_{450}$ *(MPa.m)*	-0.8858	-0.8823
$(\sigma_{500xx})_{450}$ *(MPa)*	-513	-540
$(\sigma_{500zz})_{450}$ *(MPa)*	-580	-538

5.7 Conclusion

A high-fidelity finite element (FE) model has been developed to predict the axial and tangential residual stress profiles induced by double-sided DCR process on Ti64 thin plate at the room temperature and the following thermal relaxation at elevated temperature. The process was modeled under both force and displacement control modes of the rolling ball and the results show

that the residual stress profiles for displacement and force control configuration are basically very similar in the surface layer while diverge slightly in higher depth. The results obtained from the developed FE model are in good agreement with available experimental measurements.

The developed FE model was then utilized to generate training data at intelligently identified design points using DoE techniques. Regression-based machine learning was subsequently employed to train and validate predicative analytical models. The developed surrogate analytical models can efficiently replace full-scale and computationally expensive FE simulation and accurately predict the residual stress profiles at room temperature and after thermal relaxation at 450°C.

The effects of ball diameter, feed and rolling pressure on the induced residual stress profiles and their relaxations at elevated temperature were systematically investigated using the developed surrogate models. A design optimization problem was formulated to enhance fatigue life at high stress locations of a generic compressor blade considering different operating temperatures. The developed analytical surrogate models were used to describe the objective and constraint functions. The conclusions and highlights of the present study are outlined as follows:

1. The residual stress profile induced by double-sided DCR process is significantly different than that induced by the conventional DCR process performed on the same workpiece under identical processing parameters.
2. The process generates residual stress profiles which are anisotropic and significantly different in axial and tangential directions. Therefore, the stress distribution in the component due to external load should be known prior to selection of rolling direction.
3. Higher rolling pressure and larger ball diameters with lower feed are required to achieve a more compressive residual stress in the axial direction $(\sigma_{oxx})_{RT}$. The tangential residual stress is mainly affected by feed as it significantly influences the tangential plastic deformation and higher feed values are required to achieve more compressive residual stress in tangential direction.
4. At any given ball diameter, the level of thermal relaxation is higher for deeper and more compressive residual stress which is due to high plastic deformation and thermal instability of dislocations. While the rate of thermal relaxation of axial residual stress is more

pronounced at lower feed and higher pressure, the tangential residual stress relaxes more when the process is conducted under higher levels of pressure and feed.

5. The operating temperature of the components and the stress imposed by external loading need to be considered in the optimization problem.

6 Conclusions, Contributions and future Works

This chapter outlines the main conclusions of the present PhD dissertation and its major contributions to the advancement of knowledge in the field of FE modeling and optimization of Deep Cold Rolling. Based on the knowledge gained through the course of the current research some possible future extensions have been identified which will be presented along with recommendations. Finally, an outlook on FE-based machine learning and optimizations of cold deep rolling and the potential industrial applications to save time, material and resources will be discussed.

6.1 Summary and Conclusions

Ti-6Al-4V (Ti64) is a titanium alloy with a high strength-to-weight ratio and excellent corrosion resistance making it an excellent material for gas turbine applications. The main usage of Ti64 is in compressor blades and discs which their lives are mainly limited by fatigue. Therefore, improving the fatigue life to enhance durability and reliability of such highly stressed expensive component while maintaining the original design can play an important role in design stage and life cycle cost of the engine.

Deep Cold Rolling (DCR) was presented as a promising mechanical surface treatment to improve the fatigue life of components by introducing deep and high compressive residual stresses on the surface and sub-surface layers. However, the exposure to elevated temperatures can relaxes most of the residual stressed induced by the process at the room temperature. Therefore, in order to account for the impact of beneficial residual stress on the fatigue life of the treated component, developing a design tool which can predict the residual stresses induced by the process and after thermal relaxation at elevated temperature is required.

In the present research work, first a high-fidelity FE model was developed to simulate DCR process on a Ti64 plate and the following thermal exposure to elevated temperature 450 °C. The capability of the developed FE model to predict residual stresses was validated to experimental measurements available in the literature. It has been shown that the finite element predictions correlate well with experimental results with error generally less than 10%. The developed model can be effectively utilized for parametric studies to understand the effect of different process parameters on the induced residual stresses without performing expensive experimental tests.

The application of the developed FE model was extended to predict the residual stress profiles in a deep-rolled Ti64 thin plate at room temperature as well as elevated temperature 450 °C. It was discussed that rolling speed does not have a significant impact on the residual stresses and the number of the rolling pass cannot be considered as design variable. Three key design variables ball diameter (6-12 mm), feed (0.05-0.200 mm) and rolling pressure (10-30 MPa) were considered to form the design domain. DoE was used to discretize the design to main at the design points. The FE models were then run at the design points to generate a data set to train surrogate models using well-stablished machine learning techniques. The surrogate models are considerably lower in order than a full-scale finite element simulation and can efficiently approximate FE models to perform sensitivity analysis and design optimization of process parameters.

Based on the comprehensive literature review, the tensile balancing residual stress created in component was identified as a detrimental secondary effect of the process which results in crack nucleation under HCF regime and needs a particular attention in the design optimization of the process. Operating temperature of the treated component and fatigue behaviour of Ti64 were considered in formulating an optimization problem to achieve the best residual stress profiles in a thin plate using conventional deep rolling. The results revealed that the optimal design variables achieved at the room temperature will not guarantee an optimal solution at the elevated temperature and the operating temperature needs to be considered to derive an optimal solution.

The FE results presented in Chapter 4 show that conventional DCR of thin plate (performing rolling only on one side of the component) can result in unfavorable tensile residual stresses on the untreated side of the components. It was further discussed that the process inherits manufacturing challenges as in can bend and damage thin component. In addition, high gradient asymmetric residuals stress and strain hardening can lead to thermal distortion of the component at elevated temperatures. Double-sided deep rolling was presented as an alternative solution as it treats the both sides of the thin-walled components simultaneously and can be efficiently employed to introduce compressive residual stress on both sides.

A high-fidelity non-linear finite element model has also been developed to simulate the double-sided DCR process on thin Ti64 plate and to predict the residual stress profile introduced by the process and after thermal relaxation due to subsequent exposure to high temperature. The accuracy

of the developed finite element model was validated by comparison with the experimental measurement available in the literature.

The residual stress profile induced by double-sided DCR process is significantly different than that induced by the conventional DCR process performed on the same workpiece under identical processing parameters. The process generates residual stress profiles which are anisotropic and significantly different in axial and tangential directions. Therefore, the stress distribution in the component due to external load should be known prior to selection of rolling direction.

The sensitivity analysis showed that higher rolling pressure and larger ball diameters with lower feed is required to achieve a more compressive residual stress in the axial direction. The tangential residual stress is mainly affected by feed as it significantly influences the tangential plastic deformation and higher feed value are required to achieve more compressive residual stress in tangential direction.

At any given ball diameter, the level of thermal relaxation is higher for deeper and more compressive residual stress which is due to high plastic deformation and thermal instability of dislocations. While the rate of thermal relaxation of axial residual stress is more at lower feed and higher pressure, the tangential residual stress relaxes more when the process is done under higher levels of pressure and feed.

Well-established machine learning principles were then carried out on data generated by the high-fidelity FE model to develop predictive analytical models to approximate residual stresses induced by the double-sided DCR process. The developed analytical functions efficiently replace FE models to perform design optimization of process parameters. Load distribution at high stress areas of a generic compressor blade was considered to formulate a design optimization problem of double-sided DCR process in order to achieve optimal residual stress distributions at room temperature and after thermal relaxation at elevated temperature of 450°C. The optimization study revealed that the operating temperature of the components and the stress imposed by external loading need to be considered in the optimization problem.

6.2 Contributions

The main contributions of the current study to the research field of Deep Cold Rolling process can be summarized as follow:

1. Development of a high-fidelity FE model to simulate conventional and double-sided DCR processes. The developed models were validated using available experimental results in literature and thus can be effectively utilized to fundamentally investigate the effect of process parameters on induced residual stresses instead of expensive and experimental measurements.
2. Extension of the developed FE models to simulate short-term exposure of deep-rolled Ti64 components to elevated temperature 450°C in order to investigate the thermal relaxation of the induced residual stresses.
3. Development of approximate response surface functions using well-established machine learning techniques and the developed FE models to evaluate the desired output responses accurately and efficiently. The developed surrogate models are smooth analytical functions which are explicitly related to design variables and thus can replace computationally expensive FE models.
4. Conducting extensive parametric studies to investigate the effect of design process parameters on the induced residual stresses both at room and elevated temperature.
5. Development of design optimization strategies to identify the optimal process parameters in both single and double-sided DCR processes.

The results and contributions of the current PhD research work have been published or under review to be published in form of journal articles, as follows:

1- Hadadian, A. and Sedaghati, R., 2019. Investigation on thermal relaxation of residual stresses induced in deep cold rolling of Ti–6Al–4V alloy. The International Journal of Advanced Manufacturing Technology, 100(1-4), pp.877-893.

2- Hadadian A, Sedaghati R, 2019. Design Optimization of Deep Cold Rolling of Ti-6Al-4V for Elevated Temperature Operations. Submitted to Journal of Manufacturing Processes, Ms. Ref. No.: SMEJMP-D-19-00860 (Under review)

3- Hadadian A, Sedaghati R, 2019. Analysis and Design Optimization of Double-Sided Deep Cold Rolling Process of a Ti-6Al-4V Blade. To be submitted to Production Engineering

6.3 Future Works and Recomendations

The design optimization in the current work was formulated with the emphasise on enhancing fatigue strength of Ti64 components. FOD and DOD are very common reported damages in compressor stage blades. Therefore, optimization of the process parameters to enhance the FOD ad DOD resistance of the component is an absolute need for aerospace and power generation industries.

Another main application of Ti64 is in compressor discs of gas turbines with life limited features located on negative curvature surfaces such as dovetails [101]. The developed FE model in the current thesis has been validate for flat and positive curvature surfaces. However, it has not been validated for surfaces with negative curvature due to lack of experimental measurements available in the literature. The experimental measurements and FE modeling need to be undertaken to address this caveat.

The thermal relaxation model developed in the current study is limited to short term thermal exposure due to lack of available experimental measurements to validate the model. Although the main thermal relaxation is prompt and occurred in the first hours of exposure to elevated temperature, the long-term thermal exposure must be experimentally investigated. In the absence of available measurement, updating the creep law of the current FE thermal model to include longer hours creep strains may be considered as invalidated approach to estimate the thermal relaxation.

Although the aerospace applications of Ti64 was emphasised in the current research work, the titanium alloy has long been favored for biomedical applications such as orthopedic, spinal, dental and trauma surgical implants. The design intent in such applications is to avoid any failure even at very high number of cycles. However, predicting boundary conditions for implant designers is a highly challenging task. Therefore, DCR process can be considered for HCF endurance enhancement of such implants and giving the designer a reserved factor.

To the best knowledge of the author, the design optimization of the DCR process on other super alloys such as IN738 and IN718 nickel alloys has not been addressed in the available literatures which can be considered in the future works.

6.4 Outlook

High strength-to-density ratio, high corrosion resistance and superior biocompatibility are the main advantages of titanium making it a long been favored metal for aerospace and biomedical applications. However, high environmental damage, difficulty in casting, rarity and high selling price are disadvantages of using titanium. Therefore, designing to last longer or refurbishing and rehabilitation of aged titanium components has both commercials and environmental benefits.

Optimization of the production processes and lowering the final cost while producing more reliable products in a shorter design time with minimum experimental validation is a widespread challenge for all industries under the current intense competition. FE methods have found their unique place particularly in high-tech industries to reduce the project lead times and manufacturing costs by virtually simulating the manufacturing processes scenarios and predicting the effect of manufacturing process parameters on the final product.

Advances in machine learning techniques is having a dramatic impact on the design methodologies as is it allows to continually learn from available data to predict outcomes. These techniques are getting more attention to develop analytics based on results obtained from computationally expensive FE models, in order to perform simulation-based optimizations. Hopefully, this new trend in mechanical design will result in a more durable and reliable products which are also environmentally friendly.

References

[1] Trauth, D., Klocke, F., Mattfeld, P., 2013, "Time-Efficient Prediction of the Surface Layer State After Deep Rolling using Similarity Mechanics Approach," Procedia CIRP, 9(0) pp. 29-34.

[2] Tsuji, N., Tanaka, S., and Takasugi, T., 2008, "Evaluation of Surface-Modified Ti–6Al–4V Alloy by Combination of Plasma-Carburizing and Deep-Rolling," Materials Science and Engineering: A, 488(1) pp. 139-145.

[3] Nalla, R. K., Altenberger, I., Noster, U., 2003, "On the Influence of Mechanical Surface Treatments-Deep Rolling and Laser Shock Peening-on the Fatigue Behavior of Ti-6Al-4V at Ambient and Elevated Temperatures," Materials Science and Engineering: A, 355(1-2) pp. 216-230.

[4] Bäcker, V., Klocke, F., Wegner, H., 2010, "Analysis of the Deep Rolling Process on Turbine Blades using the FEM/BEM-Coupling," IOP Conference Series: Materials Science and Engineering, 10(1) pp. 012134.

[5] Liu, Y., Wang, L., and Wang, D., 2011, "Finite Element Modeling of Ultrasonic Surface Rolling Process," Journal of Materials Processing Technology, 211(12) pp. 2106-2113.

[6] Altenberger, I., 2005, "Deep Rolling—The Past, the Present and the Future," Proceedings of 9th International Conference on Shot Peening, pp. 144-155.

[7] Hadadian, A., and Sedaghati, R., 2018, "Investigation on Thermal Relaxation of Residual Stresses Induced in Deep Cold Rolling of Ti–6Al–4V Alloy," The International Journal of Advanced Manufacturing Technology, pp. 1-17.

[8] Altenberger, I., Nalla, R. K., Sano, Y., 2012, "On the Effect of Deep-Rolling and Laser-Peening on the Stress-Controlled Low-and High-Cycle Fatigue Behavior of Ti–6Al–4V at Elevated Temperatures Up to 550 C," International Journal of Fatigue, 44pp. 292-302.

[9] Mohammadi, F., Sedaghati, R., and Bonakdar, A., 2013, "Finite Element Analysis and Design Optimization of Low Plasticity Burnishing Process," Int J Adv Manuf Technol, 70(5-8) pp. 1337-1354.

[10] El-Axir, M., 2000, "An Investigation into Roller Burnishing," International Journal of Machine Tools and Manufacture, 40(11) pp. 1603-1617.

[11] Klocke, F., Bäcker, V., Wegner, H., 2009, "Influence of Process and Geometry Parameters on the Surface Layer State After Roller Burnishing of IN718," Production Engineering, 3(4-5) pp. 391-399.

[12] Klocke, F., Bäcker, V., Wegner, H., 2011, "Finite Element Analysis of the Roller Burnishing Process for Fatigue Resistance Increase of Engine Component," Proceedings of the Institution of Mechanical Engineers, Part B: Journal of Engineering Manufac, 225(1) pp. 2-11.

[13] Klocke, F., and Mader, S., 2005, "Fundamentals of the Deep Rolling of Compressor Blades for Turbo Aircraft Engines," Steel Research International, 76(2-3) pp. 229-235.

[14] Prevéy, P., Hombach, D., and Mason, P., 1998, "Thermal residual stress relaxation and distortion in surface enhanced gas turbine engine components," Proceedings of the 17th Heat Treating Society Conference, D. L. Milam, ed. ASM, .

[15] ECOROLL© Corporation TOOL TECHNOLOGY, 2006, "Tools & Solutions for Metal Surface Improvement, Roller Burnishing, Deep Rolling, Combined Skive-Burnishing," (http://www.utech.co.th/files/ecoroll_catalog_en_web.pdf), 2019.

[16] Gill, C., Fox, N., and Withers, P., 2008, "Shakedown of Deep Cold Rolling Residual Stresses in Titanium Alloys," Journal of Physics D: Applied Physics, 41(17) pp. 174005.

[17] Schulze, V., 2006, "Modern mechanical surface treatment: states, stability, effects," Wiley-VCH, New York, .

[18] Zaroog, O. S., Ali, A., Sahari, B., 2009, "Modelling of Residual Stress Relaxation: A Review," Pertanika Journal of Science & Technology, 17(2) pp. 211-218.

[19] Altenberger, I., 2003, "Shot Peening,"Wiley-VCH Verlag GmbH & Co., KGaA, Weinheim, FRG, pp. 419-434.

[20] Stanojevic, A., Angerer, P., and Oberwinkler, B., 2016, "Thermal Stability of Residual Stresses in Ti-6Al-4V Components," IOP Conference Series: Materials Science and Engineering, 119(1) pp. 012007.

[21] Nikitin, I., Altenberger, I., Maier, H., 2005, "Mechanical and Thermal Stability of Mechanically Induced Near-Surface Nanostructures," Materials Science and Engineering: A, 403(1) pp. 318-327.

[22] Prevéy, P. S., Shepard, M. J., and Smith, P. R., 2001, "The Effect of Low Plasticity Burnishing (LPB) on the HCF Performance and FOD Resistance of Ti-6AI-4V," the 6th National Turbine Engine High Cycle Fatigue (HCF) Conference, DTIC Document, .

[23] Zhou, Z., Bhamare, S., Ramakrishnan, G., 2012, "Thermal Relaxation of Residual Stress in Laser Shock Peened Ti–6Al–4V Alloy," Surface and Coatings Technology, 206(22) pp. 4619-4627.

[24] Junjie, X., Dongsheng, L., and Xiaoqiang, L., 2015, "Modeling and Simulation for the Stress Relaxation Behavior of Ti-6Al-4V at Medium Temperature," Rare Metal Materials and Engineering, 44(5) pp. 1046-1051.

[25] Stanojevic, A., Maderbacher, H., Angerer, P., 2016, "Stability of Residual Stresses in Ti-6Al-4V Components Due to Mechanical Loads," Proceedings of the 13th World Conference on Titanium, V. Venkatesh, ed. Wiley Online Library, Hoboken, NJ, USA., pp. 1593-1598.

[26] Jayaraman, N., and Prevéy, P., 2003, "Application of low plasticity burnishing (LPB) to improve the corrosion fatigue performance and FOD tolerance of alloy 450 stainless steel," Proceedings of the Tri-Service Corrosion Conference, pp. 17-21.

[27] Zay, K., Maawad, E., Brokmeier, H., 2011, "Influence of Mechanical Surface Treatments on the High Cycle Fatigue Performance of TIMETAL 54M," Materials Science and Engineering: A, 528(6) pp. 2554-2558.

[28] Ludian, T., and Wagner, L., 2008, "Mechanical Surface Treatments for Improving Fatigue Behavior in Titanium Alloys," Advances in Materials Sciences, 8(2) pp. 44-52.

[29] Prevéy, P. S., Ravindranath, R. A., Shepard, M., 2003, "Case studies of fatigue life improvement using low plasticity burnishing in gas turbine engine applications," ASME Turbo Expo 2003, collocated with the 2003 International Joint Power Generation Conference, American Society of Mechanical Engineers, pp. 657-665.

[30] Prevey, P., Hornbach, D., Ravindranath, R., 2003, "Application of Low Plasticity Burnishing to Improve Damage Tolerance of a Ti-6Al-4V First Stage Fan Blades," 44th AIAA/ASME/ASCE/AHS/ASC Structures, Structural Dynamics, and Materials Conference, pp. 1524.

[31] Altenberger, I., Nalla, R., Noster, U., 2002, "On the Fatigue Behavior and Associated Effect of Residual Stresses in Deep-Rolled and Laser Shock Peened Ti-6Al-4V Alloys at Ambient and Elevated Temperatures," University of California, Berkeley, 94720.

[32] Sonntag, R., Reinders, J., Gibmeier, J., 2015, "Fatigue Performance of Medical Ti6Al4V Alloy After Mechanical Surface Treatments," PloS One, 10(3) pp. e0121963.

[33] Mhaede, M., Sano, Y., Altenberger, I., 2011, "Fatigue Performance of Al7075-T73 and Ti-6Al-4V: Comparing Results After Shot Peening, Laser Shock Peening and Ball-Burnishing," International Journal Structure Integrity, 2pp. 185-199.

[34] Wagner, L., Mhaede, M., Wollmann, M., 2011, "Surface Layer Properties and Fatigue Behavior in Al 7075-T73 and Ti-6Al-4V: Comparing Results After Laser Peening; Shot Peening and Ball-Burnishing," International Journal of Structural Integrity, 2(2) pp. 185-199.

[35] Cherif, M., Sano, Y., Rüppel, C., 2007, "Fatigue behaviour and residual stress relaxation of laser-shock peened and deep rolled Ti-6Al-4V," 11th World Titanium Conference, Kyoto, pp. 1711.

[36] Wagner, L., 1999, "Mechanical Surface Treatments on Titanium, Aluminum and Magnesium Alloys," Materials Science and Engineering: A, 263(2) pp. 210-216.

[37] Oberwinkler, B., 2016, "On the Anomalous Mean Stress Sensitivity of Ti-6Al-4V and its Consideration in High Cycle Fatigue Lifetime Analysis," International Journal of Fatigue, 92pp. 368-381.

[38] Lanning, D. B., and Nicholas, T., 2007, "Constant-Life Diagram Modified for Notch Plasticity," International Journal of Fatigue, 29(12) pp. 2163-2169.

[39] Lindemann, J., and Wagner, L., 1997, "Mean Stress Sensitivity in Fatigue of A,(Aβ) and B Titanium Alloys," Materials Science and Engineering: A, 234pp. 1118-1121.

[40] Dassault Systèmes, 2013, "ABAQUS 6.13, Analysis User's Guide,".

[41] Cook, R.D., 2007, "Concepts and applications of finite element analysis," John Wiley & Sons, New York, .

[42] Zhuang, W., and Wicks, B., 2004, "Multipass Low-Plasticity Burnishing Induced Residual Stresses: Three-Dimensional Elastic-Plastic Finite Element Modelling," Proceedings of the Institution of Mechanical Engineers, Part C: Journal of Mechanical Engineering Science, 218(6) pp. 663-668.

[43] Guo, Y., and Barkey, M. E., 2004, "FE-Simulation of the Effects of Machining-Induced Residual Stress Profile on Rolling Contact of Hard Machined Components," International Journal of Mechanical Sciences, 46(3) pp. 371-388.

[44] Bijak-Żochowski, M., and Marek, P., 1997, "Residual Stress in some Elasto-Plastic Problems of Rolling Contact with Friction," International Journal of Mechanical Sciences, 39(1) pp. 15-32.

[45] Demurger, J., Forestier, R., Kieber, B., 2006, "Deep rolling process simulation: impact of kinematic hardening on residual stresses," Proc ESAFORM, pp. 1-5.

[46] Yoshida, T., Uenishi, A., Isogai, E., 2013, "Material Modeling for Accuracy Improvement of the Springback Prediction of High Strength Steel Sheets," Nippon Steel Technical Report, (103) pp. 63-69.

[47] Lesuer, D.R., 2000, "Experimental investigation of material models for Ti-6Al-4V and 2024-T3." FAA Report DOT/FAA/AR-00/25, .

[48] Nițu, E., Iordache, M., Marincei, L., 2011, "FE-Modeling of Cold Rolling by in-Feed Method of Circular Grooves," Strojniški Vestnik-Journal of Mechanical Engineering, 57(9) pp. 667-673.

[49] Kıranlı, E., 2009, "Determination of Material Constitutive Equation of a Biomedical Grade Ti6AI4V Alloy for Cross-Wedge Rolling," .

[50] Sun, J., and Guo, Y., 2009, "Material Flow Stress and Failure in Multiscale Machining Titanium Alloy Ti-6Al-4V," The International Journal of Advanced Manufacturing Technology, 41(7) pp. 651-659.

[51] Rohatgi, A., 2018, "WebPlotDigitizer Version: 4.1," Austin, TX, .

[52] Majzoobi, G., Jouneghani, F. Z., and Khademi, E., 2016, "Experimental and Numerical Studies on the Effect of Deep Rolling on Bending Fretting Fatigue Resistance of Al7075," The International Journal of Advanced Manufacturing Technology, 82(9-12) pp. 2137-2148.

[53] Klocke, F., Bäcker, V., Timmer, A., 2009, "Innovative FE-analysis of the roller burnishing process for different geometries," X international conference on computational plasticity fundamentals and application, pp. 1-4.

[54] Ali, M., and Pan, J., 2012, "Effect of a Deformable Roller on Residual Stress Distribution for Elastic-Plastic Flat Plate Rolling Under Plane Strain Conditions," SAE International Journal of Materials and Manufacturing, 5(2012-01-0190) pp. 129-142.

[55] Balland, P., Tabourot, L., Degre, F., 2013, "Mechanics of the Burnishing Process," Precision Engineering, 37(1) pp. 129-134.

[56] Balland, P., Tabourot, L., Degre, F., 2013, "An Investigation of the Mechanics of Roller Burnishing through Finite Element Simulation and Experiments," International Journal of Machine Tools and Manufacture, 65pp. 29-36.

[57] Sayahi, M., Sghaier, S., and Belhadjsalah, H., 2013, "Finite Element Analysis of Ball Burnishing Process: Comparisons between Numerical Results and Experiments," The International Journal of Advanced Manufacturing Technology, 67(5-8) pp. 1665-1673.

[58] Fischer-Cripps, A.C., 2007, "Introduction to Contact Mechanics,"Springer, New York, pp. 137-150.

[59] Lim, A., Castagne, S., and Wong, C. C., 2016, "Effect of Deep Cold Rolling on Residual Stress Distributions between the Treated and Untreated Regions on Ti–6Al–4V Alloy," Journal of Manufacturing Science and Engineering, 138(11) pp. 111005.

[60] Guagliano, M., and Vergani, L., 1998, "Residual Stresses Induced by Deep Rolling in Notched Components," Journal of the Mechanical Behavior of Materials, 9(2) pp. 129-140.

[61] Jiang, Y., Xu, B., and Sehitoglu, H., 2002, "Three-Dimensional Elastic-Plastic Stress Analysis of Rolling Contact," Journal of Tribology, 124(4) pp. 699-708.

[62] Courtin, S., Henaff-Gardin, C., and Bezine, G., 2003, "Finite Element Simulation of Roller Burnishing in Crankshafts," WIT Transactions on Engineering Sciences, 39.

[63] Sai, W. B., and Saï, K., 2005, "Finite Element Modeling of Burnishing of AISI 1042 Steel," The International Journal of Advanced Manufacturing Technology, 25(5-6) pp. 460-465.

[64] Yen, Y., Sartkulvanich, P., and Altan, T., 2005, "Finite Element Modeling of Roller Burnishing Process," CIRP Annals-Manufacturing Technology, 54(1) pp. 237-240.

[65] Sartkulvanich, P., Altan, T., Jasso, F., 2007, "Finite Element Modeling of Hard Roller Burnishing: An Analysis on the Effects of Process Parameters upon Surface Finish and Residual Stresses," Journal of Manufacturing Science and Engineering, 129(4) pp. 705-716.

[66] Manouchehrifar, A., and Alasvand, K., 2009, "Finite Element Simulation of Deep Rolling and Evaluate the Influence of Parameters on Residual Stress," Recent Researches in Applied Mechanics.WSEAS Press, Athens, pp. 121-127.

[67] Li, F., Xia, W., and Zhou, Z., 2010, "Finite element calculation of residual stress and cold-work hardening induced in Inconel 718 by Low Plasticity Burnishing," 2010 Third International Conference on Information and Computing, IEEE, 2, pp. 175-178.

[68] Bougharriou, A., Saï, W. B., and Saï, K., 2010, "Prediction of Surface Characteristics obtained by Burnishing," The International Journal of Advanced Manufacturing Technology, 51(1-4) pp. 205-215.

[69] Majzoobi, G., Motlagh, S. T., and Amiri, A., 2010, "Numerical Simulation of Residual Stress Induced by Roll-Peening," Transactions of the Indian Institute of Metals, 63(2-3) pp. 499-504.

[70] Fu, C., Guo, Y., McKinney, J., 2012, "Process Mechanics of Low Plasticity Burnishing of Nitinol Alloy," Journal of Materials Engineering and Performance, 21(12) pp. 2607-2617.

[71] Bougharriou, A., Saï, K., and Bouzid, W., 2013, "Finite Element Modelling of Burnishing Process," Materials Science and Technology, .

[72] Liou, J., and El-Wardany, T., 2014, "Finite Element Analysis of Residual Stress in Ti-6Al-4V Alloy Plate Induced by Deep Rolling Process Under Complex Roller Path," International Journal of Manufacturing Engineering, 2014.

[73] Perenda, J., Trajkovski, J., Žerovnik, A., 2015, "Residual Stresses After Deep Rolling of a Torsion Bar made from High Strength Steel," Journal of Materials Processing Technology, 218pp. 89-98.

[74] Perenda, J., Trajkovski, J., Žerovnik, A., 2015, "Modeling and Experimental Validation of the Surface Residual Stresses Induced by Deep Rolling and Presetting of a Torsion Bar," International Journal of Material Forming, pp. 1-14.

[75] Prevey, P. S., 1986, "X-Ray Diffraction Residual Stress Techniques," ASM International, ASM Handbook., 10pp. 380-392.

[76] Loh, N., Tam, S., and Miyazawa, S., 1989, "A Study of the Effects of Ball-Burnishing Parameters on Surface Roughness using Factorial Design," Journal of Mechanical Working Technology, 18(1) pp. 53-61.

[77] Prabhu, P., Kulkarni, S., and Sharma, S., 2010, "Influence of Deep Cold Rolling and Low Plasticity Burnishing on Surface Hardness and Surface Roughness of AISI 4140 Steel," World Academy of Science, Engineering and Technology, 72pp. 619-624.

[78] Seemikeri, C., Brahmankar, P., and Mahagaonkar, S., 2008, "Investigations on Surface Integrity of AISI 1045 using LPB Tool," Tribology International, 41(8) pp. 724-734.

[79] Scheil, J., Müller, C., Steitz, M., 2013, "Influence of Process Parameters on Surface Hardening in Hammer Peening and Deep Rolling," Key Engineering Materials, 554pp. 1819-1827.

[80] Hadadian, A., Sedaghati, R., and Esmailzadeh, E., 2013, "Design Optimization of Magnetorheological Fluid Valves using Response Surface Method," Journal of Intelligent Material Systems and Structures, 25(11) pp. 1352-1371.

[81] Hadadian, A., Prabhakar, S., Sjodin, B., 2018, "Application of surrogate models and probabilistic design methodology to assess creep growth limit of an uncooled turbine blade," Proceedings of ASME Turbo Expo 2018: Turbomachinery Technical Conference and Exposition, American Society of Mechanical Engineers, .

[82] Yen, Y., 2004, "Modeling of Metal Cutting and Ball Burnishing - Prediction of Tool Wear and Surface Properties," .

[83] El-Taweel, T., and El-Axir, M., 2009, "Analysis and Optimization of the Ball Burnishing Process through the Taguchi Technique," The International Journal of Advanced Manufacturing Technology, 41(3-4) pp. 301-310.

[84] Babu, P. R., Ankamma, K., T SIVA, P., 2012, "Optimization of Burnishing Parameters and Determination of Select Surface Characteristics in Engineering Materials," Sadhana, 37(4) pp. 503-520.

[85] Basak, H., and Goktas, H. H., 2009, "Burnishing Process on Al-Alloy and Optimization of Surface Roughness and Surface Hardness by Fuzzy Logic," Materials & Design, 30(4) pp. 1275-1281.

[86] MRE, U. U. N., and NAPOVED, Z., 2008, "Use of Artificial Neural Networks in Ball Burnishing Process for the Prediction of Surface Roughness of AA 7075 Aluminum Alloy," Materiali in Tehnologije, 42(5) pp. 215-219.

[87] Esme, U., 2010, "Use of Grey Based Taguchi Method in Ball Burnishing Process for the Optimization of Surface Roughness and Microhardness of AA 7075 Aluminum Alloy," Materiali in Tehnologije, 44(3) pp. 129-135.

[88] Lee, W., and Lin, C., 1998, "Plastic Deformation and Fracture Behaviour of Ti–6Al–4V Alloy Loaded with High Strain Rate Under various Temperatures," Materials Science and Engineering: A, 241(1) pp. 48-59.

[89] Haight, S., Wang, L., Du Bois, P., 2016, "Development of a Titanium Alloy Ti-6Al-4V Material Model Used in LS-DYNA," U.S. Department of Transportation, Federal Aviation Administration, DOT/FAA/TC-15/23, .

[90] Loh, N., Tam, S., and Miyazawa, S., 1989, "Statistical Analyses of the Effects of Ball Burnishing Parameters on Surface Hardness," Wear, 129(2) pp. 235-243.

[91] Buchanan, D. J., John, R., Brockman, R. A., 2010, "A Coupled Creep Plasticity Model for Residual Stress Relaxation of a Shot-Peened Nickel-Based Superalloy," JOM Journal of the Minerals, Metals and Materials Society, 62(1) pp. 75-79.

[92] Jenkins, J.M., 1984, "Effect of creep in titanium alloy Ti-6Al-4V at elevated temperature on aircraft design and flight test," NASA Ames Research Center, NASA-TM-86033, H-1228, NAS 1.15:86033, Moffett Field, CA, United States.

[93] Badea, L., Surand, M., Ruau, J., 2014, "Creep Behavior of Ti-6Al-4V from 450° C to 600° C," University Polytechnica of Bucharest Scientific Bulletin, Series B, 76(1) pp. 185-196.

[94] Gutierrez, D.D., 2015, "Machine learning and data science: an introduction to statistical learning methods with R," Technics Publications, .

[95] Shiraiwa, T., Briffod, F., Miyazawa, Y., 2017, "Fatigue Performance Prediction of Structural Materials by Multi-scale Modeling and Machine Learning," Proceedings of the 4th World Congress on Integrated Computational Materials Engineering (ICME 2017), Springer, pp. 317-326.

[96] "Minitab 18 Statistical Software (2018). [Computer Software]. Minitab, Inc. (www.Minitab.Com)," 2019(1/1) .

[97] Hadadian, A., 2011, "Optimal Design of Magnetorheological Dampers Constrained in a Specific Volume using Response Surface Method," .

[98] Dowling, N. E., 2004, "Mean Stress Effects in Stress-Life and Strain-Life Fatigue," SAE Technical Paper 2004-01-2227, .

[99] Tokaji, K., 2006, "High Cycle Fatigue Behaviour of Ti–6Al–4V Alloy at Elevated Temperatures," Scripta Materialia, 54(12) pp. 2143-2148.

[100] Altenberger, I., Noster, U., Boyce, B., 2002, "Effects of mechanical surface treatment on fatigue failure in Ti-6Al-4V: Role of residual stresses and foreign-object damage," Materials science forum, Trans Tech Publications, Switzerland, 404, pp. 457-462.

[101] Gowda, B. A., Yeshovanth, H., and Siddaraju, C., 2014, "Investigation and Efficient Modeling of an Dovetail Attachment in Aero-Engine," Procedia Materials Science, 5pp. 1873-1879.